TECHNISCHE UNIVERSITÄT MÜNCHEN

Fakultät für Medizin

The Impact of Platelet Soluble Guanylyl Cyclase Deficiency on Atherosclerotic Plaque Formation and Vascular Inflammation

Carina Maria Mauersberger

Vollständiger Abdruck der von der Fakultät für Medizin der Technischen Universität München zur Erlangung des akademischen Grades einer

Doktorin der Naturwissenschaften (Dr. rer. nat.)

genehmigten Dissertation.

Vorsitz: Prof. Dr. Lars Mägdefessel

Prüfer der Dissertation:

1. Prof. Dr. Hendrik Sager

2. Prof. Dr. Franz Hagn

Die Dissertation wurde am 17.01.2023 bei der Technischen Universität München eingereicht und durch die Fakultät für Medizin am 21.03.2023 angenommen.

Acknowledgment

First of all, I would like to thank my first advisor Prof. Hendrik Sager for his open mind and motivating spirit, and his support throughout my research projects. I am grateful for the high degree of freedom I was offered in developing new methods and research approaches, which allowed me to continuously develop both scientifically and personally. I would also like to express my thanks to Prof. Franz Hagn for his support as a member of my thesis committee and the friendly atmosphere in all our meetings, as well as Prof. Heribert Schunkert for his valuable input during our lab meetings. Furthermore, I would like to extend my sincere thanks to my mentor Dr. Thorsten Keßler for his attentive supervision of my dissertation project.

I also would like to thank all my colleagues who accompanied me throughout my doctorate for being amazing teammates and real friends. Special thank goes to Jana Wobst, Tan An Dang, and Julia Werner for their continuous scientific and personal support, Christopher Wolf for always offering a practical hand, and Julia Hinterdobler, Philipp Müller, and Amin Sharifi for being the best Ph.D. crew I could have wished for. I would also like to thank Ulrike Meyer-Lindemann and David Khangholi for their diligent work on our joint projects, and last but not least, Zhifen Chen and Aldo Moggio for their highly appreciated scientific input.

Finally, I owe my deepest gratitude to my parents Anita and Michael, my siblings Melanie and Christopher, and my partner Ludwig for their unconditional support during all stages of my doctorate. I would not have reached this point without you.

Table of Contents

Abstract

Atherosclerosis is one of the leading causes of morbidity and mortality in the world. The disease is characterized by lipoproteins and inflammatory cells infiltrating the inner layer of arteries and progressively narrowing and stiffening the vessels, which may eventually lead to serious complications such as myocardial infarction or stroke. Although efforts have been made worldwide to elucidate the circumstances that cause atherosclerotic plaque formation, only parts of the answer have been unraveled so far. Just within the last decades, it has become increasingly clear that beyond classical risk factors such as hypercholesterolemia or hypertension, also genetic risk factors affecting so far unrelated pathways may strongly impact the course of the disease. One of these newly revealed players is the nitric oxide, soluble guanylyl cyclase (sGC) pathway – a key molecular pathway with several important functions throughout the organism. Genetic risk variants associated with coronary artery disease (CAD), the manifestation of atherosclerosis in the coronary vasculature, have, *e.g.*, been shown to interfere with the pathway's beneficial impact on blood pressure. The effect that is explained by genetic variation, however, is greater than that explained by changes in blood pressure. It is therefore not yet clear how the nitric oxide-sGC pathway contributes to the progression of atherosclerosis. Consequently, to further elucidate the pathway's effects on atherosclerosis, the primary objective of this thesis was to investigate the functions of sGC specifically in platelets, one major affected cell type in human sGC risk allele carriers with vascular functions beyond blood pressure.

By using an experimental model of platelet-specific, functionally sGC-deficient mice on a pro-atherosclerotic background, it was possible to experimentally examine the role of platelet sGC in atherosclerosis *in vivo*. Subsequent analyses by flow cytometry, histology and *in vivo* fluorescence microscopy confirmed that lack of sGC in platelets promotes atherosclerotic plaque formation and inflammation, although expression of sGC in other cell types was not affected. *In vitro* experiments further revealed that the releasate of sGC-deficient platelets particularly triggers endothelium-driven leukocyte adhesion. As one potential causal factor for this phenomenon, the glycoprotein angiopoietin-1 was identified. It was released significantly less from sGC-deficient murine and sGC-impaired human platelets, while platelets stimulated with the sGC-stimulator BAY-747 released significantly more angiopoietin-1. *In vivo* treatment of atherosclerotic mice with BAY-747 could *vice versa* reduce the growth of atherosclerotic lesions and aortic leukocyte accumulation. Treating CAD patients with sGC stimulators, especially those patients with a high genetic burden within the pathway, might therefore be a novel strategy to address the impact atherosclerosis and its manifestations bear on our society.

Zusammenfassung

Die Atherosklerose, eine degenerative Erkrankung der Arterien, ist eine der Hauptursachen für Morbidität und Mortalität weltweit. Die hierbei über mehrere Jahre entstehenden atherosklerotischen Plaques gelten als die wichtigsten Auslöser lebensbedrohlicher ischämischer Ereignisse wie Herzinfarkt oder Schlaganfall. Trotz jahrelanger Bemühungen, die Umstände, die zur Entstehung dieser Erkrankung führen, zu ergründen, konnten bislang nur Teile der Antwort entschlüsselt werden. In den letzten Jahrzehnten wurde jedoch deutlich, dass neben klassischen Risikofaktoren wie Hypercholesterinämie oder Bluthochdruck auch Faktoren, die zuvor nicht mit der Atherosklerose in Zusammenhang gebracht wurden, den Krankheitsverlauf beeinflussen. Ein solcher Faktor ist der Stickstoffmonoxid-Signalweg: Mehrere Varianten in Genen, die für diesen Signalweg kodieren, wurden mit einem erhöhten Risiko für die Inzidenz der koronaren Herzkrankheit (KHK), der Manifestation von Atherosklerose in den Herzkranzgefäßen, assoziiert. Die Risikovarianten beeinträchtigen nachweislich die positive Wirkung des Signalwegs auf den Blutdruck. Tatsächlich ist der Effekt jedoch größer als der, der allein durch eine Veränderung des Blutdrucks erklärt werden kann. Daher bestand das Hauptziel dieser Arbeit darin, den Einfluss dieses Signalwegs innerhalb von Thrombozyten – einem weiteren, deutlich von diesen Risikovarianten betroffenen Zelltyp – auf die Entstehung der Atherosklerose zu beleuchten.

Zu diesem Zweck wurden atherosklerotische Mäuse mit einem funktionellen Mangel der löslichen Guanylatzyklase (sGC), einem zentralen Bestandteil des Stickstoffmonoxid-Signalwegs, mittels Durchflusszytometrie, Histologie und *In vivo*-Fluoreszenzmikroskopie untersucht. Dabei konnte bestätigt werden, dass ein sGC-Mangel in Thrombozyten die Bildung atherosklerotischer Plaques und die Ansammlung entzündlicher Leukozyten innerhalb der Gefäßläsionen deutlich fördert. Ein zugrundeliegender Mechanismus hierfür könnte die veränderte Freisetzung von löslichen Faktoren aus Thrombozyten sein, die *in vitro* die Adhäsion von Leukozyten an Endothelzellen begünstigten. Ein Faktor mit möglicherweise ursächlicher Beteiligung ist Angiopoetin-1: Das Glykoprotein wurde nach mechanischer Stimulation deutlich weniger sowohl aus murinen als auch humanen Thrombozyten mit beeinträchtigter sGC-Funktion ausgeschüttet, wohingegen Thrombozyten, die mit dem sGC-Stimulator BAY-747 behandelt wurden, erheblich mehr Angiopoetin-1 freisetzten. Die *In vivo*-Behandlung von atherosklerotischen Mäusen mit BAY-747 konnte umgekehrt das Fortschreiten der Atherosklerose in der Aorta verringern. Die Behandlung von KHK-Patienten mit sGC-Stimulatoren, insbesondere von Patienten mit einem individuell erhöhten genetischen Risiko, könnte daher eine neue, zusätzliche Strategie zur Eindämmung der erheblichen Bedrohung sein, die diese Erkrankung für unsere Gesellschaft darstellt.

List of Figures

List of Tables

Abbreviations

2-APB	2-aminoethoxydiphenyl borate
ADP	adenosine diphosphate
AEC	3-amino-9-ethylcarbazole
ANGPT1	angiopoietin-1
ANOVA	analysis of variance
APC	allophycocyanin
Apoe	gene encoding for apolipoprotein E
AU	arbitrary units
AUC	area under the curve
BAC	bacterial artificial chromosome
BCA	bicinchoninic acid
bp	base pairs
BSA	bovine serum albumin
BV	brilliant violet
CAD	coronary artery disease
cAMP	cyclic adenosine-3',5'-monophosphate
CCL	C-C motif ligand
CCT7	gene encoding for human chaperonin containing T-complex protein 1 subunit 7
CD	cluster of differentiation
CDK	cyclin-dependent kinase(s)
cGMP	cyclic guanosine-3',5'-monophosphate
Ct	cycle threshold
CXCL	C-X-C motif ligand
Cy7	cyanine 7
DMSO	dimethyl sulfoxide
DNA	deoxyribonucleic acid
DPBS	Dulbecco's phosphate-buffered saline
EC	endothelial cell(s)
EDTA	ethylenediaminetetraacetic acid
ELISA	enzyme-linked immunosorbent assay(s)
eNOS	endothelial NO-synthase

ERK	extracellular signal-regulated kinase(s)
FACS	fluorescence-activated cell separation
FSC	forward scatter
g	gram
g	gravitational acceleration
GAPDH	glyceraldehyde 3-phosphate dehydrogenase
GFP	green fluorescent protein
GTP	guanosine 5'-triphosphate
GUCY1A1/Gucy1a1	gene encoding for human/murine α_1-sGC
GUCY1B1/Gucy1b1	gene encoding for human/murine β_1-sGC
GWAS	genome-wide association study
h	hour(s)
HEPES	4-(2-hydroxyethyl)-1-piperazineethanesulfonic acid
HRP	horseradish peroxidase
IL	interleukin
IMDM	Iscove's Modified Dulbecco's Medium
IP_3-R	inositol 1,4,5-trisphosphate receptor
IRAG	IP_3R-associated cGMP-kinase substrate
Irag1	gene encoding for murine IRAG
kg	kilogram
l	liter(s)
LDL	low-density lipoprotein
Ldlr	gene encoding for the low-density lipoprotein receptor
LED	light-emitting diode
LIX	alternative name for: murine CXCL5
LoxP	locus of X(cross)-over in P1
Ly6C	lymphocyte antigen 6 complex, locus C1
M	mol/l
m	milli-
µ	micro-
MACS	magnet-activated cell separation
mAoEC	murine aortic endothelial cells
MAPK	p38α mitogen-activated protein kinase
MI	myocardial infarction

min	minute(s)
MK	megakaryocyte(s)
MLCP	myosin light-chain phosphatase
mRNA	messenger ribonucleic acid
NET	neutrophil extracellular traps
NK	natural killer cells
NO	nitric oxide
NOS3/*Nos3*	gene encoding for human/murine eNOS
ORO	oil red O
oxLDL	oxidized low-density lipoprotein
PAR4-AP	platelet-activated receptor 4 agonist peptide
PBMC	peripheral blood mononuclear cells
PBS	phosphate-buffered saline
PCR	polymerase chain reaction
PDE	phosphodiesterase
PE	phycoerythrin
PerCP/Cy5.5	Peridinin-chlorophyll-protein complex/cyanine 5.5
PF4	platelet factor 4
Pf4	gene encoding for mouse PF4
PKC	protein kinase C
PKG	protein kinase G
PPP	platelet-poor plasma
PRP	platelet-rich plasma
PVDF	polyvinylidene fluoride
qPCR	quantitative polymerase chain reaction
RBC	red blood cell
RBP4	retinol binding protein 4
RIPA	radioimmunoprecipitation assay
RNA	ribonucleic acid
ROS	reactive oxygen species
rpm	revolutions per minute
RPMI	Roswell Park Memorial Institute
RT	room temperature
s	second(s)

s.e.m.	standard error of mean
sGC	soluble guanylyl cyclase
SMC	vascular smooth muscle cell
SNP	sodium nitroprusside
SSC	side scatter
TIE2	tyrosine kinase with immunoglobulin-like and EGF-like domains 2
TPO	thrombopoietin
TREML1	triggering receptor expressed on myeloid cells like 1
V	Volt
VASP	vasodilator-stimulated phosphoprotein
VEGF	vascular endothelial growth factor
vs.	versus
vWF	von Willebrand factor
ZEB1	zinc finger E-box-binding homeobox 1

1 Introduction

1.1 Cardiovascular diseases and atherosclerosis

Cardiovascular diseases account for the majority of deaths worldwide (World Health Organisation, 2021). They comprise a class of disorders affecting the heart or blood vessels, *e.g.*, coronary artery disease (CAD) including myocardial infarction (MI), stroke, or peripheral artery disease. CAD is the most common cardiovascular disease, estimated at 197 million prevalent cases globally in 2019 (Roth et al., 2020). It is responsible for 45% of mortality in women and 39% of mortality in men in Europe (Timmis et al., 2022).

The underlying cause of CAD is atherosclerosis, a chronic inflammatory disease of large- and medium-sized arteries that supply the heart with oxygen-rich blood. It is characterized by the continuous accumulation of lipoproteins and inflammatory cells – morphologically perceptible as fatty streaks or, in later stages, atherosclerotic plaques – within the tunica intima, the inner layer of arteries (Libby, 2021).

Usually, the disease process initiates early in life and develops over several years without clinical symptoms appearing (Berenson et al., 1998; Raitakari et al., 2022) until the increasing stiffness and narrowing of the coronary arteries may become apparent, for example, in the form of chronic or acute coronary syndromes, presenting with chest pain due to insufficient oxygen supply to the heart muscle under exertion or at rest, respectively (Joshi & de Lemos, 2021). The most dreadful complication is observed in the event of rupture or erosion of plaques which can result in thrombotic occlusion of, *e.g.*, coronaries leading to MI (Anderson & Morrow, 2017) or cerebral arteries leading to ischemic stroke (Campbell & Khatri, 2020). Despite the high prevalence of CAD, the exact circumstances for the development of atherosclerosis (a process commonly referred to as atherogenesis) are not fully clarified. According to current understanding, however, it seems to be a fine interplay of genetic and lifestyle factors to cause this both menacing and common disease (Khera et al., 2016).

1.1.1 Atherogenesis

While the initial atherogenic stimulus is unknown, three factors have been identified to play a fundamental role in the development of atherosclerotic lesions: endothelial activation, lipoprotein

accumulation, and leukocyte ingress (Figure 1).

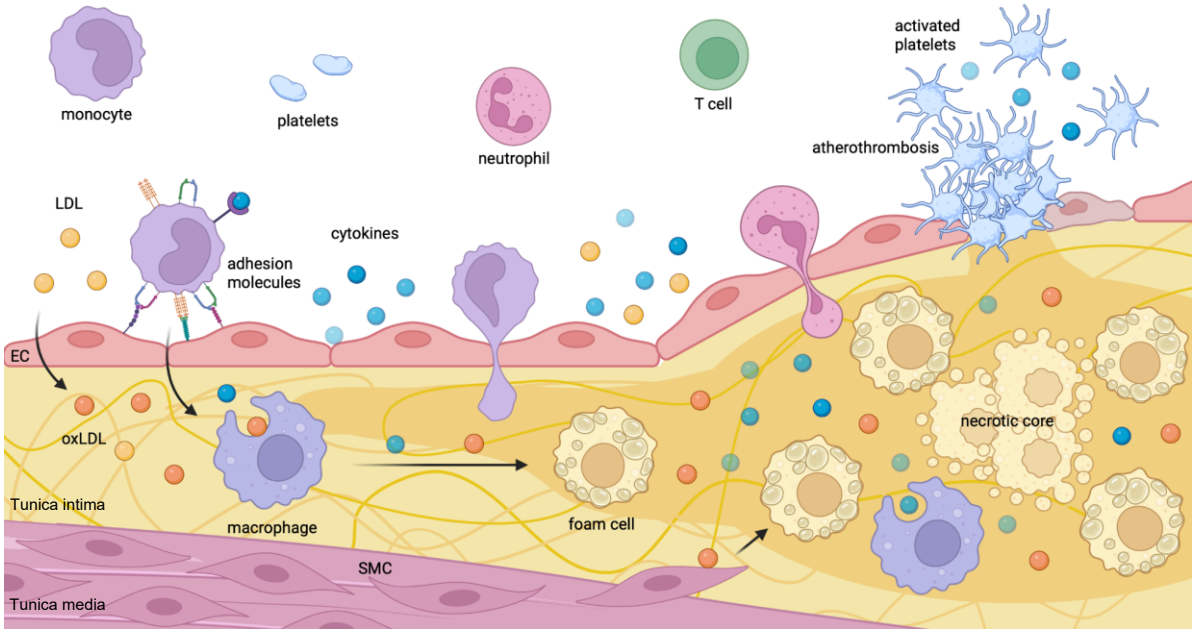

Figure 1 Atherosclerotic plaque formation and rupture. Accompanied by endothelial activation and lipid accumulation, leukocytes are recruited to the subendothelial intima of arteries via adhesion molecules. In the tissue, monocytes differentiate into macrophages and foam cells following lipoprotein particle uptake. Continuous foam cell formation and smooth muscle cell migration into the intima sustain a chronic inflammatory milieu that fosters constant plaque growth, with debris of dead cells accumulating in the necrotic core. Exposure of the inflammatory plaque content due to fibrous cap rupture or erosion triggers platelet activation and thrombus formation that can critically impede blood flow. Abbreviations: *EC*, endothelial cell; *LDL*, low-density lipoprotein; *oxLDL*, oxidized low-density lipoprotein; *SMC*, smooth muscle cell. Created with BioRender.com.

Endothelial cells (EC) are the innermost layer of vessels and serve as a physical barrier to the blood. In an inflammatory setting, though, they can act as gateways for leukocytes and other blood components by upregulating cell-surface adhesion molecules. In atherosclerosis, such endothelial activation is particularly mediated by i) inflammatory influxes such as modified low-density lipoprotein (LDL) and ii) disturbed flow (Marchini et al., 2021). Hyperlipidemia, and particularly a high level of plasma cholesterol which is transported in the blood by LDL, provokes the uptake of LDL via EC into the subendothelial space. There, under the influence of enzymes and reactive oxygen species (ROS), the particles are chemically modified to form highly inflammatory products such as oxidized LDL, and as such, trigger expression of adhesion molecules and release of pro-inflammatory cytokines by macrophages and EC (Poznyak et al., 2020). At the same time, disturbed flow, which especially occurs in branched or curved sites of vessels, stimulates ROS production and the expression of pro-inflammatory chemokines and adhesion molecules on EC by activating transcription (co)factors (Förstermann et al., 2017; Tzima et al., 2005). Also, the activity of the endogenous vasodilator nitric oxide (NO), which has broad anti-inflammatory properties, is regulated by shear stress (Zhou et al., 2014) and likewise leads to endothelial activation (Förstermann et al., 2017).

As a composite result of these stimuli, on the one hand, intima resident macrophages are activated, engulf modified LDL and expand by local proliferation, thus fueling lesion growth (Williams et al., 2020). On the other hand, blood leukocytes are triggered to locally ingress into the arterial intima – following a precise recruitment process of capture, rolling, firm arrest, crawling, and transmigration (Figure 2). There, these cells strongly contribute to an inflammatory milieu by releasing pro-inflammatory cytokines in a vicious and tightly intertwined cycle of EC activation, LDL uptake, and further accumulation of leukocytes.

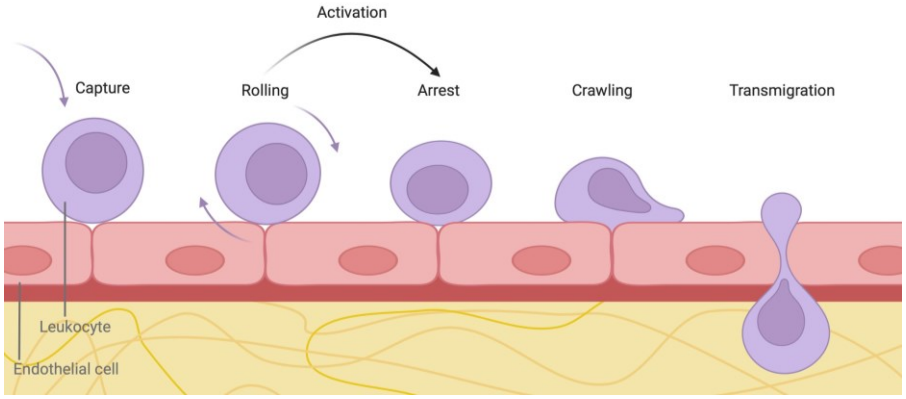

Figure 2 Leukocyte recruitment into atherosclerotic plaques. Leukocytes are recruited into atherosclerotic lesions following a precise scheme of capture, rolling, chemokine-triggered leukocyte activation leading to arrest, spreading, intravascular crawling, and transmigration. The process is mainly driven by endothelial adhesion molecules and chemokines that capture leukocytes via complementary molecules on their surface – with different adhesion molecules being important at different steps. Based on reference (Ley et al., 2007). Created with BioRender.com.

Among the invading leukocytes, monocytes play a pivotal role. There are two main subsets of monocytes in mice, inflammatory Ly6C^{high} and anti-inflammatory Ly6C^{low} cells. Although their exact correspondence to the human subsets is still a matter of debate (Ziegler-Heitbrock et al., 2010), it is commonly appreciated that murine Ly6C^{high} and Ly6C^{low} monocytes share fundamental properties with classical and nonclassical monocytes in humans, respectively. While Ly6C^{low} monocytes are typically patrolling the vessel in a potentially endothelium-protective manner (Quintar et al., 2017) but rarely transmigrate (Tacke et al., 2007), Ly6C^{high} monocytes are vastly recruited into atherosclerotic plaques (Gerhardt & Ley, 2015). In the tissue, they usually differentiate to macrophages in addition to their self-proliferating, tissue-resident counterparts and, attracted by modified LDL, turn into so-called foam cells after engulfing their lipophilic target (Gerrity, 1981). However, also vascular smooth muscle cells (SMC) are believed to be able to transform into foam cells and as such, might contribute to plaque growth in mice and men (Shankman et al., 2015). Despite the important role of foam cells in atherosclerosis, recent findings, though, suggest that it is rather the non-foamy macrophages that intensely promote the pro-inflammatory signaling within atherosclerotic plaques by releasing pro-inflammatory cytokines (Kim et al., 2018).

Also, neutrophils, which have long been regarded as mere bystanders of monocyte infiltration in atherosclerosis, emerged as important actors in atherogenesis. When activated, *e.g.*, by local chemokine gradients in the blood, they secrete granule proteins, chemokines, ROS, and proteases breaking the endothelial barrier, thus paving the way for leukocyte invasion (Silvestre-Roig et al., 2020). By depositing chemotactic proteins such as cathepsin G on the endothelium, they can directly stimulate monocyte recruitment (Ortega-Gomez et al., 2016). Neutrophils have also been shown to stimulate LDL oxidation, macrophage pro-inflammatory activity and foam cell formation (Delporte et al., 2014; Soehnlein et al., 2008). In advanced atherosclerotic lesions, they contribute to plaque destabilization by secreting neutrophil extracellular traps (NET), web-like structures composed of DNA and antimicrobial as well as cytotoxic proteins that strongly promote inflammation (Warnatsch et al., 2015).

Lastly, although the role of cells of the adaptive immune system in atherogenesis is not elucidated in detail, it is becoming increasingly clear that also T cells, a highly abundant population in human atherosclerotic plaques, contribute to atherosclerosis progression in various ways. Specifically, they are suspected to stimulate an autoimmune response against LDL peptides (Saigusa et al., 2020), shedding new light on atherosclerosis as a potential autoimmune disease.

1.1.2 Role of platelets in atherosclerosis

While the role of leukocytes in atherosclerosis is well established, the involvement of platelets – small cellular fragments circulating in large numbers within the blood – is just increasingly uncovered. Platelets are derived from megakaryocytes (MKs), giant cells residing in the bone marrow which continuously slough off large quantities of platelets, fully equipped with their proteome but without a nucleus, into the bloodstream (Patel et al., 2005). In a resting status, platelets are discoid-shaped, but can rapidly change their morphology upon activation and secrete a plethora of bioactive molecules from endogenous compartments. α-granules are the main protein storage compartment in platelets, containing over 300 distinct molecules including chemokines, growth factors, angiogenic and hemostatic mediators, proteases, and necrotic agents (Maynard et al., 2007), while dense granules store small molecules such as serotonin, adrenaline, Ca^{2+}, and ADP, and lysosomes specifically contain proteolytic enzymes (Pagel et al., 2017).

Platelets are typically activated by platelet agonists binding to dedicated surface receptors on their membrane. In hemostasis, exposed collagen from damaged vessels binds to platelets either directly or via endothelial or platelet-released von Willebrand factor (vWF), thereby stimulating

glycoprotein receptors, while soluble agonists, such as adenosine diphosphate (ADP), thromboxane A_2, and thrombin trigger platelet activation via G protein-coupled receptors (Davì & Patrono, 2007). All these receptors increase to varying degrees the cytosolic Ca^{2+} concentration followed by an actin-myosin-based contraction that supports both platelet activation and granule release (Rink & Sage, 1990; Varga-Szabo et al., 2009). Thereby, platelets undergo morphological changes by forming protrusions of their plasma membrane, thus increasing the platelet surface and supporting the release of granule factors into the extracellular space via the open canalicular system, a large intracellular tunneling network directly connected to the cell surface (Heijnen & Korporaal, 2017). Crucial for platelet aggregation is ultimately the transition of platelet surface integrin αIIbβ3 from its resting to an activated state, which allows crosslinking of platelets via fibrinogen and thrombus formation (Nieswandt et al., 2009).

The maintenance of hemostasis by clogging injured vessels for preventing blood loss is regarded as the main task of platelets. However, in the context of atherosclerosis, this life-saving function can be turned into a vicious threat by promoting excessive thrombosis up to subsequent occlusion of arteries. Thereby, platelets may be activated by collagen/vWF and tissue factor exposed at ruptured or eroded plaques and thrombus formation potentiated by proinflammatory cytokines and thrombogenic mediators, for instance, neutrophils undergoing NETosis (Libby et al., 2019). Yet, just in recent years, it has come apparent that platelets also contribute to atherosclerosis at a much earlier step in atherogenesis. In pro-atherosclerotic mice, they were observed to adhere to intact endothelium even before atherosclerotic lesions were manifest (Massberg et al., 2002). Potential causal factors for enhanced platelet reactivity in atherosclerosis are circulating lipoproteins, *e.g.*, oxidized lipids binding via platelet surface CD36 (Magwenzi et al., 2015; Podrez et al., 2007) or phospholipid products as generated under the influence of oxidative stress (Panigrahi et al., 2013). Also, disturbed flow increases platelet reactivity, particularly mediated by vWF which is conformationally activated upon shear stress (Rana et al., 2019). Subsequently, platelets express surface receptors such as P-selectin or CD40 ligand which were shown to initiate adhesion molecule expression and inflammatory chemokine release in EC, thus promoting local leukocyte recruitment (Burger & Wagner, 2003; Henn et al., 1998; May et al., 2002).

Another crucial function of platelets in atherosclerosis is their interaction with leukocytes. Endothelium-adherent platelets can form protrusions from their membrane in regions of high shear stress to activate rolling monocytes and neutrophils (Tersteeg et al., 2014). Additionally, platelets commonly aggregate with circulating monocytes and neutrophils (Li et al., 2000), a process primarily mediated by platelet P-selectin and CD40 ligand derived from α-granules upon

activation. Platelet leukocyte aggregate formation promotes leukocyte invasion into atherosclerotic lesions but also triggers foam cell formation and cytokine production in macrophages beyond the circulation (Badrnya et al., 2014; Barrett et al., 2019).

Apart from favoring leukocyte recruitment by direct leukocyte or EC contact, platelets also release a myriad of pro-atherogenic factors upon stimulation. One key factor is chemokine (C-C motif) ligand (CCL) 5 which is deposited on activated EC and significantly fosters monocyte and neutrophil recruitment by attracting leukocytes to atherosclerosis-prone regions of arteries (Schober et al., 2002; Veillard et al., 2004; von Hundelshausen et al., 2001). Also, platelet factor 4 (PF4), an important mediator in coagulation, is released in high abundancy from platelets and particularly induces pro-atherosclerotic functions in macrophages (Erbel et al., 2015; Gleissner et al., 2010). Further important platelet-derived chemokines are C-X-C motif ligand (CXCL) 12, which has been genome-wide significantly associated with CAD by genetic risk variants affecting its encoding gene (Samani et al., 2007), CXCL5, and CXCL16, but also matrix metalloproteinases 2 and 9, *e.g.*, which promote extracellular matrix degradation and thereby support leukocyte ingress into atherosclerotic plaques (Bakogiannis et al., 2019). Although platelets are incapable of *de novo* transcription, they are endowed with a specific repertoire of transcripts by their progenitors (Supernat et al., 2021). This allows also for the time-dependent synthesis of protein mediators such as interleukin (IL) 1β (Denis et al., 2005). Furthermore, a fairly recent finding is that platelets can also release microvesicles, containing a similar cargo to platelets themselves into the circulation, thus modulating inflammation distal from the site of their activation (Konkoth et al., 2021). This cargo may also include nucleic acids, particularly microRNAs, which have been found to target EC, thus affecting adhesion molecule expression or angiogenesis *in vitro* – with *in vivo* implications remaining to be explored (Coenen et al., 2021).

Strikingly and in contrast to their pro-atherogenic properties, platelets also emerged as essential components to maintain the integrity of the endothelium, thus impeding vascular leukocyte recruitment. Although these functions have yet to be studied in detail, discussed causal mechanisms include maintenance and promotion of EC growth particularly by releasing soluble factors such as adenine nucleotides, angiopoietin-1 (ANGPT1), platelet-derived growth factor, stromal cell-derived factor-1 or lipid mediators (Gros et al., 2014). Besides, they also contribute to inflammation-resolving processes, *e.g.*, by emitting prostaglandin E2, transforming growth factor β, or expressing C-type lectin-like receptor 2 which increase expression of anti-inflammatory factors in leukocytes and direct the cells towards a reparative phenotype (Ludwig et al., 2022).

To summarize, platelets contribute in a multifaceted and multidirected manner to both the

development and progression of atherosclerosis and atherothrombotic complications, as well as to its containment (Figure 3). This is in line with the plethora of pro-atherogenic, but also anti-inflammatory factors discovered within the platelet granule cargo (Maynard et al., 2007) which can, released into the circulation, affect a broad range of cell types even beyond the endothelium.

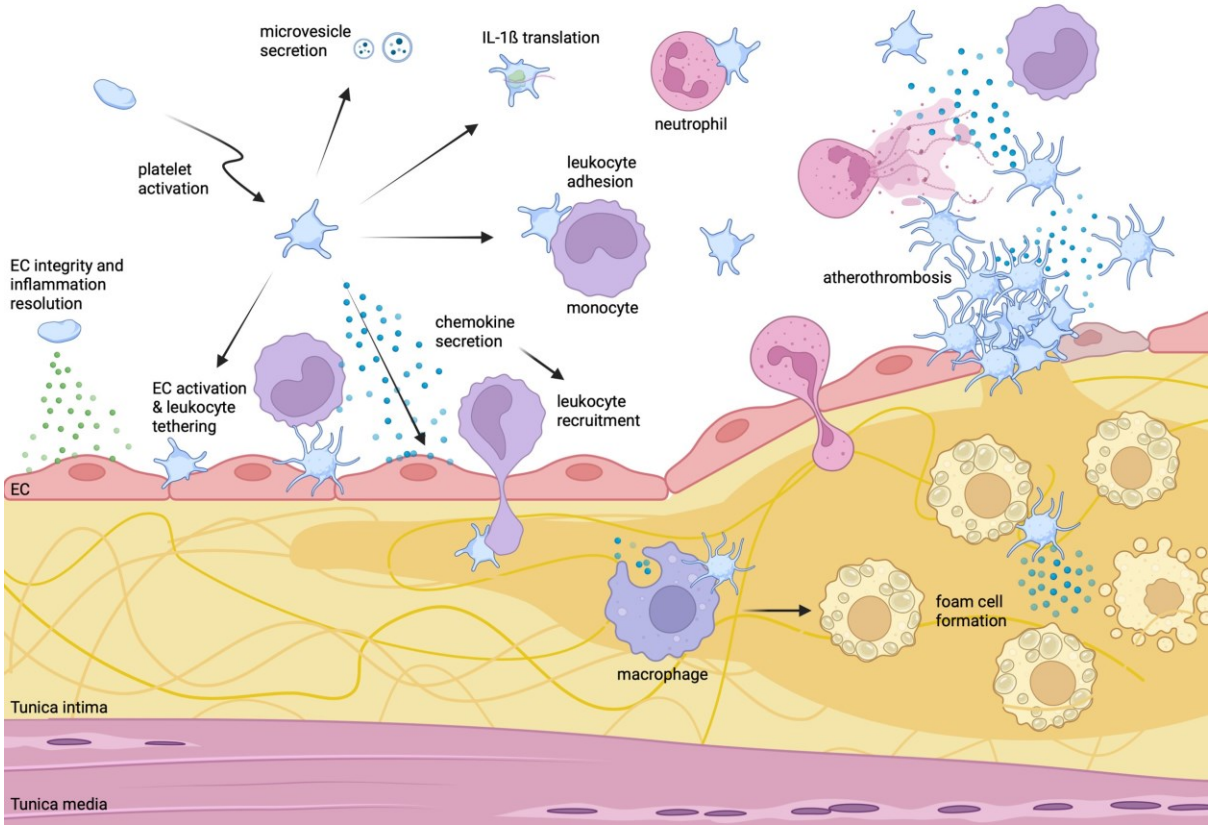

Figure 3 Role of platelets in atherosclerosis. a. Platelets are involved in early steps of atherogenesis. Upon stimulation, *e.g.*, triggered by hypercholesterolemia or shear forces, platelets facilitate leukocyte recruitment by depositing chemokines on the endothelium, binding to endothelial cells and capturing circulating leukocytes, or by directly binding and activating leukocytes in the circulation. Additionally, platelets can also synthesize IL-1β from progenitor mRNA stored in their cytoplasm upon activation or release microvesicles containing bioactive proteins or genetic material, thus triggering inflammatory actions beyond their local environment. Platelets were also shown to mediate macrophage activation and foam cell formation in the arterial wall. Still, platelets also carry a plethora of factors important for angiogenesis and inflammation resolution, thus fulfilling anti-inflammatory properties in atherosclerosis. **b**. In the acute event of plaque rupture or erosion, exposed collagen or vWF induces platelet aggregation and thrombus formation. This is accompanied by the secretion of various immunomodulatory granule components from platelets and the activation of neutrophils, which in turn contribute to platelet activation and thrombosis via NET formation. Abbreviations: *EC*, endothelial cell; *IL*, interleukin. Created with BioRender.com.

1.1.3 Risk factors for atherosclerosis

As elucidated above, hypercholesterolemia is a crucial risk factor for atherosclerosis development. Elevated levels of circulating lipoproteins, especially LDL, are indisputably linked to atherosclerosis (Borén et al., 2020) and therefore the main target of atherosclerosis prevention strategies today. However, also hypertension, smoking, diabetes mellitus, and obesity have long

been recognized as risk factors for the incidence of atherosclerosis, and interventions aimed at mitigating their hazard are among the holistic approaches targeting atherosclerosis progression, particularly in high-risk patients (Visseren et al., 2021). Yet, atherosclerosis-related diseases continue to present as the leading cause of death in Western countries (Timmis et al., 2022) and even though intensified lipid-lowering treatment strategies markedly reduce major cardiovascular events in treated individuals, a high residual risk for such events remains (Baigent et al., 2010; Ridker, 2017). Therefore, it has become clear that to fight atherosclerosis, broader therapeutic strategies are warranted.

A positive family history represents another important risk factor for atherosclerosis, but until 20 years ago, few genetic mutations causally involved in the disease were identified. Then, genome-wide association studies (GWAS) emerged as a novel tool to potentially expand the horizon of known factors causally involved in atherogenesis by comparing genome-spanning characteristic genetic variants between large groups of CAD patients and healthy individuals. As a result, today, more than 300 genomic variants significantly associated with CAD and MI risk have been revealed (for an overview see Chen & Schunkert, 2021). Importantly, many of the affected genes do not impact classical risk factors but pathways not previously linked to the pathophysiology of atherosclerosis. Among these recently associated players are several inflammation-related factors such as the IL-6 receptor (CARDIoGRAMplusC4D Consortium, 2013), platelet EC adhesion molecule (PECAM) 1 (Howson et al., 2017), or CXCL12 (Samani et al., 2007).

Another pathway brought into the cardiovascular research spotlight as a result of GWAS is the nitric oxide (NO)- cyclic guanosine-3',5'-monophosphate (cGMP) pathway. Strikingly, variants in several of its coding genes have been associated with CAD risk in recent years, rendering it a highly interesting target for further atherosclerosis-related research, as discussed in detail in the following.

1.2 Cardiovascular implications of sGC-signaling

1.2.1 The NO-sGC-cGMP pathway

NO is a gaseous molecule, in the vasculature mainly produced from EC through the action of the endothelial NO-synthase (eNOS). It has been identified several years ago as a central mediator of vasodilatation (Furchgott & Zawadzki, 1980; Ignarro et al., 1987). The soluble guanylyl cyclase (sGC) is the primary receptor for NO in cells and is mainly composed as a heterodimer of one α_1- and one β_1-subunit encoded by the genes *GUCY1A1* and *GUCY1B1*, respectively. Although also

α_2- and β_2-isoforms have been described, the $\alpha_1\beta_1$-heterodimer is regarded as the canonical sGC enzyme due to its high abundance and activity in human cells (for an overview see Wobst et al., 2018). sGC consists of four functionally different domains: An N-terminal heme-NO/oxygen (H-NOX) domain, a Per/Arnt/Sim (PAS) domain, a coiled-coil (CC) domain, and a C-terminal catalytic domain (CD) where guanosine 5'-triphosphate (GTP) is converted to cGMP (Figure 4). The binding of NO to the heme cofactor located in the β_1-sGC subunit induces conformational changes, thus catalyzing the enzymatic formation of the second messenger cGMP from GTP.

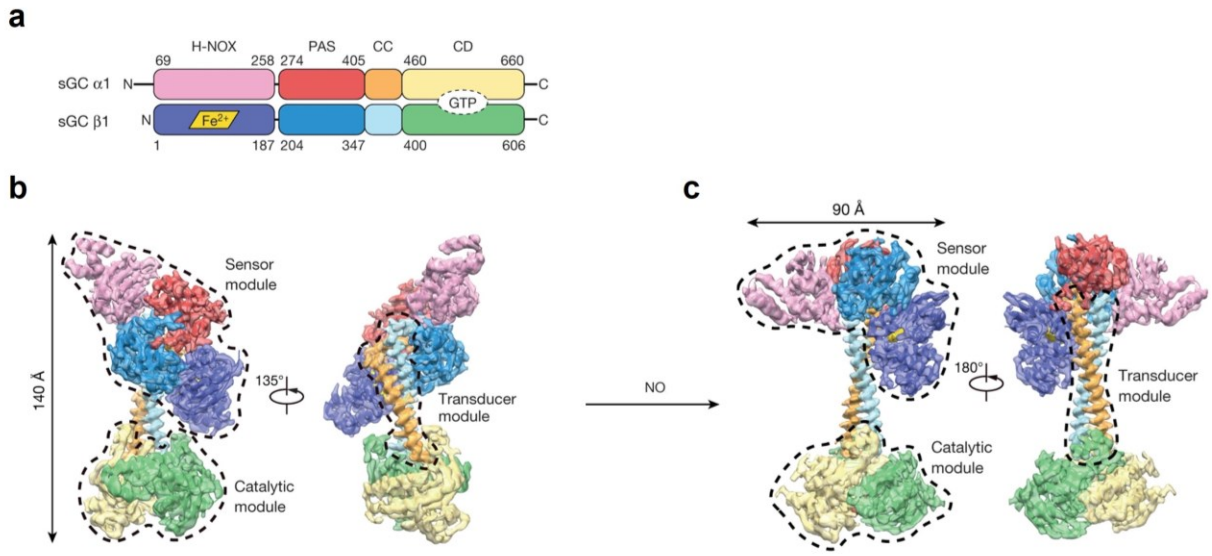

Figure 4 Protein structure of human sGC. a. Domain organization depicting the four modular domains and the heme and GTP substrate binding sites of human $\alpha_1\beta_1$-sGC. **b+c.** cryo-electron microscopy structure of the inactive **b**) and activated state **c**) during NO-triggered conformational changes. Abbreviations: *GTP*, guanosine 5'-triphosphate; *NO*, nitric oxide; *sGC*, soluble guanylyl cyclase; *H-NOX*, *PAS*, *CC*, and *CD* designate the protein domains, for more information see text. Reprinted with permission from Springer Nature: Figure 1a,c,d, and Figure 2a,b from reference (Kang et al., 2019), copyright © 2019.

Downstream effects of cGMP are mediated by cGMP-dependent protein kinases (PKG) and ion channels, while phosphodiesterases (PDE) catalyze its degradation (Schmidt et al., 1993). PKG I is regarded as the central regulator of the pathway's vascular effects, leading to SMC relaxation (Warner et al., 1994) and inhibition of platelet aggregation (Dangel et al., 2010). These effects are mainly mediated by inositol 1,4,5-trisphosphate receptor (IP_3-R)-associated cGMP-kinase substrate (IRAG), vasodilator-stimulated phosphoprotein (VASP), and myosin light-chain phosphatase (MLCP) (Francis et al., 2010).

IRAG forms a trimeric complex with PKG I and IP_3-R and reduces Ca^{2+} release from the endoplasmic reticulum. In SMC, this leads to decreased myosin light-chain phosphorylation and subsequent vasorelaxation, whereas in platelets, the decreasing intracellular Ca^{2+} concentration retards cytoskeletal rearrangement preceding platelet aggregation (Schlossmann & Desch, 2011).

Similarly, PKG I-mediated activation of MLCP promotes SMC dilation and subsequently, lowers blood pressure by disrupting actin-myosin light-chain binding and muscle contraction (Lincoln, 2007). VASP, by contrast, is a substrate of both cAMP- and cGMP-dependent protein kinases and is closely involved in integrin αIIbβ3 activation as a crucial step in platelet aggregation (Aszódi et al., 1999). The NO-sGC-cGMP pathway is schematically depicted in Figure 5.

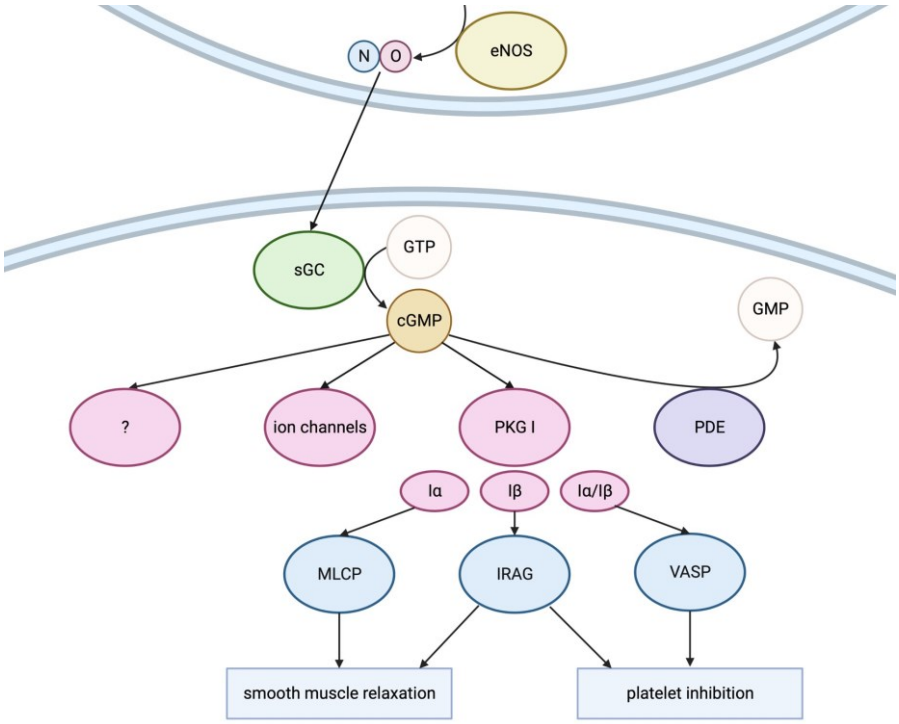

Figure 5 Overview of the NO-sGC-cGMP signaling pathway. The endothelial NO-synthase catalyzes the formation of NO which subsequently stimulates sGC in effector cells to form cGMP. The main downstream targets of cGMP are protein kinases, ion channels, and cGMP-degrading phosphodiesterases. The protein kinase G is a central regulator of sGC function by phosphorylating different effector proteins, thus promoting the pathway's most famous functions, smooth muscle cell relaxation and inhibition of platelet aggregation. Abbreviations: *cGMP*, cyclic guanosine-3',5'-monophosphate; *eNOS*, endothelial NO synthase; *GMP*, guanosine 5'-monophosphate; *GTP*, guanosine 5'-triphosphate; *IRAG*, inositol trisphosphate receptor-associated cGMP-kinase substrate, *MLCP*, myosin light-chain phosphatase; *NO*, nitric oxide; *PDE*, phosphodiesterase; *PKG*, protein kinase G; *sGC*, soluble guanylyl cyclase; *VASP*, vasodilator-stimulated phosphoprotein. Adapted with permission from John Wiley and Sons: Figure 1 from reference (Feil & Kemp-Harper, 2006). Created with BioRender.com.

1.2.2 sGC-signaling and atherosclerosis

Endothelial dysfunction is a hallmark of atherogenesis and is characterized by impaired vascular NO availability. It leads to several pro-atherogenic responses which ultimately promote endothelial adhesion molecule expression and leukocyte recruitment (Förstermann et al., 2017). Mechanistically, disturbed flow, LDL, and intimal leukocyte accumulation as central pillars of atherogenesis may all lead to endothelial dysfunction by either downregulating expression of the eNOS encoding gene *NOS3* (Davis et al., 2004), uncoupling eNOS leading to superoxide formation (Lu & Kassab, 2004), or decreasing eNOS accessibility (Blair et al., 1999), respectively.

Moreover, oxidative stress promotes the formation of heme-oxidized sGC, hence strongly impairing the sensitivity of sGC for NO (Stasch et al., 2006). In line, CAD patients display impaired sGC function in platelets compared with healthy controls (Ahrens et al., 2011). To conclude, atherogenesis is strongly correlated with decreased NO-sGC-cGMP signaling. Yet, genetic studies in recent years have made it increasingly clear that impaired NO signaling may not only be a consequence but also a potential causal factor in the development of atherosclerosis. Particularly, GWAS and exome-sequencing revealed several variants in NO-sGC pathway-related coding genes to be significantly associated with CAD or MI risk in humans; affecting eNOS (Nikpay, 2015), α_1-sGC (CARDIoGRAMplusC4D Consortium, 2013), PDE3 and 5 (Klarin et al., 2017; Nelson et al., 2017), and IRAG (Webb, 2017).

Common and rare risk variants impacting the pathway's two key enzymes eNOS and sGC were found to be associated with reduced sGC signaling or activity and *vice versa*, genetic predisposition to enhanced NO-sGC-signaling was related to reduced CAD risk (Emdin et al., 2018). Importantly, a subsequent mediation analysis suggested that these effects exceed those explained by their impact on vascular pressure alone (Emdin et al., 2018). The first direct genetic link between impaired sGC signaling and MI risk was uncovered in 2013 in a family severely affected by premature MI (Erdmann et al., 2013). As a causal factor, private mutations in both *GUCY1A1* and *CCT7*, a gene encoding for a modulator of sGC function, were identified. Collectively, these mutations strongly reduced both α_1- and β_1-sGC protein expression, particularly in platelets, and could be linked to accelerated thrombus formation as a potential cause of premature MI (Erdmann et al., 2013). In the same year, the risk variant G of the rs7692387 locus in *GUCY1A1* was genome-wide significantly associated with CAD risk (CARDIoGRAMplusC4D Consortium, 2013). Importantly, this variant is highly frequent in the European population, with only 4% homozygous carriers of the non-risk allele (CARDIoGRAMplusC4D Consortium, 2013; for an overview see Wobst et al., 2018). rs7692387 is located in an enhancer region, where the risk variant decreases the region's affinity for binding of the transcription factor ZEB1, leading to significantly less α_1-sGC expression in platelets and SMC of homozygous risk allele carriers (Kessler et al., 2017).

In line, lower *Nos3* or *Gucy1a1* expression were also associated with increased aortic atherosclerotic lesions (Bennett et al., 2015; Kuhlencordt et al., 2001) and platelet aggregation (Dangel et al., 2010) in rodents. Further studies linked enhanced sGC activity with reduced leucocyte adhesion to atherosclerotic plaques (Ahluwalia et al., 2004), neointimal formation (Sinnaeve et al., 2001), and atherosclerotic plaque formation (Tsou et al., 2014). Also, previous work from our group indicated larger atherosclerotic plaques (Figure 6) and increased vascular inflammation in mice particularly

lacking platelet sGC (Stroth, 2022). To summarize, genetic and mechanistic studies provide sharp evidence for a link between sGC signaling and atherosclerosis; yet, the underlying cellular and molecular mechanisms are poorly understood.

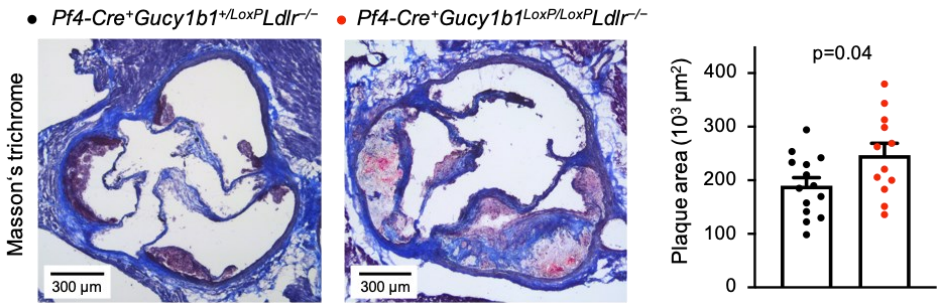

Figure 6 Atherosclerotic plaque formation in aortic roots of platelet sGC-deficient mice. Larger atherosclerotic plaques in aortic roots of *Pf4-Cre*$^{+}$*Gucy1b1*$^{LoxP/LoxP}$*Ldlr*$^{-/-}$ compared with *Pf4-Cre*$^{+}$ *Gucy1b1*$^{+/LoxP}$*Ldlr*$^{-/-}$ mice after 10 weeks of Western diet. Reprinted under the terms of the Creative Commons CC BY license: Figure 1a from reference (Mauersberger et al., 2022). The experiment was conducted by Marlène Stroth (Deutsches Herzzentrum München).

1.3 Therapeutic options to counter atherosclerosis

1.3.1 Anti-atherosclerotic therapies

Due to the important role of lipids in atherogenesis, the treatment of hyperlipidemia is currently the dominant strategy to lower atherosclerosis-related risk. Apart from lifestyle modifications, decreasing plasma LDL levels can be achieved pharmaceutically either by statins, which lower endogenous LDL production, by ezetimibe, which reduces intestinal absorption of dietary LDL, or by novel intensified therapeutics such as proprotein convertase subtilisin kexin (PCSK) 9 inhibitors which increase LDL receptor function. A 2010 meta-analysis calculated that with each 1 mM of LDL reduction, the annual rate of major vascular events can be reduced by 20% (Baigent et al., 2010). Despite their primary effect on LDL biosynthesis, several pleiotropic, *i.e.*, LDL-independent, effects of statins have been described in the literature. For instance, statins were reported to upregulate eNOS expression and activity and reduce SMC proliferation as well as platelet reactivity (Oesterle et al., 2017). Whether these effects indeed occur independently from LDL or are rather secondary effects of lower LDL plasma concentrations is, however, still a matter of debate (Yu & Liao, 2022).

Nonetheless, even intensified LDL lowering leaves a considerable residual risk for cardiovascular complications in atherosclerosis patients (Guedeney et al., 2019). In this regard, the role of triglyceride-rich lipoproteins has gained much attention in the last years as another lipid-related

risk factor in atherosclerosis (Nordestgaard, 2016). Indeed, the omega-3 fatty acid ester icosapent ethyl was reported to further decrease the risk of major cardiovascular events in patients treated with statins (Bhatt et al., 2019). However, this effect was accompanied by decreased plasma LDL concentrations in the treatment group and therefore not directly attributable to triglyceride-lowering alone. The triglyceride-lowering class of fibrates, on the other hand, could so far not confirm an additive beneficial effect on CAD risk in statin-treated patients – while notably not affecting LDL values (Virani, 2022). As other metabolic diseases such as hypertension or type 2 diabetes mellitus often coincide alongside atherosclerosis and are causally involved in its pathogenesis, affected patients are likewise treated with antihypertensive and antihyperglycemic agents (Visseren et al., 2021). Two classes of antidiabetic agents in particular, sodium-glucose cotransporter-2 (SGLT2) inhibitors and glucagon-like peptide-1 (GLP-1) receptor agonists, have attracted considerable attention in recent years as valuable agents for lowering cardiovascular mortality – making SGLT2 inhibitors a mainstay of heart failure treatment today, even in the absence of diabetes (Marx et al., 2022; Vaduganathan et al., 2022).

Additionally, anti-platelet drugs are commonly used in the context of secondary prevention of major cardiovascular events, for example in patients who have already undergone MI (Visseren et al., 2021). Two such frequently used agents, aspirin, and clopidogrel, inhibit platelet aggregation by blocking the formation of thromboxane A2 or by antagonizing the ADP-receptor $P2Y_{12}$, respectively. Still, due to the inherently increased risk of bleeding, anti-thrombotic agents are not equally suitable for all patients. As a matter of fact, clinical trials did not show a clear benefit of aspirin in primary prevention (for an overview see Ridker, 2018). Interestingly, a recent study found a direct association between the rs7692387 *GUCY1A1* risk variant and the benefit of aspirin in primary prevention: homozygous carriers of the G risk variant had less, whereas A allele carriers, in contrast, had even more cardiovascular events under aspirin (Hall et al., 2019). As a result, such tailored treatment strategies could also gain a foothold in future atherosclerosis therapy to better weigh the risk-benefit ratio of different treatment options for different subgroups or individuals – as already common, *e.g.*, in oncology (Ashley, 2016).

Nonetheless, despite major advances in treatment options, atherosclerosis-related diseases continue to be the world's major cause of death, including in high-income countries such as Germany (Statistisches Bundesamt (Destatis), 2021). One causal factor is certainly insufficient targeting of at-risk individuals through early treatment. Another could be that the existing treatment options are not comprehensive enough. Therefore, treatment options beyond currently available strategies are necessary to fight this global threat.

1.3.2 Outlook to potential future therapeutic targets

The broad involvement of immune cells in atherogenesis makes the potential of anti-inflammatory therapies a hot topic in the cardiovascular community (Libby, 2021). Indeed, several randomized controlled trials are underway or have been already conducted to investigate the effect of anti-inflammatory drugs in atherosclerotic patients. Canakinumab, an IL-1β neutralizing antibody, was the first solely anti-inflammatory drug to prove efficient for lowering the incidence of major cardiovascular events in high-risk CAD patients (Ridker et al., 2017). Due to a relatively poor cost-benefit ratio and higher risk of infections, canakinumab did not move into clinical use for atherosclerosis-related indications. However, another anti-inflammatory agent, colchicine, has only recently emerged as a suitable tool to reduce the risk of MI, stroke, or cardiovascular death in CAD patients by 25% in addition to standard care treatment (Fiolet et al., 2021). Consequently, colchicine has already entered European guidelines as an additional therapeutic option in high-risk patients and may herald a new era of anti-inflammatory drugs in CAD (Visseren et al., 2021).

The striking advent of the NO-sGC-pathway in the context of CAD risk in GWAS also makes this pathway a promising therapeutic target, all the more so because such treatment options are already available (Figure 7). Nitrates, a class of NO donors including nitroglycerine, are established

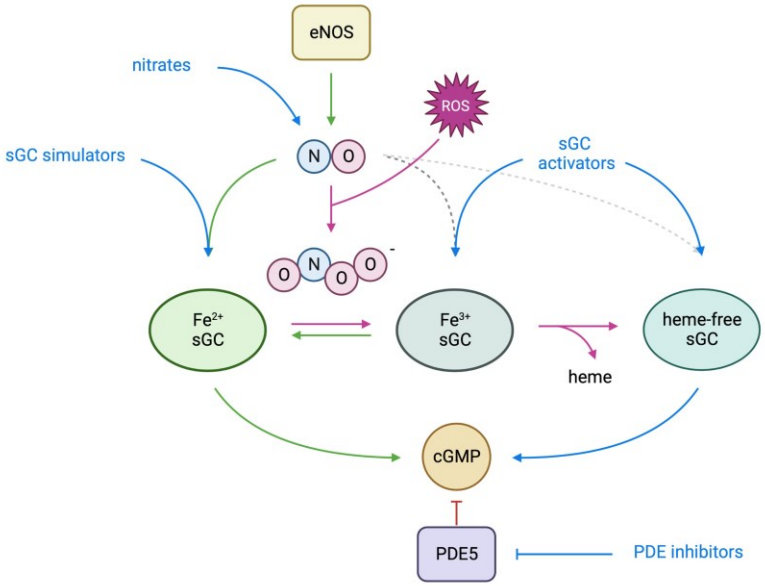

Figure 7 Mechanism of action of commonly used NO-sGC-cGMP pathway-targeting drugs. Endogenously produced or pharmaceutically delivered NO activates the reduced (Fe^{2+}), heme-containing form of sGC and promotes the subsequent formation of cGMP. sGC stimulators target Fe^{2+}-sGC and trigger cGMP formation by stabilizing the NO-heme complex. Oxidative stress, as involved in atherogenesis, enhances peroxynitrite formation from NO and oxidizes sGC (Fe^{3+}) which promotes loss of the heme group, rendering it unresponsive to NO. Such functionally inactive sGC can be targeted by sGC activators. Further downstream, inhibitors of phosphodiesterase isoforms 3 or 5 increase cGMP availability by inhibiting its enzymatic degradation. Abbreviations: *cGMP*, cyclic guanosine-3',5'-monophosphate; *eNOS*, endothelial NO synthase; *NO*, nitric oxide; *ONOO⁻*, peroxynitrite; *PDE*, phosphodiesterase; *ROS*, reactive oxygen species; *sGC*, soluble guanylyl cyclase. Based on reference (Sandner et al., 2021).

drugs for rapidly improving oxygen supply to the heart in acute angina pectoris attacks due to their local antihypertensive effect. The rapid decrease in effectiveness with frequent use known as nitrate tolerance, though, is a major drawback of these agents (Kraehling & Sessa, 2017). PDE inhibitors such as sildenafil target further down the pathway and increase cGMP bioavailability indirectly by inhibiting its degradation (for an overview see Dang et al., 2020). They are commonly used due to their beneficial effect on blood pressure for example in pulmonary hypertension (PH).

Just recently, the novel class of sGC stimulators and activators, which directly stimulate sGC, entered the market. Importantly, both groups can activate the enzyme independently of NO. sGC stimulators stabilize the active state of sGC in the absence or synergically in presence of NO (Figure 8), whereas sGC activators specifically target inactive oxidized or heme-free sGC (Liu et al., 2021).

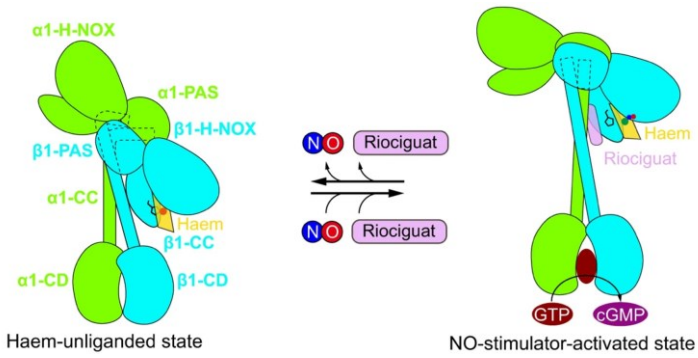

Figure 8 Schematic model of sGC activation following sGC stimulator binding. Conformational change from inactive to NO- and riociguat-bound state. The sGC stimulator riociguat binds to heme between H-NOX and CC domains and thereby stabilizes the active, cGMP-formation catalyzing conformation of α1β1-sGC. Reprinted under the terms of the Creative Commons CC BY license: Parts of Figure 5 from reference (Liu et al., 2021).

Inactive sGC particularly forms under the impact of oxidative stress, a risk factor strongly involved in atherogenesis, and promotes loss of the ferrous heme group bound to β_1-sGC (Sandner et al., 2021). Therefore, sGC activators might be interesting candidates to restore sGC activity in diseases critically implicating oxidative stress. Riociguat was the first sGC stimulator available for patients and is used for treating PH, whereas vericiguat was just approved for the treatment of heart failure with reduced ejection fraction (HFrEF) in 2021 (Armstrong et al., 2020). Further indications and substances are currently investigated in clinical trials.

1.4 Aim

Although efforts have been made worldwide to elucidate the exact circumstances that cause atherosclerotic plaques to form in arteries, only parts of the answer have been unraveled so far. With help of genome-wide association studies, the NO-sGC-cGMP-pathway has attracted attention among cardiovascular researchers, as several genetic variants impairing the functions of its mediators were associated with CAD in humans. Despite many important functions in various cell types, it is not completely clear how exactly impaired functions of this pathway promote CAD risk.

Two key vascular functions which are both transmitted via sGC activity are platelet inhibition and SMC relaxation leading to decreased blood pressure (Thoonen et al., 2015). In line, studies showed that both SMCs and platelets are crucially affected by CAD risk variants in sGC-encoding genes in humans (Kessler et al., 2017). However, it was indicated that the effect of sGC on atherosclerosis extends beyond the pathway's most famous function, lowering blood pressure (Emdin et al., 2018). This renders a role beyond SMC likely. Together with the fact that the involvement of platelets in atherosclerosis is increasingly but still not well understood, this led to the central aim of this thesis: To specifically investigate the role of sGC in platelets in the context of atherosclerosis.

Therefore, two different approaches were pursued: *in vivo* experiments on functionally sGC-deficient as well as atherosclerotic mice treated with an sGC stimulator, complemented by *in vitro* cell culture and platelet functional assays.

2 Materials

2.1 Mice

2.1.1 C57BL/6 J

C57BL/6 J represents the most widely used inbred wildtype (WT) strain and is commercially available via The Jackson Laboratory, Bar Harbor, ME, USA (#000664). Both female and male animals were used for experiments at 10 to 25 weeks of age, representing wildtype mice. All other mouse strains used were on the genetic background of C57BL/6 J.

2.1.2 Ldlr$^{-/-}$

Ldlr$^{-/-}$ mice were purchased from the Jackson Laboratory (full name: B6.129S7-*Ldlr*^{tm1Her}/J, #002207) and expanded for in-house breeding. By the insertion of a neomycin resistance cassette into exon 4, this strain is predicted to encode a truncated non-functional low-density lipoprotein receptor protein unable to bind LDL. The mice present with elevated serum cholesterol levels and develop atherosclerotic plaques when fed a high-cholesterol diet. Both female and male animals at 8 to 12 weeks of age were subjected to the experiments.

2.1.3 *Pf4-Cre^{+}Gucy1b1^{LoxP}* and *Pf4-Cre^{+}Gucy1b1^{LoxP}Ldlr$^{-/-}$*

Platelet-specific sGC knockout mice (*Pf4-Cre*$^{+}$*Gucy1b1*$^{LoxP/LoxP}$) were received from the group of Prof. Andreas Friebe (Universität Würzburg, Germany). *Pf4-Cre*$^{+}$*Gucy1b1*$^{+/LoxP}$ and *Pf4-Cre*$^{+}$*Gucy1b1*$^{LoxP/LoxP}$ mice were bred to receive control (*Pf4-Cre*$^{+}$*Gucy1b1*$^{+/LoxP}$) and platelet-specific sGC knockout (*Pf4-Cre*$^{+}$*Gucy1b1*$^{LoxP/LoxP}$) littermates used for *in vitro* experiments. For *in vivo* experiments, *Pf4-Cre*$^{+}$*Gucy1b1*^{LoxP} strains were crossbred with *Ldlr*$^{-/-}$ mice to generate a homozygous, pro-atherosclerotic *Ldlr*$^{-/-}$ background and mated to receive control (*Pf4-Cre*$^{+}$*Gucy1b1*$^{+/LoxP}$*Ldlr*$^{-/-}$) and platelet-specific sGC knockout (*Pf4-Cre*$^{+}$*Gucy1b1*$^{LoxP/LoxP}$*Ldlr*$^{-/-}$) animals. Male and female littermates at 8 to 12 weeks of age were included in the experiments.

2.1.4 Irag1-Pf4-Cre

Pf4-Cre^{+}*Irag1*$^{LoxP/LoxP}$ mice were received from the group of Prof. Jens Schlossmann (Universität

Regensburg, Germany). The strain was generated by *LoxP*-flanking of exon 3 in the *Irag1* gene (Desch et al., 2010) and crossbreeding with transgenic *Pf4-Cre*$^{+}$ mice as described above. Obtained platelet-specific *Irag1*-deficient mice were backcrossed on a C57BL/6 J background for ten generations.

2.1.5 UBC-GFP

C57BL/6- Tg(UBC-GFP)30 Scha/J mice, abbreviated UBC-GFP in the following, ubiquitously express the green fluorescent protein (GFP) and are therefore a useful tool for cell tracking analyses such as adoptive transfer experiments (3.1.3). The strain was purchased from The Jackson Laboratory (#004353) and expanded by in-house breeding. For experiments, both female and male animals were used at 10 to 12 weeks of age.

2.2 Primary cells

2.2.1 C57BL/6 primary aortic endothelial cells

Primary murine aortic endothelial cells (#C57-6052, mAoEC) were purchased from Cell Biologics (Chicago, IL, USA).

2.3 Antibodies

2.3.1 Flow cytometry antibodies

Table 1 Antibodies used for flow cytometry

Reactivity	Clone	Conjugate	Manufacturer	Catalogue #
mouse B220	RA3-6B2	PE	BioLegend	103208
mouse CD115	AFS98	BV510	BD Biosciences	750893
mouse CD11b	M1/70	APC-Cy7	BioLegend	101225
mouse CD45	30-F11	BV605	BioLegend	103140
mouse CD45.2	104	PerCP/Cy5.5	BioLegend	109827
mouse CD49b	DX5	PE	BioLegend	108908
mouse CD90.2	53-2.1	PE	BioLegend	140308
mouse F4/80	BM8	PE-Cy7	BioLegend	123113
mouse Ly6C	HK4.1	BV421	BioLegend	128031

mouse Ly6G	1A8	PE	BioLegend	127608
mouse NK-1.1	PK136	PE	BioLegend	108708
mouse Ter119	TER-119	PE	BioLegend	116208

2.3.2 Further antibodies

Table 2 Antibodies used for histology, Western blotting, and *in vivo* fluorescence

Reactivity	Clone	Conjugate	Manufacturer	Catalogue #
GAPDH	D16H11	-	Cell Signaling Technology	5174
mouse β_1-sGC	polyclonal	-	self-raised – kindly provided by Prof. Andreas Friebe (Würzburg)	
mouse CD115	AFS98	Biotin	BioLegend	135508
mouse CD11b	M1/70	-/PE	BioLegend	101201/101225
mouse Ly6C	HK1.4	AF488	BioLegend	128022
mouse Ly6G	1A8	PE	BioLegend	127608
mouse monocytes + macrophages	MOMA-2	-	Abcam	ab33451
rabbit IgG H&L	polyclonal	HRP	Cell Signaling Technology	7074
rat IgG H&L	polyclonal	HRP	Abcam	ab6734

2.4 Enzymes and growth factors

Table 3 Enzymes and growth factors used

Product	Manufacturer	Catalogue #	Headquarters
Collagenase from *Clostridium histolyticum*, Type I	Sigma-Aldrich/ Merck	C0130	St. Louis, MO, USA
Collagenase from *Clostridium histolyticum*, Type XI	Sigma-Aldrich/ Merck	C7657	St. Louis, MO, USA
Deoxyribonuclease I bovine	Sigma-Aldrich/ Merck	D5319	St. Louis, MO, USA
FBS Superior	Sigma-Aldrich/ Merck	S0615	St. Louis, MO, USA
Hyaluronidase from bovine testes, Type I-S	Sigma-Aldrich/ Merck	H3506	St. Louis, MO, USA
Phosphatase Inhibitor Cocktail (100X)	Thermo Fisher Scientific	78428	Waltham, MA, USA
Protease Inhibitor Cocktail (100X)	Thermo Fisher Scientific	87785	Waltham, MA, USA

SCF (mouse)	Miltenyi Biotec	130-101-693	Bergisch Gladbach, Germany
TPO (mouse)	Miltenyi Biotec	130-096-301	Bergisch Gladbach, Germany
Trypsin/EDTA (0.04% (w/v)/0.03% (w/v))	Promocell	C-41020	Heidelberg, Germany

2.5 Nucleic acids

2.5.1 TaqMan probes

Table 4 TaqMan probes used

Target	TaqMan probe	Dye
Gapdh	Mm99999915_g1	VIC-MGB_PL
Gucy1a1	Mm01220285_m1	FAM-MGB
Gucy1b1	Mm00516926_m1	FAM-MGB
Gucy1a2	Mm01253540_m1	FAM-MGB
Gucy1b2	Mm00555742_m1	FAM-MGB
rs7692387	C__29125113_10	FAM-MGB

2.5.2 Primers

Table 5 Sequences of primers used for genotyping of mice

Gene of interest	Target site	Primer sequence
Gucy1b1	(LoxP-)*Gucy1b1* (forward)	AAG ATG CTG AAG GGA AGG ATG C
	(LoxP-)*Gucy1b1* (reverse)	CAG CCC AAA GAA ACA AGA AGA AAG
Irag1	(LoxP-)*Irag1* Intron E2/3 (forward)	AAG GAG CTC CGT GTT TTG CA
	(LoxP-)*Irag1* Intron E2/3 (reverse)	CAC TAC GCC ATT CTG CTG CC
Pf4-Cre	Pf4-promoter (forward)	CCC ATA CAG CAC ACC TTT TG
	Cre (reverse)	TGC ACA GTC AGC AGG TT
Ldlr	*Ldlr* (forward)	TAT GCA TCC CCA GTC TTT GG
	Ldlr wildtype-specific (reverse)	CTA CCC AAC CAG CCC CTT AC
	Ldlr mutant-specific (reverse)	ATA GAT TCG CCC TTG TGT CC

The synthesis of the primers was commissioned to the company Eurofins Genomics (Ebersberg, Germany) and products diluted 1:10 to a concentration of 10 µM prior to use.

2.6 Chemicals and solutions

2.6.1 Chemicals

Table 6 Chemicals used

Chemical	Manufacturer	Catalogue #	Headquarters
2-APB	Tocris Bioscience	1224	Bristol, UK
2-Methylbutane	Sigma Aldrich/ Merck	277258	St. Louis, MO, USA
2-propanol ≥99.8%	Carl Roth	6752	Karlsruhe, Germany
Acetic acid, 100% Ph. Eur.	Carl Roth	6755.1	Karlsruhe, Germany
Acetone ≥99.5%	Sigma Aldrich/ Merck	179124	St. Louis, MO, USA
Adenosin-5-diphosphat (ADP)	mölab	0203001	Langenfeld, Germany
Agarose, LE	Biozym Scientific	840004	Hessisch Oldendorf, Germany
BAY-747	Bayer AG	n.a.	Wuppertal, Germany
BAY-826	Tocris Bioscience	6579	Bristol, UK
Bovine Serum Albumin (BSA)	Sigma Aldrich/ Merck	A2153	St. Louis, MO, USA
Chloroform	Sigma Aldrich/ Merck	372978	St. Louis, MO, USA
Dimethyl sulfoxide (DMSO)	Carl Roth	A994.1	Karlsruhe, Germany
Dinaciclib	Selleck Chemicals	S2768	Houston, TX, USA
Ethanol absolute	Merck Millipore	1070172511	Billerica, MA, USA
Ethanol denatured ≥96%	Carl Roth	T171	Karlsruhe, Germany
Ficoll-Paque PREMIUM	GE Healthcare	17-5442-02	Chicago, IL, USA
Hydrochloric acid (HCl), 6 M	Carl Roth	0281	Karlsruhe, Germany
Kaiser's glycerol gelatin	Carl Roth	6474.1	Karlsruhe, Germany
KT-5823	Santa Cruz Biotechnology	sc-3534	Dallas, TX, USA
MK-2206 hydrochloride	Selleck Chemicals	S1078	Houston, TX, USA
Nonfat dry milk powder	AppliChem	A0830	Darmstadt, Germany
O.C.T. Compound	Sakura Finetek	62550	Tokyo, Japan
Oil red O	Sigma Aldrich/ Merck	O0625	St. Louis, MO, USA
PAR4-AP (Ala-Tyr-Pro-Gly-	Sigma Aldrich/	A3227	St. Louis, MO, USA

Lys-Phe-NH_2)	Merck		
peqGREEN DNA/RNA dye	VWR International	732-3196	Radnor, PA, USA
Ravoxertinib (GDC-0994)	Selleck Chemicals	S7554	Houston, TX, USA
Ro 32-0432	Merck Millipore	557525	Burlington, MA, USA
Sodium chloride	AppliChem	A2942	Darmstadt, Germany
Sodium nitroprusside dihydrate (SNP)	Carl Roth	HN34.1	Karlsruhe, Germany
TRIS hydrochloride ≥99%	Carl Roth	9090	Karlsruhe, Germany
Tween 20	AppliChem	A1389	Darmstadt, Germany
U46619	Tocris Bioscience	1932	Bristol, UK
UltraPure Distilled Water (DNase/RNase Free)	Thermo Fisher Scientific	10977	Waltham, MA, USA
Xylene (isomers)	Carl Roth	4436.2	Karlsruhe, Germany
β-mercaptoethanol	Sigma Aldrich/ Merck	M3148	St. Louis, MO, USA

2.6.2 Buffers, solutions, and media

2.6.2.1 Commercial buffers and solutions

Table 7 Commercially available buffers and solutions used

Product	Manufacturer	Catalogue #	Headquarters
10X PBS, pH 7.4	Thermo Fisher Scientific	70011044	Waltham, MA, USA
10X RBC Lysis Buffer	BioLegend	420301	San Diego, CA, USA
10X RIPA	Cell Signaling Technology	9806S	Danvers, MA, USA
10X TRIS-borate-EDTA (TBE) buffer	Thermo Fisher Scientific	15581028	Waltham, MA, USA
10X Tris/Glycine/SDS	Bio-Rad	161-0772	Hercules, CA, USA
2X Laemmli Sample Buffer	Bio-Rad	1610737	Hercules, CA, USA
32% Formaldehyde Aqueous Solution	Electron Microscopy Sciences	15714	Hatfield, PA, USA
6X Gel Loading Dye	New England Biolabs	B7024S	Ipswich, MA, USA
AEC Substrate	Abcam	ab64252	Cambridge, UK
Bouin's solution	Sigma Aldrich/ Merck	HT10132	St. Louis, MO, USA
Buffer RLT Plus	QIAGEN	1053393	Hilden, Germany

Collagen (horse tendon), 100 µg/ml	mölab	0203009	Langenfeld, Germany
Color Prestained Protein Standard, Broad Range (10-250 kDa)	New England Biolabs	P7712	Ipswich, MA, USA
DPBS (without Ca^{2+}, Mg^{2+})	Thermo Fisher Scientific	14190144	Waltham, MA, USA
Ethylenediaminetetraacetic acid (EDTA) disodium salt solution (0.5 M)	Sigma-Aldrich/ Merck	E7889	St. Louis, MO, USA
Haematoxylin (Gill II)	Merck Millipore	1051752500	Darmstadt, Germany
Heparin sodium (25,000 U/5 ml)	Panpharma	PZN: 16200037	Luitré, France
HEPES solution (1 M)	Sigma-Aldrich/ Merck	83264	St. Louis, MO, USA
M-PER Mammalian Protein Extraction Reagent	Thermo Fisher Scientific	78503	Waltham, MA, USA
Mountex	MEDITE	41-4021	Burgdorf, Germany
Normal Rabbit Serum Blocking Solution	Vector Laboratories	S5000	Newark, CA, USA
Trypan Blue Solution 0.4%	Sigma-Aldrich/ Merck	93595	St. Louis, MO, USA
VX-702 solution (10 mM in DMSO)	Selleck Chemicals	S6005	Houston, TX, USA

2.6.2.2 General buffers and solutions

1X phosphate buffered saline (PBS)

100 ml	10X PBS
ad 1000 ml	Millipore water

containing a final concentration of 1.1 mM KH_2PO_4, 0.16 M NaCl, 2.97 mM Na_2HPO_4, pH 7.4; stored at room temperature (RT) for up to two weeks

1X red blood cell (RBC) lysis buffer

10 ml	10X RBC lysis buffer
ad 100 ml	Millipore water

containing ammonium chloride, potassium carbonate, EDTA at unpublished concentrations, pH 7.1-7.4; stored at RT, prepared anew each day

1X radioimmunoprecipitation assay (RIPA) buffer

2 ml	10X RIPA
ad 20 ml	Millipore water

containing a final concentration of 20 mM Tris-HCl (pH 7.5), 150 mM NaCl, 1 mM Na_2EDTA, 1

mM EGTA, 1% NP-40, 1% sodium deoxycholate, 2.5 mM sodium pyrophosphate, 1 mM beta-glycerophosphate, 1 mM Na_3VO_4, 1 µg/ml leupeptin; aliquoted and stored at -20 °C

M-PER lysis buffer

50 µl	Protease Inhibitor Cocktail
50 µl	Phosphatase Inhibitor Cocktail
ad 5 ml	M-PER extraction reagent

Prepared freshly prior to use, stored at 4°C

1X TBE buffer

100 ml	10X TRIS-borate-EDTA (TBE) buffer
ad 1000 ml	Millipore water

containing a final concentration of 0.1 M TRIS, 90 mM boric acid, 1 mM EDTA, pH 8.3; stored at RT

70% (v/v) ethanol

35 ml	Ethanol absolute
ad 50 ml	UltraPure Distilled Water

prepared under DNAse/RNase-free conditions, stored at RT

2.6.2.3 Cell isolation solutions

MACS buffer

5 g	Bovine Serum Albumin (BSA)
4 ml	Ethylenediaminetetraacetic acid (EDTA) disodium salt solution (0.5 M)
ad 1000 ml	1X PBS (see 2.6.2.2)

containing a final concentration of 5 mg/ml BSA, 2 mM EDTA, 1 mM KH_2PO_4, 0.16 M NaCl, 2.97 mM Na_2HPO_4, pH 7.4; sterile filtered and stored at 4°C, prepared anew for each experiment

Collagenase I stock solution

10,000 U	Collagenase Type I
1 ml	DPBS

aliquoted and stored at -20°C

Collagenase XI stock solution

12,500 U	Collagenase Type XI
1 ml	DPBS

aliquoted and stored at -20°C

Hyaluronidase stock solution

12,000 U	Hyaluronidase Type I-S
1 ml	DPBS

aliquoted and stored at -20°C

2.6.2.4 Flow cytometry buffers and solutions

FACS buffer

5 g	Bovine Serum Albumin (BSA)
ad 1000 ml	1X PBS (see 2.6.2.2)

containing a final concentration of 5 mg/ml BSA, 1 mM KH_2PO_4, 0.16 M NaCl, 2.97 mM Na_2HPO_4, pH 7.4; stored at 4°C, prepared anew for each experiment

2.6.2.5 Histology solutions

4% formaldehyde solution

12.5 ml	32% Formaldehyde Solution
ad 100 ml	1X PBS (see 2.6.2.2)

stored at 4°C for up to two weeks

10% rabbit serum blocking solution

10 ml	Normal Rabbit Serum Blocking Solution
0.5 g	Bovine serum albumin
ad 100 ml	1X PBS (see 2.6.2.2)

stored at 4°C for up to three days

Oil red O stock solution

0.5 g	Oil red O
100 ml	2-propanol

Filtered through filter paper and stored at RT

2.6.2.6 In vitro treatment solutions

50 U/ml heparin

10 µl	Heparin sodium (25,000 U/5 ml)
ad 1000 µl	DPBS

stored at RT, prepared anew shortly before each experiment

BAY-747 stock solution

15 mg	BAY-747
200 µl	DMSO

stored at 4°C, prepared anew weekly

SNP stock solution

30 mg	sodium nitroprusside (SNP)
500 µl	DMSO

vortexed until fully dissolved, stored at RT, prepared anew for each experiment

ADP stock solution

42.72 mg (1 vial)	Adenosine diphosphate (ADP)
500 µl	UltraPure Distilled Water

stored at 4°C, prepared anew each month

PAR4-AP stock solution

1 mg	PAR4-AP
500 µl	UltraPure Distilled Water

aliquoted and stored at -20°C

U46619 stock solution

1 mg	U46619
100 µl	UltraPure Distilled Water

aliquoted and stored at -20°C

2-APB stock solution

10 mg	2-APB
888 µl	DMSO

aliquoted and stored at -20°C

Ro 32-0432 stock solution

1 mg	Ro 32-0432
409 µl	DMSO

aliquoted and stored at -20°C

KT-5823 stock solution

100 µg	KT-5823
40.4 µl	DMSO

aliquoted and stored at -20°C

Dinaciclib stock solution

5 mg	Dinaciclib
252 µl	DMSO

aliquoted and stored at -20°C

MK-2206 stock solution

5 mg	MK-2206
208 µl	DMSO

aliquoted and stored at -20°C

Ravoxertinib stock solution

5 mg	Ravoxertinib
227 µl	DMSO

aliquoted and stored at -20°C

BAY-826 stock solution

5 mg	BAY-826
88,8 µl	DMSO

aliquoted and stored at -20°C

2.6.2.7 Western blotting solutions

2X Laemmli buffer

50 µl	β-mercaptoethanol
950 µl	2X Laemmli

containing 65.8 mM Tris-HCl, pH 6.8, 26.3 g/ml glycerol, 2.1% (v/v) SDS, 0.01% bromophenol blue, 710 mM β-mercaptoethanol; stored at -20 °C

1X running buffer

100 ml	10X Tri/Glycine/SDS
ad 1000 ml	Millipore water

containing 25 mM Tris, 192 mM glycine, 0.1% SDS, pH 8.3; stored at RT

1X PBS-T

100 ml	10X PBS
2 ml	Tween 20
ad 1000 ml	Millipore water

containing a final concentration of 1 mM KH_2PO_4, 0.16 M NaCl, 2.97 mM Na_2HPO_4, 0.2% v/v Tween 20, pH 7.4; stored at RT

25/50 mg/ml milk in PBS

2.5/5 g	nonfat dry milk powder
ad 100 ml	1X PBS (2.6.2.2)

stored at 4 °C for up to two days

2.6.2.8 Media and cell culture solutions

Table 8 Commercially available media and cell culture solutions used

Product	Manufacturer	Catalogue #	Headquarters
Complete Mouse Endothelial Cell Medium /w Kit	CellBiologics	M1168	Chicago, IL, USA
DPBS (without Ca^{2+}, Mg^{2+})	Thermo Fisher Scientific	14190144	Waltham, MA, USA
Gelatin-Based Coating Solution	CellBiologics	6950	Chicago, IL, USA
HEPES buffered saline solution	Promocell	C-40020	Heidelberg, Germany
IMDM + GlutaMAX supplement	Thermo Fisher Scientific	31980030	Waltham, MA, USA
Penicillin-Streptomycin (5,000 U/ml)	Thermo Fisher Scientific	15070063	Waltham, MA, USA
RPMI 1640 Medium (ATCC-Modification)	Thermo Fisher Scientific	A1049101	Waltham, MA, USA

kept under sterile conditions, stored at 4°C for up to four weeks

MK isolation medium

50 ml	FBS Superior
5 ml	Penicillin-Streptomycin
ad 500 ml	IMDM, GlutaMAX

prepared under sterile conditions, stored at 4°C for up to four weeks

MK growth medium

50 ml	FBS Superior
5 ml	Penicillin-Streptomycin
200 µl	0.5 mg/ml TPO solution in UltraPure Distilled Water
100 µl	0.1 mg/ml SCF solution in UltraPure Distilled Water
ad 500 ml	IMDM, GlutaMAX

containing 200 ng/ml TPO and 20 ng/ml SCF, prepared under sterile conditions, stored at 4°C for up to four weeks

2.7 Commercially available kits

Table 9 Commercially available kits used

Product	Manufacturer	Catalogue #	Headquarters
Adrenaline High Sensitive ELISA	DLD Diagnostika	EA632	Hamburg, Germany
blackPREP Rodent Tail DNA Kit	IST Innuscreen	845-BP-0010250	Berlin, Germany
CytoSelect Leukocyte-Endothelium Adhesion Assay	Cell Biolabs	CBA-210	San Diego, CA, USA
High Capacity RNA-to-cDNA kit	Thermo Fisher Scientific	4388950	Waltham, MA, USA
Human Angiopoietin-1 Quantikine ELISA Kit	R&D Systems	DANG10	Minneapolis, MN, USA
KAPA2G Fast HotStart Genotyping PCR Mix	Kapa Biosystems/ Roche	KK5621	Wilmington, MA, USA
Mouse Angiopoietin-1 PicoKine ELISA Kit	Boster Biological Technology	BOS-EK1296	Pleasanton, CA, USA
Mouse CXCL15 ELISA Kit	Abcam	ab193720	Cambridge, UK
Mouse CXCL4/PF4 Quantikine ELISA Kit	R&D Systems	MCX400	Minneapolis, MN, USA
Mouse CXCL7 / PBP ELISA Kit	Abcam	ab236713	Cambridge, UK
Mouse Endostatin ELISA Kit	Abcam	ab263894	Cambridge, UK
Mouse GRO gamma ELISA Kit (CXCL3)	Abcam	ab272191	Cambridge, UK

Mouse LIX Quantikine ELISA Kit	R&D Systems	MX000	Minneapolis, MN, USA
Mouse RBP4 Quantikine ELISA Kit	R&D Systems	MRBP40	Minneapolis, MN, USA
Mouse sP-Selectin/CD62P Quantikine ELISA Kit	R&D Systems	MPS00	Minneapolis, MN, USA
Mouse TREML1 PicoKine ELISA Kit	Boster Biological Technology	BOS-EK1522	Pleasanton, CA, USA
Mouse VEGF ELISA Kit	Abcam	ab209882	Cambridge, UK
Pierce BCA Protein Assay Kit	Thermo Fisher Scientific	23225	Waltham, MA, USA
Pierce Coomassie Plus (Bradford) Assay Kit	Thermo Fisher Scientific	23236	Waltham, MA, USA
Proteome Profiler Mouse XL Cytokine Array	R&D Systems	ARY028	Minneapolis, MN, USA
Puregene Blood Kit	QIAGEN	158489	Hilden, Germany
RNeasy Plus Mini Kit	QIAGEN	74139	Hilden, Germany
Serotonin ELISA Kit	Abcam	ab133053	Cambridge, UK
SuperSignal West Dura Extended Duration Substrate	Thermo Fisher Scientific	34075	Waltham, MA, USA
TaqMan Fast Universal PCR Master Mix (2X)	Thermo Fisher Scientific	4364103	Waltham, MA, USA
TaqMan Universal Master Mix II, no UNG	Thermo Fisher Scientific	4440040	Waltham, MA, USA
Trichrome Stain (Masson) Kit	Sigma Aldrich/ Merck	HT15	St. Louis, MO, USA
Weigert's Iron Hematoxylin Solution	Sigma Aldrich/ Merck	HT1079	St. Louis, MO, USA

2.8 Consumables

Table 10 Special consumables used

Consumable	Manufacturer	Catalogue #	Headquarters
4–20% Mini PROTEAN TGX™ Precast Protein Gels, 10-well	Bio Rad	4561094	Hercules, CA, USA
40 µm cell strainer	Corning	352340	Corning, NY, USA
70 µm pluriStrainer mini	pluriSelect Life Science	43-10070-40	Leipzig, Germany
Anti-PE MicroBeads	Miltenyi Biotec	130-048-801	Bergisch Gladbach, Germany
Biotin-Dynabeads	Thermo Fisher Scientific	11047	Waltham, MA, USA

CS&T Research Beads	BD Biosciences	655050	San Jose, CA, USA
Hard and Soft Tissue Omni Tip Plastic Homogenizing Probes	Omni International	32750H/ 32750	Kennesaw, GA, USA
Heparin-coated micro capillaries	Brand	749311	Wertheim, Germany
LS columns	Miltenyi Biotec	130-042-401	Bergisch Gladbach, Germany
MicroAmp fast optical 96 well reaction plate, 0.1 ml	Thermo Fisher Scientific	4346907	Waltham, MA, USA
Microvette 500 K3 EDTA, 500 µl	Sarstedt	20.1341	Nümbrecht, Germany
Minutien Pins	Fine Science Tools	26002-20	Foster City, CA, USA
Phase Lock Gel Heavy 1.5 ml vials	5PRIME	2302810	Hilden, Germany
Pipette tips for aggregometry	möLab	0303032	Langenfeld, Germany
S-Monovette Hirudin, 1.6 ml	Sarstedt	04.1959.001	Nümbrecht, Germany
S-Monovette K3 EDTA, 9 ml	Sarstedt	02.1066.001	Nümbrecht, Germany
Ser/Thr Kinase array	PamGene International	PamChip	's-Hertogenbosch, the Netherlands
Stir bars (micro)	möLab	0403013	Langenfeld, Germany
Streptavidin MicroBeads	Miltenyi Biotec	130-048-101	Bergisch Gladbach, Germany
SuperFrost Plus microscope slides	Menzel	J1800AMNZ	Braunschweig, Germany
Test tubes – micro (7.25 x 55 mm)	möLab	0303014	Langenfeld, Germany
UltraComp eBeads	Thermo Fisher Scientific	01-2222-42	Waltham, MA, USA
Whatman filter paper grade 1	Cytiva	1001-125	Marlborough, MA, USS

2.9 Devices and utensils

Table 11 Devices and utensils used

Device	Manufacturer	Type	Headquarters
Automated hematology analyzer	Sysmex	XP-300	Kobe, Japan
Benchtop centrifuge	Eppendorf	Centrifuge 5425 R	Hamburg, Germany
Biomolecular imager	GE Healthcare	Amersham ImageQuant 800	Chicago, IL, USA
CO_2 incubator	Thermo Fisher	Heracell VIOS 160i	Waltham, MA, USA

Cryostat	Leica Biosystems	CM3050 S	Wetzlar, Germany
Digital microscope cameras	Leica Microsystems	DFC450 C	Wetzlar, Germany
	Carl Zeiss	Axiocam ERc 5s	Oberkochen, Germany
Electron multiplier CCD camera	Hamamatsu Photonics	9100-02	Hamamatsu, Japan
Electrophoresis power supply	Consort	EV215	Turnhout, Belgium
Flow cytometer	BD Biosciences	LSRFortessa	San Jose, CA, USA
Fluorescence microscopes	Olympus	BX51	Tokyo, Japan
	Leica	DMRB	Wetzlar, Germany
Hemocytometer	Brand	717805	Wertheim, Germany
Kinase array station	Pam Gene International	PamStation	's-Hertogenbosch, the Netherlands
Large centrifuge	Thermo Fisher Scientific	Heraeus Megafuge 16R	Waltham, MA, USA
Microtiter shaker	IKA-Werke	MTS 4	Staufen, Germany
Millipore water system	Merck Millipore	Milli-Q Reference	Burlington, MA, USA
Omni Tissue Homogenizer	Omni International	TH220	Kennesaw, GA, USA
Orbital shaker	ELMI	Shaker S4	Riga, Latvia
Plate reader	Tecan	Infinite M200 PRO	Männedorf, Switzerland
Platelet aggregation profiler	Bio/Data	PAP-8 v2.0	Horsham, PA, USA
QuadroMACS Separator	Miltenyi Biotec	130-090-976	Bergisch Gladbach, Germany
Real-time PCR system	Thermo Fisher Scientific	Applied Biosystems ViiA 7 Real-Time PCR System	Waltham, MA, USA
Roller mixer	Bibby Sterilin	Stuart SRT9D	Stone, UK
Semi-dry protein transfer system	Bio-Rad	Trans-Blot Turbo	Hercules, CA, USA
Stereomicroscope	Carl Zeiss	Stemi 2000-C	Oberkochen, Germany
Thermal cycler	Thermo Fisher Scientific	Applied Biosystems Veriti, 4375305	Waltham, MA, USA
Thermal cycler	Thermo Fisher Scientific	Applied Biosystems Veriti Thermal Cycler, 96-Well	Waltham, MA, USA
Thermoshaker	Biosan	TS-100 C	Riga, Latvia
Ultrasonic bath	Merck Eurolab	Qualilab USR 9	Bruchsal, Germany

Spring Scissors Vannas-Tübingen	Fine Science Tools	15003-08	Foster City, CA, USA
Vertical gel electrophoresis system	Bio-Rad	Mini-PROTEAN Tetra cell	Hercules, CA, USA

2.10 Software

Table 12 Software used

Software	Distributor	Headquarters
BioNavigator (version 6.3)	PamGene International	's-Hertogenbosch, the Netherlands
FACS Diva software (version 8.0.1)	BD Biosciences	San Jose, CA, USA
FlowJo (version 9.9.6)	Tree Star	Ashland, OR, USA
GraphPad Prism (version 9.4.1)	GraphPad Software	San Diego, CA, USA
ImageJ2 (version 2.3.0)	National Institutes of Health	Bethesda, MD, USA
ImageQuant LAS TL (version 8.1)	Leica Microsystems	Wetzlar, Germany
LAS (version 4.5)	Leica Microsystems	Wetzlar, Germany
PAP-8E software (version 1.0.8)	Bio/Data	Horsham, PA, USA
TaqMan Genotyper software (version 1.3)	Thermo Fisher Scientific	Waltham, MA, USA
Tecan i-control 2.0 (version 3.9.1.0)	Tecan	Männedorf, Switzerland
ViiA 7 software (version 1.2.2)	Thermo Fisher Scientific	Waltham, MA, USA
ZEN 2.3 (blue, version 2.3.69.1000)	Carl Zeiss	Oberkochen, Germany

3 Methods

3.1 Murine models

The complexity and only partially elucidated pathogenesis of atherosclerosis require the use of animal models for many scientific questions. Due to the rapid reproduction cycle, availability of genetic manipulation, and quick development of atherosclerotic lesions under pro-atherosclerotic conditions, mice are the most widely used animal model in atherosclerosis research. Sharing about 95% of their protein-coding genes with humans, also the conservation of pathways associated with atherosclerosis between both species is highly significant (for an overview see von Scheidt et al., 2017).

3.1.1 Selection of strains

Since the sGC in platelets consists of one α_1- and one β_1-subunit which are encoded by the genes *Gucy1a1* and *Gucy1b1*, respectively, a functional knockout of sGC can be achieved by genetic depletion of either of the two genes. In this project, mice with impaired *Gucy1b1* expression were used, since in contrast to ubiquitous α_1-depletion (Mergia et al., 2006), loss of the β_1-subunit is not reported to be functionally compensated by other β-subunits.

To deplete sGC-mediated functions specifically in platelets, *Pf4-Cre*$^{+}$*Gucy1b1*$^{LoxP/LoxP}$ mice were used. The strain was generated by the group of Prof. Andreas Friebe (Universität Würzburg, Germany) using the Cre/*LoxP* system: This technology is based on the function of the protein Cre recombinase, deleting target gene sequences which are flanked by specific *LoxP* (locus of X(cross)-over in P1) recognition sequences (Orban et al., 1992; Sternberg & Hamilton, 1981). To this end, *Gucy1b1*$^{LoxP/LoxP}$ mice (Friebe et al., 2007) carrying a *LoxP*-flanked exon 10 of the β1 subunit expressing gene *Gucy1b1* were mated with *Pf4-Cre*$^{tg/+}$ mice expressing the protein Cre-recombinase in a platelet-specific manner (Rukoyatkina et al., 2011). This was achieved by introducing a Cre-encoding mouse bacterial artificial chromosome (BAC) construct into the promoter of the MK- and platelet-marker protein PF4 encoding gene. The same principle was used for the generation of *Pf4-Cre*$^{+}$*Irag1*$^{LoxP/LoxP}$ mice by the group of Prof. Jens Schlossmann (Universität Regensburg, Germany).

Wildtype mice are comparatively resistant to the development of atherosclerosis regardless of diet due to low levels of circulating lipoproteins (Gisterå et al., 2022). Therefore, the mouse model

usually requires an additional genetic modification in lipoprotein-related genes, most commonly, depletion of the LDL receptor or apolipoprotein E encoding genes *Ldlr* or *Apoe*, respectively. Due to a relatively similar cholesterol distribution compared to human plasma (Gisterå et al., 2022), $Ldlr^{-/-}$-mice were selected for backcrossing the respective mouse strains on a pro-atherosclerotic background.

3.1.2 Breeding

Mice were kept in a specific pathogen-free area with HEPA-filtered room air and received a ssniff standard diet and water *ad libitum* unless stated otherwise. Littermates of the same sex were housed together in a maximum number of 8 animals per stock cage (800 cm^2) or 5 animals per experimental cage (501 cm^2), where possible, to exclude effects of different gut microbiomes in different cages. Cages were illuminated with an automatic light regime of 12 h in a day-night rhythm and temperature was kept constant between 20-22°C at a humidity of 45-60%.

3.1.1 Western Diet

To accelerate the formation of atherosclerotic plaques in $Pf4\text{-}Cre^{+}Gucy1b1^{LoxP}Ldlr^{-/-}$, $Pf4\text{-}Cre^{+}Irag1^{LoxP}Ldlr^{-/-}$, and $Ldlr^{-/-}$ strains, respectively, animals were fed a Western diet (21.2% fat and 0.2% cholesterol by weight; TD.88137; Envigo, Indianapolis, IN) *ad libitum*. The feeding period was ten weeks for determining atherosclerotic plaque size and composition and six weeks for observational *in vivo* leukocyte adhesion experiments and analyzing atherosclerotic plaque size in early atherogenesis. The experiments were conducted in accordance with the German legislation on the protection of animals and approved by the local animal care committee (Regierung von Oberbayern, GZ: ROB-55.2-2532.Vet_02-15-176, ROB-55.2-2532.Vet_02-16-191, ROB-55.2-2532.Vet_02-18-177). According to these previously established protocols, mice were assessed for well-being daily, and weight gain was monitored weekly. Additionally, the protocol stipulated removing individual mice with increased stress levels or rare abnormalities (severe weight loss, occurrence of malignancy) from the experiments prematurely to ensure animal welfare and to preclude bias in the experimental results.

3.1.2 *In vivo* sGC stimulation

To analyze the influence of pharmacological sGC stimulation on atherogenesis, the novel sGC

stimulator BAY-747 (N-(2-amino-2-methylbutyl)-8-[(2,6-difluorobenzyl)oxy]-2,6-dimethylimidazo[1,2-a]pyridine-3-carboxamide) was kindly provided by Dr. Peter Sandner (Bayer AG, Wuppertal, Germany) and used in a concentration of 150 ppm (360 µM) for all experiments, as the substance only slightly influences blood pressure when applied in this concentration *in vivo* (Krishnan et al., 2021).

For *in vivo* sGC stimulation, *Ldlr*$^{-/-}$ mice received a Western diet (21.1% crude fat and 0.15% cholesterol, E15721-34; TD.88137 modified; ssniff, Soest, Germany) enriched with either 0 (control group) or 150 ppm (treatment group) of BAY-747 ad libitum for six or ten weeks, respectively, as stated in the respective section.

3.1.3 Adoptive transfer of leukocytes

Adoptive transfer is an established method to trace leukocyte migration from the circulation into different organs *in vivo* (Heidt et al., 2014). Thereby, leukocytes that can be distinguished from the cells of the recipients – commonly by expressing GFP – are injected intravenously into the organisms of interest. Importantly, these injected leukocytes are equally numbered and of the same origin for all experimental groups, to specifically compare the recruitment capabilities of the target tissues. By detecting the GFP signal 24 h later, presence of the adoptively transferred leukocytes can be explored, *e.g.*, in the aorta. Because the donor cells can only be found in aortic plaques after they have invaded from the blood via the recruitment cascade described in section 1.1.1, this is a suitable experimental design to study leukocyte recruitment into atherosclerotic plaques.

Table 13 Composition of antibody mix for adoptive transfer experiment

Volume (per sample)	Reagent	Final concentration
4.5 µl	anti-Ly6G-PE- antibody	0.9 µg/ml
4.5 µl	anti-CD115-biotin antibody	0.9 µg/ml
ad 1,000 µl	MACS buffer (2.6.2.3)	

In the present experiment, *Ldlr*$^{-/-}$ recipient mice were fed a Western diet for six weeks (3.1.1) to induce early atherosclerotic plaques. Bone marrow from ubiquitous GFP-expressing mice was isolated by crushing humeri, femora, tibiae, pelvis, and spine in ice-cold MACS buffer using a glass mortar and pestle after bones were cleared from muscle and fat tissue. The obtained cell suspension was filtered through a 40 µm strainer and centrifuged at 300 *g* for 10 min at 4°C. To specifically isolate monocytes and neutrophils, cells were incubated with cell-specific anti-Ly6G-PE and anti-CD115-biotin antibodies (Table 13) for 15 min on ice.

After removing excess antibodies by washing and centrifuging the samples in MACS buffer, cells were resuspended in a mixture of complementary microbeads (Table 14) for 15 min on ice in order to create magnetic bead complexes of target, Ly6G, and CD115-expressing cells via PE-anti-PE-antibody or biotin-streptavidin binding, respectively.

Table 14 Composition of microbead mix for adoptive transfer experiment

Volume (per sample)	Reagent
70 µl	Anti-PE-MicroBeads
70 µl	Streptavidin-MicroBeads
ad 500 µl	MACS buffer (2.6.2.3)

Cells were subsequently washed and positively selected over LS columns on a QuadroMACS Separator. Hereby, undesired cells not binding to the microbeads were flushed, while monocytes and neutrophils remained magnetically attached to the columns. The columns were removed from the magnetic field, and the positively selected cells were rinsed from the columns, washed, and adjusted to a concentration of 10 million cells per 300 µl in DPBS. Purity and GFP-expression of isolated monocytes and neutrophils was confirmed by flow cytometry analysis as described in section 3.3. Lastly, *Ldlr*$^{-/-}$ recipient mice were intravenously injected with 300 µl of the GFP^{+}-leukocyte suspension 24 h before harvesting organs.

3.1.4 Intravital fluorescence microscopy

Following the six weeks' Western diet (section 3.1.1), *Pf4-Cre*$^{+}$*Gucy1b1*$^{+/LoxP}$*Ldlr*$^{-/-}$ mice and *Pf4-Cre*$^{+}$*Gucy1b1*$^{LoxP/LoxP}$*Ldlr*$^{-/-}$ mice were transported to the local Institute for Cardiovascular Prevention (IPEK) and anesthetized with a combination of midazolam, medetomidine, and fentanyl (5, 0.5, and 0.05 mg per kg body weight, respectively). After confirming the desired deepness of anesthesia, mice were subjected to intravital microscopy of the right carotid artery bifurcation by Prof. Oliver Söhnlein (Universität Münster, Germany) as described previously (Winter et al., 2018). Shortly, circulating leukocytes were labeled *in vivo* by intravenous injection of 1 µg/mouse PE-conjugated anti-Ly6G, Alexa Fluor 488-conjugated anti-Ly6C, and, in a second round, PE-conjugated anti-CD11b antibodies (2.3.2). The right common carotid artery was exposed at the level of the bifurcation and adhesion of the stained leukocytes to the atherosclerotic vessel wall documented by recording 30-second movies using an Olympus BX51 microscope with a Hamamatsu 9100-02 EMCCD camera and a 10X saline-immersion objective. Neutrophils (Ly6G-PE^{+}), monocytes (Ly6C-Alexa Fluor 488^{+}), and myeloid cells (CD11b-PE^{+}) remaining stationary within the specified 30 s were regarded as adherent and absolute numbers were

determined in a blinded manner by Prof. Söhnlein.

3.2 Harvesting of target tissues

Untreated or atherosclerotic mice (section 3.1.1) were sacrificed under deep isoflurane anesthesia (4% V/V) by retrobulbar exsanguination using heparin-coated capillaries.

If applicable, an antibody directed against the pan-leukocyte marker CD45 (Table 15) was injected intravenously 5 min before sacrificing animals to distinguish blood leukocytes from tissue-resident or -invaded leukocytes in subsequent flow cytometry analyses.

Table 15 *in vivo* labeling of blood leukocytes for flow cytometry analysis

Volume (per mouse)	Reagent	Final concentration
10 µl	anti-CD45-antibody	20 µg/ml
ad 100 µl	DPBS	

3.2.1 Isolating blood leukocytes

Per mouse, 50 µl of blood was transferred to 5 ml polystyrene tubes for flow cytometry analyses and residual blood was collected into EDTA-coated microvettes, stored on ice, and centrifuged at 1,000 *g* for 15 min at 4°C. The supernatant plasma was stored at -80°C for routine plasma cholesterol determination by the in-house clinical chemistry department or enzyme-linked immunosorbent assays (section 3.7.4). Blood samples for flow cytometry were subjected to 1X RBC lysis buffer and incubated for 5 min at room temperature (RT) to lyse red blood cells. The reaction was stopped by adding 3 ml of 1X PBS. Cells were spun down at 400 *g* for 8 min at 4°C and resuspended in FACS buffer (section 3.3).

For isolating peripheral blood mononuclear cells (PBMC) for Western blotting (3.7.2), 1 ml of blood was diluted with DPBS in a 1:1 ratio and carefully layered on top of a 1.5 ml Ficoll-Paque PREMIUM layer at RT in a 5 ml polystyrene tube. After a 30-min centrifugation at 400 *g* without brake, the interphase containing PBMC was washed in DPBS and spun down at 400 *g* for 10 min. The cell pellet was subjected to red blood cell lysis in 5 ml 1X RBC lysis buffer at RT for 5 min. After washing samples in DPBS, cells were manually counted in a 1:100 dilution of trypan blue using a hemocytometer, centrifuged at 100 *g* for 10 min to remove platelets, and, per million cells, resuspended in 20 µl of 1X RIPA buffer containing 1:100 protease inhibitor. Samples were stored at -80°C until further processing.

3.2.2 Dissecting aortae, aortic roots, and lung

After opening the chest and cutting the vena cava, the right ventricle was flushed with 20 ml of 1X PBS. The superior lobe of the right lung was excised, washed in DPBS, and snap-frozen in liquid nitrogen. After removing residual lung and gastrointestinal organs as well as perivascular fat and surrounding other tissue, aortae were excised 2 mm distant from the aortic root and 1 mm distal from the common iliac artery bifurcation. Aortae were either stored for up to 2 h in ice-cold 1X PBS for flow cytometry preparations (3.2.2.1), in a 4% formaldehyde solution at 4°C for subsequent histology (3.4.4), or specimens were washed in DPBS followed by snap-freezing in liquid nitrogen for protein isolation (3.7.1).

Hearts were cut transversely at the upper third level, and the surrounding tissue along the aortic roots was partially removed with a scalpel. Small portions of surrounding muscle were preserved to stabilize the vascular root, and samples were embedded in tissue molds in O.C.T. compound. Specimens were snap-frozen in -80°C cold 2-methylbutane and stored at -80°C.

3.2.2.1 Preparing single-cell suspensions of aortic leukocytes

Aortae were transferred to vials containing ice-cold aortic digestion buffer (Table 16), minced using fine scissors, and incubated for 1 h at 37°C and 750 rpm agitation.

Table 16 Leukocyte isolating digestion mix

Volume (per sample)	**Reagent**	**Final concentration**
45 µl	Collagenase I stock solution (2.6.2.3)	450 U/ml
10 µl	Collagenase XI stock solution (2.6.2.3)	125 U/ml
5 µl	Hyaluronidase stock solution (2.6.2.3)	60 U/ml
3.7 µl	Deoxyribonuclease I	60 U/ml
20 µl	1 M HEPES solution	20 mM
ad 1000 µl	DPBS	

Cell suspensions were filtered through 40 µm nylon cell strainers, washed in 40 ml FACS buffer, centrifuged at 400 *g* for 8 min at 4°C, and resuspended in 300 µl FACS buffer for flow cytometry staining (3.3).

3.2.2.2 Tissue lysing for Western blotting

Frozen aortae and lungs were transferred to 2 ml vials containing 500 µl of ice-cold 1X RIPA buffer enriched with 1:100 protease inhibitor solution and minced with scissors to a fine tissue suspension. Subsequently, samples were homogenized using the Omni Tissue homogenizer with soft (lung) or hard (aorta) tissue tips three times for 10 s on ice. Samples were lysed for 1 h on ice

and stored at -80°C until further processing (3.7.1).

3.2.1 Differentiating and culturing megakaryocytes

To obtain MK and progenitors, humeri, femora, tibiae, and os ilii of mice from both genotypes were collected and separated from the muscle and connective tissue. After removal of the proximal epiphysis, the bones were placed with the opening facing downwards into sterile 0.5 ml tubes and transferred into sterile 1.5 ml reaction tubes containing 100 µl MK isolation medium. The bottoms of the 0.5 ml tubes were previously pricked with an 18 G needle to allow the bone marrow to flow into the 1.5 ml tube during subsequent centrifugation at 2,500 *g* for 1 min (Heib et al., 2021). Cells were suspended in 1 ml MK isolation medium, centrifuged at 300 *g* for 5 min, and incubated in 4.5 ml 1X RBC lysis buffer for another 5 min. After adding 9 ml of DPBS and centrifugation at 300 *g* for 5 min, cells were vigorously pipetted up and down in 5 ml MK isolation medium, filtered through 70 µm cell strainers, and centrifuged at 300 *g* for 5 min. After manually determining cell numbers, cells were resuspended in MK growth medium to a concentration of 1×10^7 cells/ml and kept in T75 cell culture flasks in a humidified incubator with 5% CO_2 at 37°C. Cells were cultured for 9 days and fresh medium was added every second day.

Cultivation of bone marrow cells in a TPO-enriched medium resulted in the differentiation of progenitor cells into MKs, which were visible under the microscope as semi-adherent, exceptionally large cells with an irregular surface. Cells were harvested by BSA density gradient filtration as follows (Drachman et al., 1997): After detaching the cells with a cell scraper and centrifugation at 400 rpm for 10 min, they were resuspended in 4 ml of DPBS and carefully placed on top of a layer of 4 ml of 1.5% BSA solution over a second layer of 4 ml of 3% BSA solution in a 15 ml tube. Due to their high density, MKs sedimented to the bottom after 40 min at RT, while other cells were retained in the upper 0-1.5% BSA solution. The bottom, MK-containing 2 ml was collected, washed in DPBS, and resuspended in 4 ml Dulbecco's PBS before being subjected to another 0-3% BSA gradient filtration step to obtain a pure population. Cell number was determined manually and cells were resuspended in 350 µl of Buffer RLT Plus at a concentration of 50.000 cells/µl and stored at -80°C for further processing (3.8.1.1).

3.3 Flow cytometry

Flow cytometry is a valuable method to identify and quantify cell populations in single-cell samples after labeling with fluorophore-conjugated antibodies directed against characteristic cellular

antigens. In the system, one cell at a time is passed through a laser beam and, depending on its size, granularity, and antibodies bound, recognized by the light scattered from its surface or emitted from the antibody-conjugated fluorophores.

3.3.1 Flow cytometry analysis of leukocytes

Blood and aortic cells were stained for hematopoietic lineage markers by adding a mixture of phycoerythrin (PE) conjugated lineage-specific antibodies (Table 17) for 15 min at 4°C. Unbound antibody was washed off by adding 1 ml of FACS buffer and centrifuging samples at 400 *g* for 8 min at 4°C before resuspending cells in 300 µl of FACS buffer.

Table 17 Composition of antibody mix 1 for leukocyte staining

Volume (per sample)	**Reagent**	**Dilution**
0.5 µl	anti-B220-PE antibody	1:600
0.25 µl	anti-CD49b-PE antibody	1:1200
0.1 µl	anti-CD90.2-PE antibody	1:3000
0.5 µl	anti-NK1.1-PE antibody	1:600
0.5 µl	anti-Ter119-PE antibody	1:600
0.5 µl	anti-Ly6G-PE antibody	1:600
ad 50 µl	FACS buffer (2.6.2.4)	

A second round of staining was conducted using leukocyte-specific antibodies (see Table 18) for another 15 min at 4°C before cells were washed as stated above and resuspended in 300 µl of FACS buffer.

Table 18 Composition of antibody mix 2 for leukocyte staining

Volume (per sample)	**Reagent**	**Dilution**
0.5 µl	anti-Ly6C-BV421 antibody	1:600
0.5 µl	anti-CD115-BV510 antibody	1:600
1.0 µl	anti-CD45.2-PerCP/Cy5.5 antibody	1:300
0.5 µl	anti-F4/80-PE-Cy7 antibody	1:600
0.5 µl	anti-CD11b-APC-Cy7 antibody	1:600
ad 50 µl	FACS buffer (2.6.2.4)	

Cells were submitted to flow cytometry on a BD LSRFortessa. Lasers were calibrated weekly using CS&T Research Beads and compensated using UltraComp eBeads conjugated with each of the antibodies used prior to performing experiments.

Cells were submitted to flow cytometry on a BD LSRFortessa and analyzed using FlowJo software. After excluding non-viable cells (as identified by FSC-A *vs.* SSC-A) and multiplets (identified by

FSC-A *vs.* FSC-W and SSC-A *vs.* SSC-W), neutrophils were identified as lineage^{high}(CD45.2/CD11b)^{high}CD115^{low}. Monocytes were identified as lineage^{low} (CD45.2/CD11b/CD115)^{high} Ly6C$^{high/low}$ and macrophages as lineage^{low}(CD45.2/CD11b/F4/80)^{high}Ly6C$^{low/int}$.

In adoptive transfer experiments, the number of CD45.2^{high}/CD11b^{high}/GFP^{high} cells within the aorta was assessed and normalized to the exact number of injected cells.

3.4 Histology

3.4.1 Preparation of samples

Frozen aortic root specimens (3.2.2) were cut into 5 µm sections using a cryostat set to -20°C and transferred onto microscope slides. Among the sections showing at least two complete cusps, every fifth slide was subjected to tissue staining.

3.4.2 Masson's trichrome staining

For Masson's trichrome staining, sections were hydrated in Millipore water and fixated in a 4% formaldehyde solution for 45 s. Afterward, slides were mordanted in Bouin's solution at 56°C for 15 min and cooled in warm tap water before being subjected to freshly prepared Weigert's iron hematoxylin solution for 5 min according to the manufacturer's recommendations, followed by a 5-minute washing step in running tap water. Subsequently, using the Trichrome Staining (Masson) kit, specimens were stained in Biebrich scarlet-acid fuchsin solution for 5 min, rinsed in Millipore water, incubated in phosphotungstic/phosphomolybdic acid solution and aniline blue solution for 5 min each, and rinsed in 1% aqueous acetic acid solution for 2 min. Slides were dehydrated in 70, 96, and 100% ethanol followed by a washing step in xylene and covered with Mountex mounting medium. Specimens were digitalized using a 5X objective on a Leica digital microscope camera, plaque size was determined per sample in a blinded fashion using ImageJ, and mean total plaque size (in µm^2) was calculated per animal.

3.4.3 Immunohistochemistry

For immunohistochemistry, specimens were fixated in ice-cold acetone for 10 min, blocked in 10% rabbit serum blocking solution for 1 h, and stained using unconjugated anti-CD11b or anti-

monocyte + macrophage antibody (diluted 1:200 or 1:50, respectively, in 10% rabbit serum blocking solution) in a humidified chamber overnight. Subsequently, samples were incubated in a 1:200 dilution of anti-rat HRP-conjugated secondary antibody in 10% rabbit serum blocking solution for 1 h at RT and staining was developed by adding AEC substrate for 10 min. Afterward, cell nuclei were counterstained in hematoxylin Gill II solution for 2 min, rinsed for 8 min in running tap water, and mounted in warm Kaiser's glycerol gelatin. Images were captured using a 5X objective on a Leica digital microscope camera and CD11b or monocyte and macrophage area per total plaque area was calculated using automated color-thresholding in ImageJ.

3.4.4 *En face* analysis

After being subjected to 4% formaldehyde solution for 24 h (3.2.2), aortae were washed in a 60% solution of 2-propanol in Millipore water for 10 min and incubated at 37°C for 30 min in Oil red O working solution which was freshly prepared as directed in Table 19 and filtered twice through filter paper.

Table 19 Oil red O working solution

Volume	Reagent	Final concentration
300 ml	Oil red O stock solution (2.6.2.5)	3 mg/ml
200 ml	Millipore water	

Subsequently, the aortae were washed in 60% 2-propanol, cut opened longitudinally using spring scissors, and pinned on a black pad with Minutien pins. Specimens were imaged on a Stemi 2000-C microscope connected to an Axiocam ERc 5s camera using ZEN 2 software. Percent of lesion area was determined manually in a blinded fashion as ORO-positive area of total *en face* aortic area from the aortic root to the branch of the right renal artery using Image J software.

3.5 *In vitro* activation of platelets

3.5.1 Generation of murine platelet suspensions

Per mouse, 800 µl of blood was collected from the retrobulbar plexus into 2.0 ml tubes containing 200 µl of 50 U/ml heparin solution and gently mixed after adding 1 ml of DPBS. Samples were centrifuged for 10 min at 100 *g* and RT without active deceleration and platelet-rich plasma (PRP) was either used directly (3.5.3) or subjected to a second 10-min centrifugation step at 700 *g*.

Supernatant platelet-poor plasma (PPP) was stored at -80°C and pelleted platelets either resuspended in 100 µl of 1X RIPA buffer containing 1:100 protease inhibitor and stored at -80°C for protein measurements or further processed by shake-activation (3.5.4). Platelet count was measured using an automated hematology analyzer.

3.5.2 Generation of human platelet suspensions

Venous blood from healthy volunteers was collected into hirudin Monovettes using an approved study protocol by the local ethics committee of the Technical University of Munich (387/17 S). All participants gave written informed consent. Samples were centrifuged at 170 *g* for 13 min at RT without active deceleration. PRP was subjected to shake-activation (3.5.4) and platelet count was determined using an automated hematology analyzer.

3.5.3 Aggregometry

In aggregometry, platelet aggregation can be monitored by measuring differences in light transmission caused by aggregating platelets in suspension in response to added platelet agonists. 10X working solutions of required substances were prepared freshly from the respective stock solutions (2.6.2.6) by serial dilutions in UltraPure Distilled Water (Table 20). Vehicle solutions were prepared accordingly.

Table 20 Concentrations of substances used for aggregometry

Substance	**Final concentration**	**Vehicle** (final concentration)
SNP	10 µM	0.4% DMSO
BAY-747	150 ppm	0.4% DMSO
ADP	2 µM	UltraPure Distilled Water
PAR4-AP	75 nM	UltraPure Distilled Water
U46619	5 µM	UltraPure Distilled Water
Collagen	1 µg/ml	UltraPure Distilled Water

Per tested condition and mouse, 200 µl of PRP were transferred to glass cuvettes and, after adding either 25 µl of sodium nitroprusside (SNP), BAY-747 solution, or vehicle, incubated at 37°C with constant stirring on a PAP-8 turbidimetric platelet aggregation profiler. Residual PRP was centrifuged at 700 *g* for 10 min to receive PPP used for blanking. Thrombocyte aggregation was induced by adding 25 µl of ADP, PAR4-AP, U46619, or collagen working solutions and platelet aggregation was recorded over 5 min to measure area under the curve (AUC) using the respective software. Subsequently, samples were transferred to 1.5 ml vials and spun down for 15 min at

maximum speed and 4°C. The supernatant was transferred to new vials and stored at -80°C for further processing (3.7.4).

3.5.4 Shake-activation

If not stated otherwise, pelleted platelets (3.5.1, 3.5.2) were carefully resuspended in 370 µl of RPMI 1640 and activated by orbital shaking for 30 min at 1000 rpm in a thermoshaker set to 25°C. Subsequently, samples were centrifuged at 12,000 *g* for 10 min and the supernatant was either used directly in subsequent experiments or stored at -80°C. Platelet count was analyzed simultaneously with an automated hematology analyzer.

3.5.5 sGC stimulation and protein kinase inhibition

2X BAY-747 (final concentration 150 ppm, 0.4% DMSO) and kinase inhibitor working solutions (Table 21, 0.2% DMSO) were freshly prepared from the respective stock solutions (2.6.2.6) by serial dilutions in DPBS. Vehicle solutions were prepared accordingly. Pelleted platelets (3.5.1) were gently resuspended in 870 µl RPMI 1640 and added in a 1:1 ratio to either vehicle or respective compound solutions, mixed gently, and incubated for 30 min at RT prior to shaking (3.5.4).

Table 21 Kinase inhibitor working solutions

Inhibitor	Affected kinase	Final concentration
2-APB	Inositol triphosphate receptor (IP_3-R)	10 µM
Ro 32-0432	Protein kinase C (PKC)	5 µM
KT-5823	Protein kinase G (PKG)	10 µM
Dinaciclib	Cyclin-dependent kinase (CDK) 2/5/9	100 nM
MK-2206	Akt	1 µM
Ravoxertinib	Extracellular signal-regulated kinases (ERK)	10 µM
VX-702	p38α mitogen-activated protein kinase (MAPK)	10 µM

3.5.6 PamGene Serine/Threonine Kinase Array

Following shake activation (3.5.4), BAY-747 and vehicle-treated platelets were centrifuged at 1,200 *g* for 5 min and resuspended in ice-cold M-PER lysis buffer to a concentration of 200×10^6 platelets per 100 µl. Platelets were incubated for 15 min on ice and each sample was pipetted up and down eight times every 5 min using 200 µl pipette tips to ensure proper cell dissolution. Lysates were centrifuged at 20,000 g for 15 min and protein content was determined using the Pierce Coomassie

Plus Assay Kit according to the manufacturer's recommendations. Samples were stored at -80°C until being further processed by Dr. Emiel van der Vorst (RWTH Aachen, Germany) using the PamChip Ser/Thr Kinase array as described previously (Peters et al., 2022) to determine serine/threonine kinase profiles in the platelet lysates. The array contains 144 peptide sequences harboring specified phosphorylation sites, which are subsequently phosphorylated dependent on the specificity and activity of the kinases present in the sample. By fluorescently labeled anti-phospho-detection antibodies and a respective LED imaging system, thus, the phosphopeptide fingerprints based on the kinase activity in the samples are identified and correlated to upstream kinases using the PhosphoNET database (Kinexus Bioinformatics Corporation, 2019).

3.6 Cell culture

3.6.1 Culturing murine endothelial cells

Murine aortic endothelial cells (mAoEC) were cultured in complete endothelial cell medium in gelatin-coated cell culture flasks in a humidified incubator with 5% CO_2 at 37°C. The medium was exchanged every second day and cells were split for a maximum of five cycles.

3.6.2 Leukocyte-endothelium adhesion assay

mAoEC were seeded at 30.000 cells/well in gelatin-coated 96-well plates prior to performing experiments and incubated in a humidified incubator until forming a continuous monolayer. Activated platelet supernatant was generated freshly as stated in section 3.5.4. from either C57BL/6 J (wildtype), *Pf4-Cre*$^{+}$*Gucy1b1*$^{+/LoxP}$, or *Pf4-Cre*$^{+}$*Gucy1b1*$^{LoxP/LoxP}$ mice.

Monocytes and neutrophils were isolated from the bone marrow of wildtype mice using MACS cell separation columns as described in section 3.1.3, using either anti-Ly6G-PE, anti-CD115-Biotin, or both antibodies and respective beads. Using the CytoSelect Leukocyte-Endothelium Adhesion Assay, isolated cells were resuspended in RPMI 1640 at 1.25×10^{6} cells/ml and fluorescently labeled with LeukoTracker solution (kit component, 1X final concentration) for 30 min. Cells were washed twice and resuspended in RPMI 1640 at 1×10^{6} cells/ml.

Endothelial culture medium was aspirated and 250 µl of leukocyte suspension was added to each well, followed by 50 µl of platelet supernatant. Samples were assayed in triplicates and incubated for 30 min. Afterward, plates were washed trice in 1X PBS to remove non-adherent cells, lysed in

150 µl of 1X lysis buffer (kit component) for 5 min, and fluorescence of lysed endothelium-adherent leukocytes was measured on a plate reader at 535 nm using 485 nm for excitation.

For preincubation experiments, platelets were resuspended in 540 µl RPMI 1640 and, in addition to treating samples as explained above, neutrophils or monocytes and EC separately incubated with 50 µl of activated *Pf4-Cre*$^{+}$*Gucy1b1*$^{LoxP/LoxP}$ platelet supernatant or vehicle for 30 min in 96-well-plates. Subsequently, both cell types were washed trice in RPMI 1640, incubated together for another 30 min in the absence of platelet supernatant, and readout performed as explained above.

To determine the effects of TIE2-receptor inhibition on *in vitro* leukocyte adhesion, BAY-826 or vehicle solutions were added to mAoEC culture medium to a final concentration of 0.5 µM BAY-826 and 0.1% DMSO for 5 h prior to performing the adhesion assay in the presence of activated platelet supernatant.

3.7 Qualitative and quantitative protein analyses

3.7.1 Preparation of cell or tissue protein solutions

Samples were thawed on ice and sonicated for 30 s followed by 30 s on ice for a total of three rounds and centrifuged at maximum speed for 30 min and 4°C to remove cell debris. Protein lysate was transferred to new 1.5 ml vials and protein content was determined using the Pierce bicinchoninic acid (BCA) assay kit and 2 µl of protein sample according to the manufacturer's recommendations. The assay is based on the reduction of Cu^{2+} in an alkaline environment to Cu^{+}, which forms a violet complex with BCA that is photometrically detectable at 562 nm. Protein content was determined using a standard series of BSA solutions of known concentration (stock solution included in the kit).

3.7.2 Western blotting

Following electrophoretic separation, Western blotting enables the visualization of particular proteins via specific antibodies using a chemiluminescent reaction of the enzyme horseradish peroxidase (HRP) and its respective substrate.

In the first step, a sample volume equivalent to 20 µg (PBMC), 25 µg (lung), or 30 µg (aorta and platelets) protein was mixed 1:1 with 2X Laemmli buffer and made up to a total volume of 30 µl

with 1X Laemmli buffer (prepared by diluting 2X Laemmli buffer in 1X RIPA buffer). Samples were denatured at 95°C for 5 min and loaded onto 4-20% gradient precast polyacrylamide gels in a vertical electrophoresis chamber. 5 µl of a broad range color prestained protein standard served as the size standard. Chambers were filled with 1X running buffer and electrophoresis was performed at 100 V for approximately 90 min to separate proteins according to their size.

Next, the gel was placed on a ready-to-use Mini 0.2 µm PVDF membrane using the Trans-Blot Turbo Transfer System and blotted by semi-dry transfer for 7 min at 1.3 Ampere and a maximum of 25 V. Membranes were incubated in 50 mg/ml milk in PBS at RT for 1 h on a rocker set to 35 rpm for blocking, transferred into a 50 ml tube containing 4 ml of the primary antibody mixture (Table 22), and incubated on a roller at 4°C overnight.

Table 22 Primary antibody solution for Western blotting

Reagent	Final dilution
Rabbit anti-mouse β_1-sGC antibody	1:1,000
Rabbit anti-GAPDH XP antibody	1:200,000
25 mg/ml milk in PBS (2.6.2.7)	carrier solution

Subsequently, membranes were washed trice for 5 min in 25 ml of 1X PBS-T and incubated in 50 ml of anti-rabbit secondary antibody in a dilution of 1:100,000 in 25 mg/ml milk in PBS for 1 h at RT on a rocker at 35 rpm. Membranes were washed three times for 10 min in 25 ml of 1X PBS-T before being incubated in 2 ml of freshly prepared SuperSignal Substrate solution according to the manufacturer's recommendations for 5 min. Proteins were subsequently visualized using the ImageQuant 800 and respective software.

3.7.3 Cytokine profiling of activated platelet releasate

To detect differential protein release in wildtype and sGC-deficient platelets, shake-activated platelet supernatant of *Pf4-Cre*$^{+}$*Gucy1b1*$^{+/LoxP}$ and *Pf4-Cre*$^{+}$*Gucy1b1*$^{LoxP/LoxP}$ mice (3.5.4) was subjected to the Proteome Profiler Mouse XL Cytokine Array according to the manufacturer's protocol. In principle, the assay consists of antibody-spotted nitrocellulose membranes able to capture over 100 different proteins which are incubated with the samples overnight at 4°C. Subsequently, membranes are exposed to a mixture of respective biotinylated detection antibodies followed by streptavidin-HRP and visualized with chemiluminescent reagents in a manner similar to Western blotting. Signals were detected using the ImageQuant 800 imager and signal intensities were digitalized using ImageQuant TL software after background subtraction. Signal intensities of target

proteins were normalized to signal intensities for reference spots in each sample. In total, six samples per genotype were tested.

3.7.4 Enzyme-linked immunosorbent assays

Enzyme-linked immunosorbent assays (ELISA) are used to quantify specific proteins in samples. Usually, well-plates pre-treated with immobilized antibodies to specifically capture the protein of interest are incubated with the sample, unbound material washed off, and well-plates again subjected to an enzyme-linked, antigen-specific detection antibody. By adding a substrate solution, the enzyme reaction yields a colored product with color intensities relative to the amount of the specific protein in the sample. Absolute protein amounts are determined from a standard curve, utilizing standard solutions measured in parallel with the samples in the assay.

The ELISA kits used to determine the amounts of adrenaline, angiopoietin-1 (ANGPT1), chemokines C-X-C motif ligand (CXCL)3, 4, 5, 7, and 15, endostatin, P-selectin, retinol binding protein 4 (RBP4), serotonin, vascular endothelial growth factor (VEGF), and triggering receptor expressed on myeloid cells like 1 (TREML1) are listed in Table 9. All assays were performed according to the manufacturer's protocol. Samples were diluted according to the recommendations in the manual or according to pre-tests performed with different dilutions of the samples. Readout was generally performed using the Infinite M200 PRO plate reader at 450 nm, followed by subtraction of the reference background values measured at 540 nm and conversion of the obtained absorbance values based on the standard curve using a Four Parameter Logistic (4PL) regression.

3.8 Genotyping and gene expression analyses

3.8.1 Isolating nucleic acids

3.8.1.1 RNA isolation and cDNA synthesis

To isolate RNA, cells were disrupted by the guanidine-isothiocyanate-containing Buffer RLT Plus to inactivate ribonucleases. Buffer RLT Plus treated samples (3.2.1) were thawed, pipetted into QIAshredder spin columns to homogenize lysates, and further processed according to the RNeasy Plus Mini Kit manual. Genomic DNA was removed using a highly concentrated salt solution by precipitating it on gDNA Eliminator spin columns. Subsequently, samples were treated with

ethanol to precipitate RNA, which was bound to silica-based columns, washed, and eluted from columns with 30 µl of UltraPure Distilled Water. RNA was quantified using a NanoQuant Plate on an Infinite M200 PRO plate reader.

Subsequently, respective volumes corresponding to 25 ng RNA per sample were subjected to cDNA synthesis using the High Capacity RNA-to-cDNA kit. The cDNA reaction mix (Table 23) was prepared in 8-well strips and incubated at 37°C for 60 min followed by 5 min at 95°C and subsequent cooling at 4°C with help of a thermal cycler. Samples were stored at -20°C until further processing.

Table 23 Preparation of cDNA synthesis reaction

Amount (per sample)	**Reagent**
10 µl	2X RT Buffer Mix
1 µl	20X RT Enzyme Buffer Mix
25 ng	RNA sample
ad 20 µl	UltraPure Distilled Water

3.8.1.2 DNA isolation

DNA was isolated from mouse ear punches obtained during the marking of each animal using the blackPREP Rodent Tail DNA Kit as recommended in the manual and eluted using 100 µl of Elution buffer.

To determine the genotype of human subjects (3.5.2), whole blood was collected into EDTA-coated tubes and DNA was isolated using the Puregene Blood Kit according to the manufacturer's protocol. Hereby, isolation followed a similar principle to that described for RNA isolation.

3.8.2 Polymerase chain reaction (PCR)

Polymerase chain reaction (PCR) is a three-step procedure to exponentially amplify a specific DNA sequence *in vitro* (Mullis et al., 1986). The reaction mix contains a *Taq* polymerase, the template DNA, nucleotides, and primers which are short sequences of complementary nucleotides specifically binding to both ends of the desired DNA sequence. In the first step, single-stranded DNA is generated by denaturing DNA at a temperature of 95-98°C, causing the break-down of hydrogen bonds between complementary bases. During the second step, a primer-specific temperature between 55-65 °C is applied to enable the annealing of primers to the DNA template. In the last step, the temperature is elevated to 68-72°C and enables the Taq polymerase to

synthesize a new, complementary DNA strand. Due to exponential amplification, a 25-fold to 40-fold repetition of this procedure allows for the generation of large amounts of the respective DNA sequences.

3.8.2.1 Endpoint polymerase chain reaction and agarose gel electrophoresis

In endpoint PCR, the resultant amplified DNA sequence can be used for qualitative analyses such as genotyping. To this end, murine DNA (3.8.1.2) was subjected to genotype-specific PCR reactions using the KAPA2G Fast HotStart Genotyping PCR Mix (Table 24) and the cycling protocol given in Table 25.

Table 24 Preparation of PCR reaction mixes

Volume (per sample)	**Reagent**
12.5 µl	2X KAPA2G Fast HotStart ReadyMix
1.25 µl (*Gucy1b1*), 0.75 µl (*Irag1*), 0.3 µl (*Pf4-Cre*), or 0.6 µl (*Ldlr*), respectively	10 µM forward primer, gene-specific
1.25 µl (*Gucy1b1*), 0.75 µl (*Irag1*), 0.3 µl (*Pf4-Cre*), or 0.6 µl (*Ldlr*), respectively	10 µM reverse primer, gene-specific
1 µl	Template DNA
ad 25 µl	UltraPure Distilled Water

PCR reactions were prepared for each region of interest using the forward and reverse primers as listed in section 2.5.2. For genotyping $Ldlr^{-/-}$ mice, samples were subjected to two separate PCR reactions using 0.6 µl of the common forward primer and the specific reverse primer to detect either the $Ldlr^{-/-}$ wildtype or mutant gene sequence.

Table 25 PCR cycling protocol

Step	**Temperature**	**Duration**	**Cycles**
Initial denaturation	95°C	3 min	1
Denaturation	95°C	15 sec	35
Annealing	60°C	15 sec	
Extension	72°C	1 sec/kb	
Final extension	72°C	1 min/kb	1

Amplification products were visualized by horizontal agarose gel electrophoresis at 120 V in 1X TBE buffer. The agarose gel was prepared by dissolving 1 g/ml agarose in 1X TBE buffer under heating. PeqGREEN dye was added to the mixture in a 1:20,000 dilution to enable DNA visualization before the gel was allowed to solidify in a specified mold. The 2-Log DNA Ladder ranging from 0.1 to 10.0 kb was used as a size reference and before loading, samples were mixed 6:1 with 6X purple loading dye. Gels were imaged under UV light in the ImageQuant 800

biomolecular imager. DNA bands were analyzed according to their size. Genotyping was performed for every single animal before inclusion in experiments.

3.8.2.2 Real-time quantitative polymerase chain reaction (qPCR)

Real-time quantitative PCR allows for the quantification of gene sequences in a sample. After enzymatically converting RNA to cDNA, this method can also be used to determine the expression of specific genes. For this purpose, i) murine cDNA (3.8.1.1) or ii) DNA from human subjects (3.8.1.2) who were enrolled for *in vitro* platelet experiments (3.5.2) was subjected to real-time quantitative PCR using gene-specific pre-designed TaqMan probes (2.5.1). The assays contain a sequence-specific primer pair and a sequence-specific probe labeled with the fluorescent dyes FAM™ or VIC™ at the 5'-end as well as a quencher at the 3'-end. After hybridization of probes and primers with their target sequences, the Taq-DNA-polymerase synthesizes the complementary strands and as soon as reaching the probes, cleaves the fluorophores from the probe and quencher, thereby releasing the fluorophore signals subsequently detected by the system.

Murine cDNA qPCR reactions were prepared according to Table 26 and performed in MicroAmp fast optical 96 well reaction plates on a ViiA 7 system (Thermo Fisher Scientific) using the cycle conditions given in Table 27 and respective software. Ct values were normalized against *Gapdh* Ct values measured in parallel with each sample to calculate ΔCt. Relative gene expression levels between samples were calculated by the ΔΔCt method using the average ΔCt of *Gucy1b1* wildtype samples as a reference. Data were log-transformed to obtain fold change.

Table 26 Preparation of qPCR gene expression reaction mix

Volume (per sample)	**Reagent**
5 µl	TaqMan Fast Universal PCR Master Mix
0.167 µl	TaqMan probe Mm99999915_g1 (*Gapdh*, 60X)
0.5 µl	Gene of interest specific Taqman probe (20X)
1 µl	cDNA sample
ad 10 µl	UltraPure Distilled Water

Table 27 Cycle conditions for gene expression qPCR

Step	**Temperature**	**Duration**	**Cycles**
Initial denaturation	95°C	20 s	1
Denaturation	95°C	1 s	45
Annealing/Extension	60°C	20 s	

Human blood leukocyte DNA was genotyped for the *GUCY1A1* risk variant using the TaqMan SNP rs7692387 Genotyping Assay. Reaction mixes were prepared according to Table 28 in 96-

well plates using the cycling conditions given in Table 29. Genotypes were analyzed with the TaqMan Genotyper software.

Table 28 Preparation of qPCR genotyping reaction mix

Volume (per sample)	**Reagent**
12.5 µl	TaqMan Universal Master Mix II, no UNG
1.25 µl	TaqMan SNP genotyping probe for rs7692387 (20X)
1 µl	DNA (10 ng/µl)
ad 25 µl	UltraPure Distilled Water

Table 29 Cycle conditions for genotyping

Step	**Temperature**	**Duration**	**Cycles**
Initial denaturation	95°C	10 min	1
Denaturation	95°C	15 s	40
Annealing/Extension	60°C	1 min	
Post-PCR read	60°C	30 s	1

3.9 Statistical analyses

The normality distribution of data was assessed using the Kolmogorov-Smirnov test or the Shapiro-Wilk test for sample sizes n<5. Normally distributed data were analyzed using a two-tailed Student's unpaired or paired t-test as appropriate. For comparison of more than two groups, a repeated measures one-way ANOVA test followed by a Dunnett's or Tukey's multiple comparisons test, or a mixed-effects analysis was performed, as appropriate. Non-normally distributed data were analyzed by the Mann-Whitney test. To determine statistical outliers, the two-sided ROUT's test was used. If applicable, the removal of outliers is indicated in the respective figure legends. Likewise, sample sizes or the numbers of replicates, respectively, are specified in the figure legends and visualized in the figures (each symbol represents one animal/biological replicate) and data are displayed as the mean and standard error of mean (s.e.m.). Statistical significance was assumed if p-values were <0.05; in the case of investigating more than two groups after adjustment for multiple testing. Statistical analyses were performed using GraphPad Prism software.

4 Results

4.1 Confirmation of platelet sGC depletion in the experimental model

4.1.1 Genotyping and β_1-sGC protein expression

Mice were enrolled in knockout and control groups according to the genotyping results obtained by agarose gel electrophoresis following sequence-specific PCR of earlobe-isolated DNA from each animal. The *LoxP*-flanked (floxed) *Gucy1b1* sequence was only deleted in presence of Cre recombinase, with protein expression limited to platelets and megakaryocytes by its dependency on *Pf4*-expression. Therefore, the genotyping strategy was to detect the floxed sequences in the earlobe DNA material. As depicted in Figure 9a, *Gucy1b1*$^{LoxP/LoxP}$ mice were identified by one band at 790 bp representing the floxed alleles, whereas a heterozygous *Gucy1b1*$^{+/LoxP}$ genotype was detected by showing both the mutant and wildtype band at 680 bp. The *Irag1*$^{+/LoxP}$ genotype was identified by two bands at 259 and 280 bp indicating the mutant allele and one band at 224 bp for the wildtype allele, whereas *Irag1*$^{LoxP/LoxP}$ was detected by only one band at 259 bp. The presence of *Pf4-Cre* was assured by a PCR amplification product of 450 bp. *Ldlr* mutated mice were detected

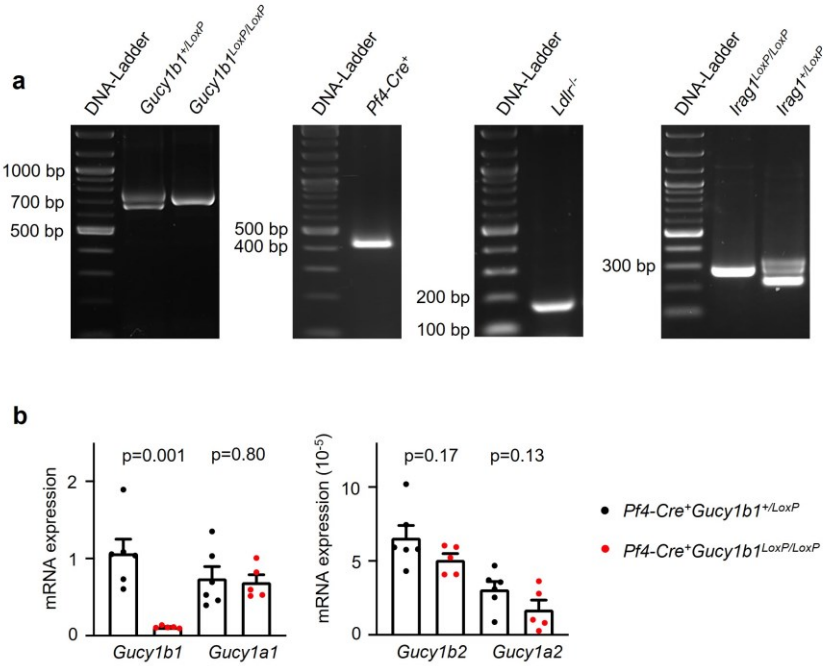

Figure 9 *Gucy* gene and transcript expression analysis. a. The desired genotype of breeding and experimental mice was assured by gel electrophoresis of sequence-specific PCR products from isolated earlobe DNA as specified in the text. **b**. *Gucy* RNA expression in megakaryocytes of *Pf4-Cre*$^{+}$*Gucy1b1*$^{+/LoxP}$ and *Pf4-Cre*$^{+}$*Gucy1b1*$^{LoxP/LoxP}$ mice. The first panel shows *Gucy1b1* and *Gucy1a1* and the second one *Gucy1b2* and *Gucy1a2* expression in relation to *Gucy1b1* wildtype expression. Each symbol represents one independent animal. Two-sided unpaired t-test (pairwise comparisons). Data are mean ± s.e.m. Abbreviations: *bp*, base pairs. Adapted under the terms of the Creative Commons CC BY license: Extended Data Figure 1b,c from reference (Mauersberger et al., 2022).

by a PCR product at 179 bp, while wildtype alleles produced a signal at 350 bp (not shown).

Next, β_1-sGC depletion in platelets of *Pf4-Cre*$^{+}$*Gucy1b1*$^{LoxP/LoxP}$ mice was verified and potential compensational upregulation of other *Gucy1* transcripts was tested. Platelets are anuclear and therefore incapable of *de novo* transcription, but are endowed with their proteome and a specific repertoire of transcripts by their progenitor megakaryocyte (MK) cells (Supernat et al., 2021). Therefore, RNA was directly extracted from MKs, which were isolated from the bone marrow of 6 *Pf4-Cre*$^{+}$*Gucy1b1*$^{+/LoxP}$ and 5 *Pf4-Cre*$^{+}$*Gucy1b1*$^{LoxP/LoxP}$ mice and cultured *ex vivo* in order to augment cellular material. RNA was subjected to qPCR using *Gucy1b1*-, *Gucy1b2*-, *Gucy1a1*-, and *Gucy1a2*-specific probes, respectively. As shown in Figure 9b, *Gucy1b1* expression was downregulated in *Pf4-Cre*$^{+}$*Gucy1b1*$^{LoxP/LoxP}$ platelet progenitors by 89.6 ± 0.7% compared with controls (p=0.001), while levels of *Gucy1a1* transcripts were unchanged. Of note, *Gucy1a2* and *Gucy1b2* expression was negligible (second panel) and numerically alone could not compensate for the β_1-sGC deficit by upregulated expression, in line with the literature reporting $\alpha_1\beta_1$-sGC to be the only relevant isoform in platelets (Makhoul et al., 2018). Therefore, it can be excluded that higher expression of other sGC-subunits thwarted the desired effect of β_1-sGC depletion in this mouse model.

Lastly, in order to ensure protein deletion of β_1-sGC in platelets, different tissues isolated from *Pf4-Cre*$^{+}$*Gucy1b1*$^{+/LoxP}$ and *Pf4-Cre*$^{+}$*Gucy1b1*$^{LoxP/LoxP}$ mice were subjected to protein isolation and Western blotting using an anti-β_1-sGC antibody. Apart from platelets, also aortae and PBMCs were assessed for β_1-sGC expression due to their relevance in atherosclerosis. Lung tissue was included because of its high content of smooth muscle cells (SMC), expressing high levels of sGC. As shown in Figure 10, β_1-sGC expression was greatly reduced in platelets (not quantified), whereas other tissues tested were not relevantly affected, suggesting a platelet-targeted β_1-sGC depletion in the *Pf4-Cre*$^{+}$*Gucy1b1*$^{LoxP/LoxP}$ mouse line.

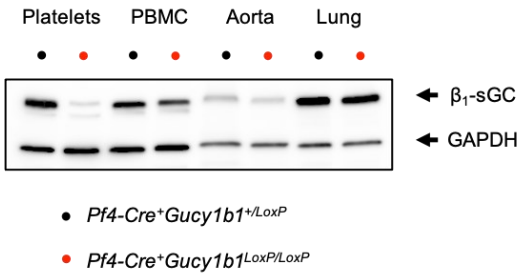

Figure 10 β_1-sGC expression in atherosclerosis-relevant tissues of platelet sGC-deficient mice. Representative Western blot of three independently performed tests shows equal β_1-sGC levels and GAPDH as loading control in peripheral blood mononuclear cells, aorta, and lung but strongly reduced β_1-sGC amount in platelets in *Pf4-Cre*$^{+}$*Gucy1b1*$^{LoxP/LoxP}$ compared with *Pf4-Cre*$^{+}$*Gucy1b1*$^{+/LoxP}$ mice. Abbreviations: *GAPDH*, glyceraldehyde 3-phosphate dehydrogenase; *PBMC*, peripheral blood mononuclear cells. Reprinted under the terms of the Creative Commons CC BY license: Extended Data Figure 1a from reference (Mauersberger et al., 2022).

4.1.2 Effects of β_1-sGC depletion on platelet aggregation

In order to confirm the functional phenotype of the mouse model in platelets, platelet aggregation was examined using PRP of *Pf4-Cre$^+$Gucy1b1$^{LoxP/LoxP}$* and *Pf4-Cre$^+$Gucy1b1$^{+/LoxP}$* mice *in vitro* and aggregation was recorded on an optical aggregometer. Samples were stimulated with the platelet agonists adenosine diphosphate (ADP), the platelet-activated receptor 4 agonist PAR4-AP, the thromboxane analog U46619, or collagen which all trigger platelet aggregation via a different receptor. Suitable concentrations of the reagents were determined in preliminary experiments. As

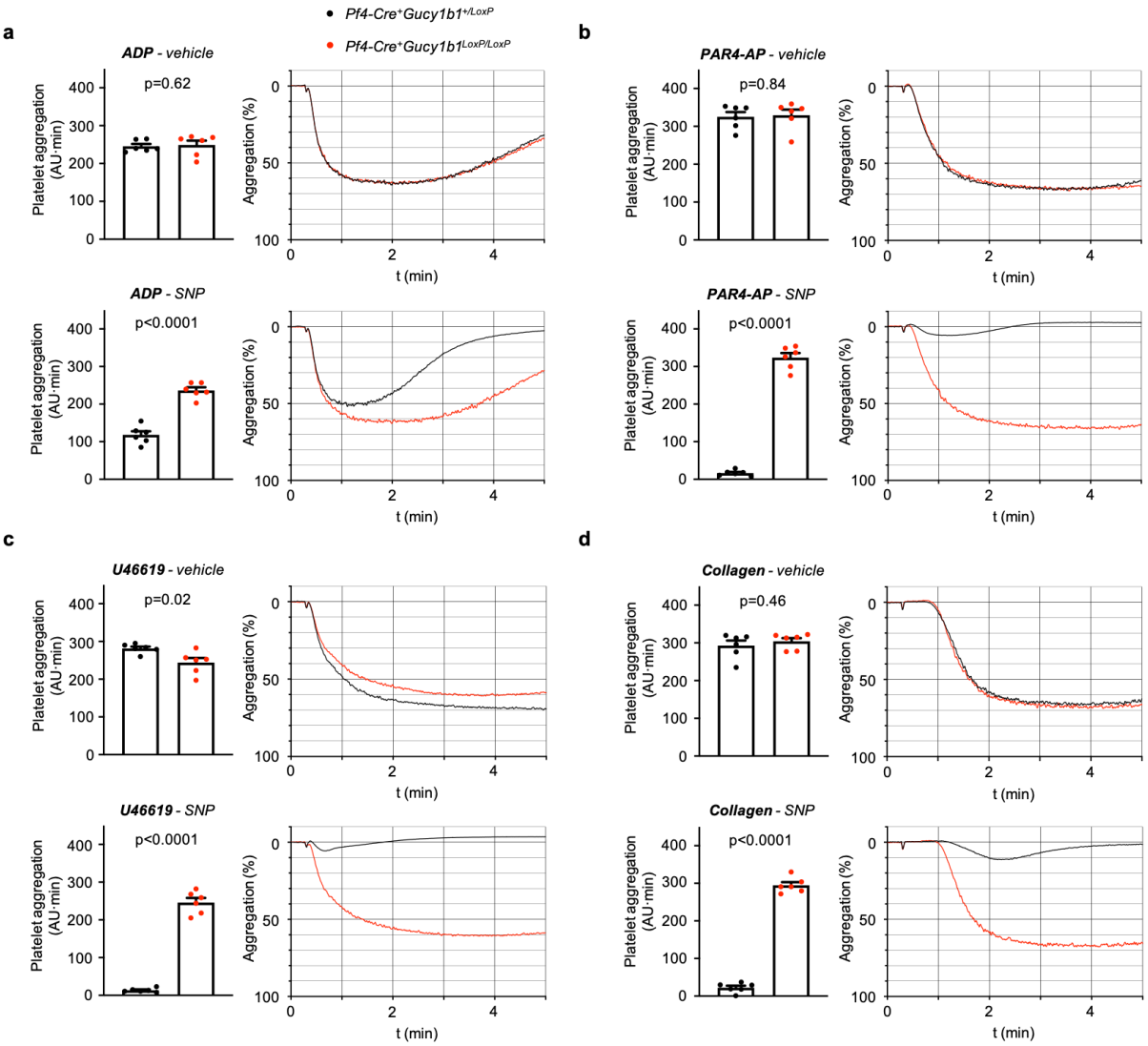

Figure 11 Platelet aggregation in presence of different platelet agonists and SNP. Aggregation profiles of platelets from control (*Pf4-Cre$^+$Gucy1b1$^{+/LoxP}$*) and platelet sGC-deficient (*Pf4-Cre$^+$Gucy1b1$^{LoxP/LoxP}$*) mice after stimulation with (**a**) 2 µM ADP, (**b**) 75 nM of the platelet-activated receptor 4 agonist PAR4-AP, (**c**) 5 µM of the thromboxane analog U46619, or (**d**) 1 µg/ml collagen. Each experiment was performed in the presence of DMSO (vehicle, 0.4%) or the nitric oxide donor sodium nitroprusside (SNP, 10 µM), which decreased platelet aggregation only in sGC wildtype platelets (*Pf4-Cre$^+$Gucy1b1$^{+/LoxP}$*). Each symbol represents one independent animal. Aggregation tracings represent the mean values of the investigated animals. Unpaired t-test (except (**a**), vehicle and (**d**), vehicle: Mann-Whitney test). Data are mean ± s.e.m. Abbreviations: *ADP*, adenosine diphosphate; *AU·min*, arbitrary units, here depicting area under the curve over 5 min of acquisition; *SNP*, sodium nitroprusside. Reprinted under the terms of the Creative Commons CC BY license: Extended Data Figure 2 from reference (Mauersberger et al., 2022).

shown in Figure 11, no differences in aggregation were detectable under baseline conditions (0.4% DMSO) when platelets of both genotypes (n=6 each) were stimulated with ADP, PAR4-AP, or collagen, while platelets lacking functional sGC showed slightly less aggregation after U46619 stimulation compared with sGC wildtype platelets as measured by area under the curve (AUC) of aggregation curves (244.0 ± 12.2 *vs.* 281.5 ± 4.9 arbitrary units (AU·min); p=0.02). Next, samples were briefly incubated with the NO donor sodium nitroprusside (SNP) before the platelet agonists were added. Importantly, this resulted in inhibited platelet aggregation in *Pf4-Cre*$^{+}$*Gucy1b1*$^{+/LoxP}$, but not in *Pf4-Cre*$^{+}$*Gucy1b1*$^{LoxP/LoxP}$ platelets following the addition of all four platelet agonists (lower panels of Figure 11a, b, c, and d; ADP: 118.2 ± 9.8 *vs.* 236.5 ± 8.2 AU·min; PAR4-AP: 16.7 ± 3.0 *vs.* 323.7 ± 12.4 AU·min; U46619: 13.5 ± 2.1 *vs.* 246.0 ± 12.1 AU·min; collagen: 22.3 ± 5.2 *vs.* 294.7 ± 8.3 AU·min). As expected, due to functional sGC-deficiency, the *Pf4-Cre*$^{+}$*Gucy1b1*$^{LoxP/LoxP}$ mice were unresponsive to the NO donor sodium nitroprusside (SNP) which inhibits platelet aggregation via sGC stimulation.

4.2 Atherosclerosis-related phenotype of mice lacking platelet sGC

4.2.1 Basic characteristics

Pf4-Cre^{+}*Gucy1b1*$^{LoxP/LoxP}$*Ldlr*$^{-/-}$ and *Pf4-Cre*$^{+}$*Gucy1b1*$^{+/LoxP}$*Ldlr*$^{-/-}$ mice were fed a high cholesterol (Western) diet for either 6 weeks (atherogenesis) or 10 weeks (advanced atherosclerosis) in order to investigate the impact of sGC deficiency in platelets on atherosclerosis-related phenotypes. Only a negligibly small number of animals (<0.5% in all groups; not shown) had to be removed prematurely from the experiments, and no genotype-specific abnormalities or increase in stress symptoms were observed between both groups.

The body weight of the animals is depicted in Figure 12a before and after Western diet and shows no significant difference between both groups (n=11), suggesting similar calorie intake. Figure 12b+c displays plasma cholesterol and PRP platelet levels at the end of the ten-weeks Western diet. Neither of the investigated values revealed significant differences between *Pf4-Cre*$^{+}$*Gucy1b1*$^{LoxP/LoxP}$*Ldlr*$^{-/-}$ and *Pf4-Cre*$^{+}$*Gucy1b1*$^{+/LoxP}$*Ldlr*$^{-/-}$ mice, indicating no relevant influence of platelet sGC on lipid metabolism or blood platelet counts in this model. Also, plasma levels of the chemokines CXCL3, 5, 7, and 15, which were introduced in an additional copy in the genome of these mice via the BAC clone used for the generation of the respective strain, were not significantly different between both groups (Appendix Figure 1).

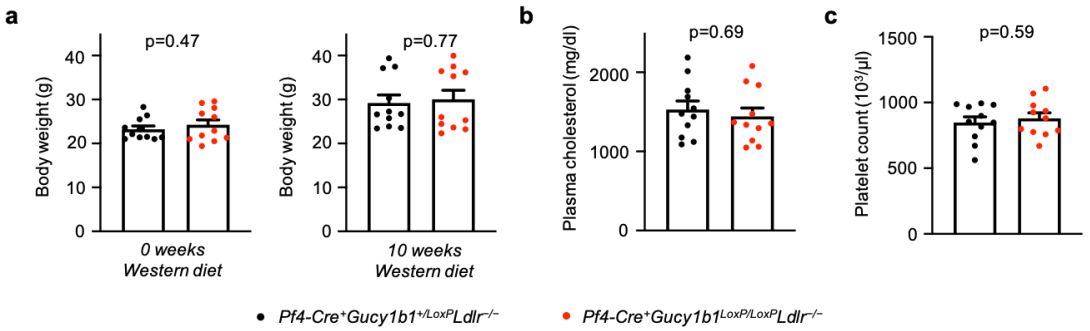

Figure 12 Body weight development and blood characteristics in mice lacking platelet sGC. No significant differences between *Pf4-Cre*$^{+}$*Gucy1b1*$^{LoxP/LoxP}$*Ldlr*$^{-/-}$ and *Pf4-Cre*$^{+}$*Gucy1b1*$^{+/LoxP}$*Ldlr*$^{-/-}$ mice regarding (**a**) body weight at baseline (left) and after ten weeks of Western diet (right), (**b**) plasma cholesterol levels, and (**c**) PRP platelet count as assessed using an automated hematology analyzer. Each symbol represents one animal. Data are mean ± s.e.m. Unpaired t-test. Reprinted under the terms of the Creative Commons CC BY license: Extended Data Figure 3a-c from reference (Mauersberger et al., 2022).

To assess blood leukocyte numbers and any related impact on leukocyte recruitment to atherosclerotic plaques, monocytes and neutrophil levels in full blood were investigated by flow

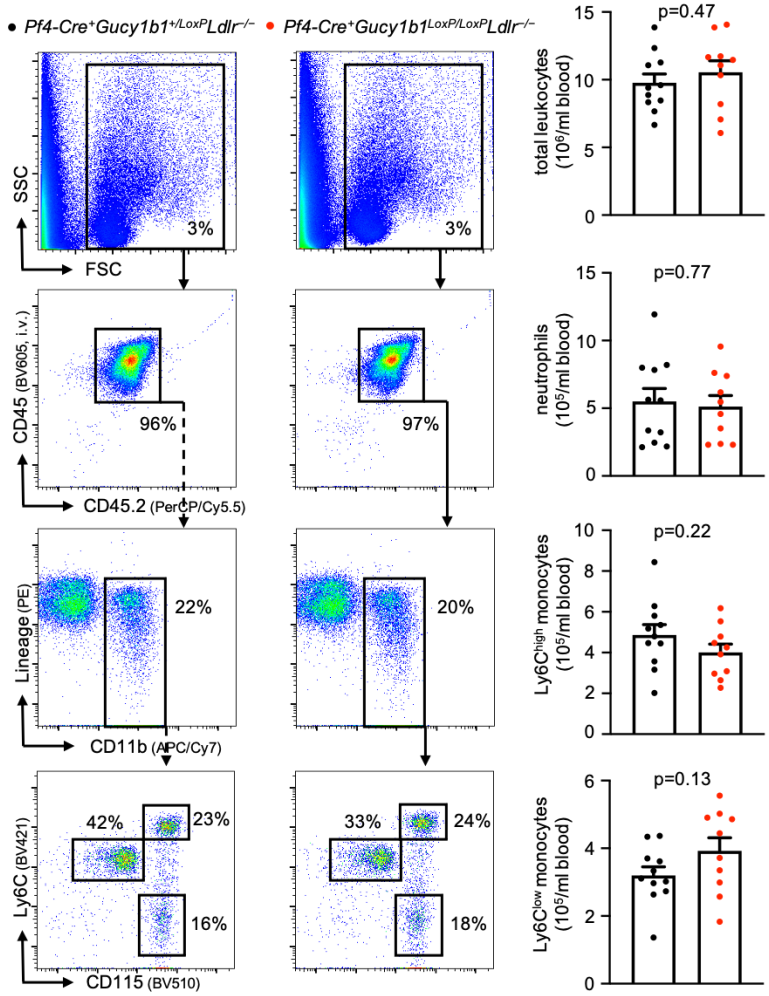

Figure 13 Blood leukocyte numbers in platelet sGC-deficient mice after Western diet. Total leukocytes, neutrophils, Ly6C^{high}, or Ly6C^{low} monocytes display no quantitative differences in the blood of *Pf4-Cre*$^{+}$*Gucy1b1*$^{LoxP/LoxP}$*Ldlr*$^{-/-}$ compared with *Pf4-Cre*$^{+}$*Gucy1b1*$^{+/LoxP}$*Ldlr*$^{-/-}$ mice after 10 weeks of Western diet (n=10 *vs.* n=11 independent animals). Each symbol represents one animal. Unpaired t-test. One outlier was removed in the analysis of Ly6C^{low} monocytes according to the ROUT method. Data are mean ± s.e.m. Reprinted under the terms of the Creative Commons CC BY license: Extended Data Figure 3d from reference (Mauersberger et al., 2022).

cytometry using fluorophore-conjugated antibodies raised against common surface markers of the respective cells. The gating strategy as well as resultant absolute cell numbers per group are depicted in Figure 13. No quantitative differences in total leukocytes, neutrophils, and pro-inflammatory Ly6C^{high} or anti-inflammatory Ly6C^{low} monocytes were detected between the blood of 10 atherosclerotic *Pf4-Cre*$^{+}$*Gucy1b1*$^{LoxP/LoxP}$*Ldlr*$^{-/-}$ and 11 *Pf4-Cre*$^{+}$*Gucy1b1*$^{+/LoxP}$*Ldlr*$^{-/-}$ mice. Therefore, it can be concluded that the blood supply for leukocyte migration into inflammatory tissues is not markedly different between both groups.

4.2.2 Atherosclerotic plaque formation

The size and cellular composition of atherosclerotic plaques are key markers of atherosclerosis progression in mice. A characteristic anatomic site to investigate for this use is the aortic root, as plaques readily form in the vicinity of aortic valves due to altered blood flow characteristics. *Pf4-Cre*$^{+}$*Gucy1b1*$^{LoxP/LoxP}$*Ldlr*$^{-/-}$ mice were already shown to exhibit significantly larger atherosclerotic lesions in aortic roots than respective controls after 10 weeks of Western diet (Figure 6). Thus, to comprehend the plaque distribution throughout the whole aorta, *en face*-opened aortae from both groups were analyzed from the aortic arch to the branch of the right renal artery by oil red O staining. This stain specifically highlights lipids as a typical marker of atherosclerotic plaques. As shown in Figure 14a, *Pf4-Cre*$^{+}$*Gucy1b1*$^{LoxP/LoxP}$*Ldlr*$^{-/-}$ mice revealed larger aortic plaques than controls after 10 weeks of Western diet (5.4 ± 0.7% (n=8) *vs.* 3.9 ± 0.2% (n=9), p=0.03).

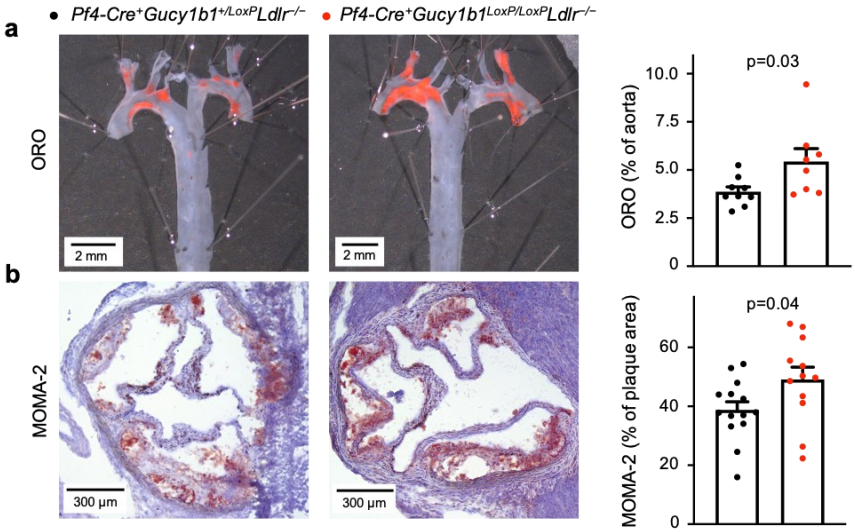

Figure 14 Atherosclerotic plaque formation in mice lacking platelet sGC. Enhanced atherosclerotic plaque formation as assessed by (**a**) aortic *en face* ORO staining and (**b**) monocyte and macrophage content in 12 (**a**: 8) *Pf4-Cre*$^{+}$*Gucy1b1*$^{LoxP/LoxP}$*Ldlr*$^{-/-}$ mice compared with 14 (**a**: 9) *Pf4-Cre*$^{+}$*Gucy1b1*$^{+/LoxP}$*Ldlr*$^{-/-}$ mice that were fed a Western diet for 10 weeks. Two-sided unpaired t-test. Each symbol represents one independent animal. Data are mean ± s.e.m. Abbreviations: *MOMA-2*: monocyte and macrophage specific antibody, *ORO*: oil red O. Reprinted under the terms of the Creative Commons CC BY license: Figure 1b,c from reference (Mauersberger et al., 2022).

Abdominal parts of the aortae were not included in the analysis, as they did not display appreciable lesions in both groups.

Next, in order to test whether larger aortic plaques were also concomitant with a higher density of leukocytes, particularly monocytes and macrophages, immunohistochemistry was performed on aortic root sections from both groups using a cell type-specific antibody. Indeed, *Pf4-Cre*$^{+}$*Gucy1b1*$^{LoxP/LoxP}$*Ldlr*$^{-/-}$ mice exhibited higher monocyte and macrophage content per plaque area, as indicated by the brown chromogenic stain in the representative images in Figure 14b (49.1 ± 4.2% (n=12) *vs.* 38.8 ± 2.8% (n=14), p=0.04). To conclude, aortic lesions were significantly larger in sGC-deficient mice compared with controls, concomitant with a higher density of monocytes and macrophages within the atherosclerotic plaques.

4.2.3 Vascular inflammation

Apart from aortic plaque size, the cellular composition of immune cells within plaques is an important marker of vascular inflammation in mice. To follow up on the finding of higher monocyte and macrophage density within aortic plaques in Figure 14b, aortic leukocyte

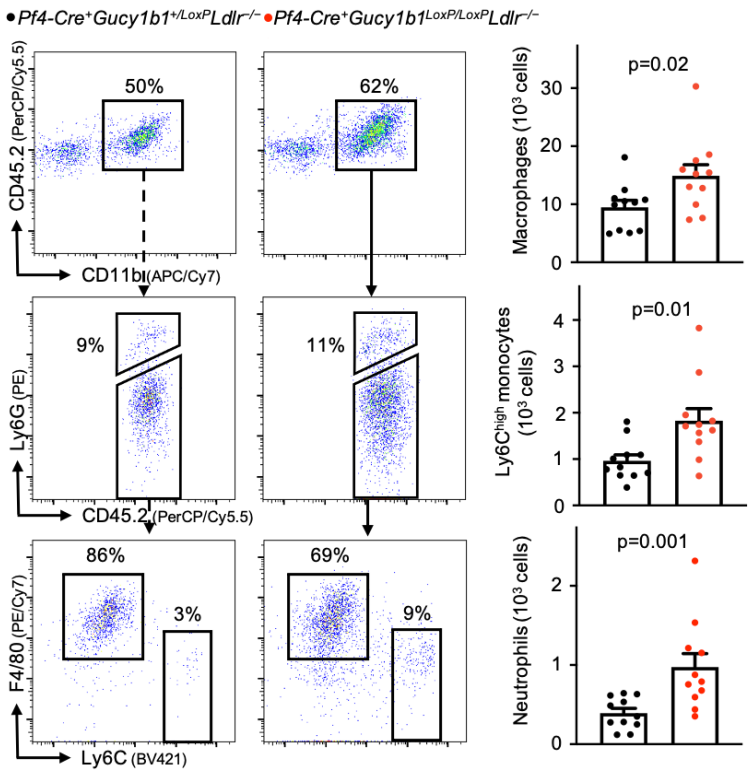

Figure 15 Vascular inflammation in mice lacking platelet sGC. Flow cytometry analysis of aortic cell suspensions reveals higher numbers of leukocyte subsets in *Pf4-Cre*$^{+}$*Gucy1b1*$^{LoxP/LoxP}$*Ldlr*$^{-/-}$ compared with *Pf4-Cre*$^{+}$*Gucy1b1*$^{+/LoxP}$*Ldlr*$^{-/-}$ mice (n=11 per group). Two-sided Mann–Whitney U-test. Each symbol represents one independent animal. Data are mean ± s.e.m. Reprinted under the terms of the Creative Commons CC BY license: Figure 1e from reference (Mauersberger et al., 2022).

subpopulations of *Pf4-Cre*$^{+}$*Gucy1b1*$^{LoxP/LoxP}$*Ldlr*$^{-/-}$ and *Pf4-Cre*$^{+}$*Gucy1b1*$^{+/LoxP}$*Ldlr*$^{-/-}$ mice were subsequently quantified by flow cytometry after 10 weeks of Western diet. As depicted in Figure 15, mice lacking platelet sGC displayed significantly higher numbers of macrophages (14,895 ± 1,912 *vs.* 9,463 ± 1,211 cells, p=0.02), inflammatory Ly6C^{high} monocytes (1,829 ± 262 *vs.* 964 ± 129 cells, p=0.01), as well as neutrophils (974 ± 170 *vs.* 392 ± 60 cells, p=0.001) within aortae than sGC-wildtype mice (n=11 each).

4.2.4 *In vivo* leukocyte adhesion

The next question addressed was whether the finding of larger plaque sizes and higher content of leukocyte populations within plaques was due to active leukocyte recruitment from the blood. Leukocyte adhesion to EC is the first step of recruitment into atherosclerotic plaques and was therefore assessed as a surrogate marker of active leukocyte recruitment *in vivo*. Therefore, intravital fluorescence microscopy was conducted on the right carotid artery bifurcation of *Pf4-Cre*$^{+}$*Gucy1b1*$^{LoxP/LoxP}$*Ldlr*$^{-/-}$ and respective control mice after six weeks of Western diet, representing an early phase of plaque growth. Imaging and subsequent analyses were conducted by Prof. Oliver Söhnlein (Universität Münster, Germany). To this end, CD11b^{+} myeloid cells were fluorescently labeled and found to adhere in higher numbers to arteries of 13 *Pf4-Cre*$^{+}$*Gucy1b1*$^{LoxP/LoxP}$*Ldlr*$^{-/-}$ compared with 11 *Pf4-Cre*$^{+}$*Gucy1b1*$^{+/LoxP}$*Ldlr*$^{-/-}$ mice (20.9 ± 1.5 *vs.* 13.6 ± 1.4, p=0.001). Similarly,

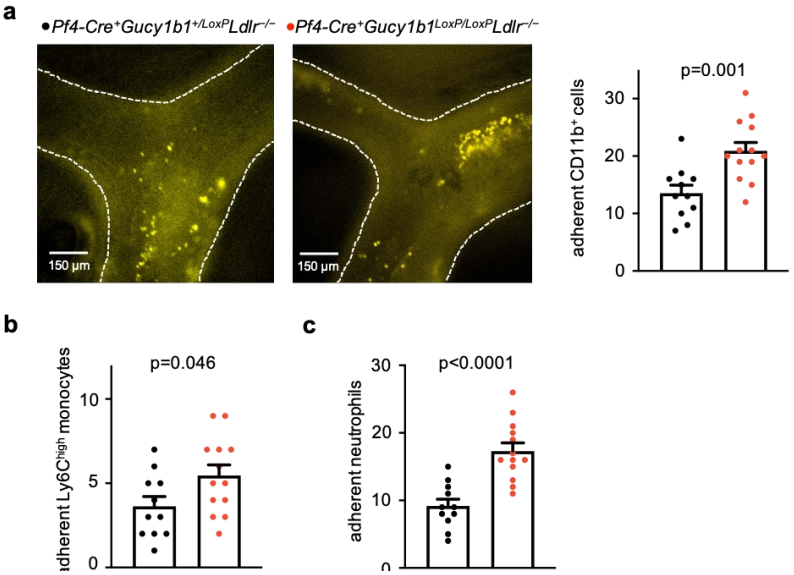

Figure 16 *In vivo* leukocyte adhesion in mice lacking platelet sGC. Leukocyte adhesion to atherosclerotic plaques was assessed by fluorescence intravital microscopy in right carotid artery bifurcations. Significantly larger amounts of adherent (**a**) CD11b^{+} cells, (**b**) Ly6C^{high} monocytes, and (**c**) neutrophils were found in *Pf4-Cre*$^{+}$*Gucy1b1*$^{LoxP/LoxP}$*Ldlr*$^{-/-}$ (n=13) compared with *Pf4-Cre*$^{+}$*Gucy1b1*$^{+/LoxP}$*Ldlr*$^{-/-}$ mice (n=11) following a 6 weeks Western diet. Each symbol represents one independent animal. Two-sided unpaired t-test. Data are mean ± s.e.m. Reprinted under the terms of the Creative Commons CC BY license: Figure 1d and Extended Data Figure 4 from reference (Mauersberger et al., 2022). Measurement and analysis were conducted by Prof. Oliver Söhnlein (Universität Münster, Germany).

Ly6C^{high} monocytes (5,5 ± 0.6 *vs.* 3.6 ± 0.6, p=0.046) and neutrophils (17.3 ± 1.2 *vs.* 9.2 ± 1.0, p<0.0001) adhered in higher numbers to atherosclerotic plaques in mice lacking platelet sGC (Figure 16). Essentially, at this early time point, aortic plaque sizes were not significantly different between both groups (Appendix Figure 2). This observation is important, as the presence of atherosclerotic lesions strongly increases leukocyte recruitment. Therefore, it can be indeed assumed likely, that leukocyte adhesion – the first step toward leukocyte ingress into plaques – is causally involved in plaque formation in platelet-specific sGC-deficient mice.

4.3 Investigating the atherogenic effects of platelet sGC deficiency *in vitro*

4.3.1 *In vitro* leukocyte-endothelium adhesion

The above results clearly indicate enhanced leukocyte adhesion to atherosclerotic plaques in platelet sGC-deficient mice. Thus, the next step was to perform *in vitro* adhesion experiments to further investigate how the mutant platelet genotype is linked to increased leukocyte-endothelium adhesion. To mimic as closely as possible the *in vivo* adhesion of leukocytes to EC in early atherosclerosis of sGC-deficient mice, wildtype EC and wildtype leukocytes isolated from C57BL/6 J mice were therefore incubated with releasate of either *Pf4-Cre^{+}Gucy1b1$^{+/LoxP}$* or *Pf4-Cre^{+}Gucy1b1$^{LoxP/LoxP}$* derived platelets. By using platelet-released factors, a key mechanism of platelets to influence early atherogenesis was targeted while avoiding platelet aggregation in the sense of atherothrombosis during the experiment. Similarly, shaking – which is intended to mimic impaired flow in atherosclerosis-prone arteries and only moderately activates platelets as shown by the reduced release of granule components as compared with platelet agonists (Appendix Figure 3) – was preferred to agonist-stimulated activation because of its stronger link to the role of platelets in early atherogenesis. The resultant experimental scheme is depicted in Figure 17a.

As a result and in line with the *in vivo* findings, *Pf4-Cre^{+}Gucy1b1$^{LoxP/LoxP}$* platelet releasate enhanced both monocyte (33,125 ± 1,313 *vs.* 27,039 ± 555 relative fluorescence units (RFU), p=0.006) and neutrophil adhesion (33,810 ± 1,139 *vs.* 27,824 ± 758 RFU, p=0.0002, n=8) to EC by over 20% compared with respective controls (Figure 17b). In contrast, using neutrophils from *Pf4-Cre^{+}Gucy1b1$^{LoxP/LoxP}$* mice did not increase their adhesion to wildtype EC when incubated with wildtype platelets compared with *Pf4-Cre^{+}Gucy1b1$^{+/LoxP}$* neutrophils (Appendix Figure 4), clearly attributing this phenotype to lack of sGC in platelets.

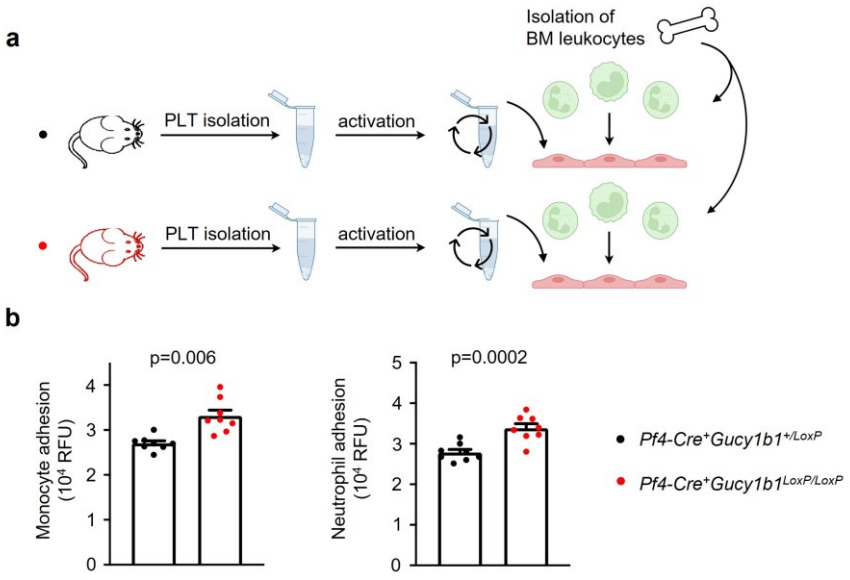

Figure 17 ***In vitro*** **leukocyte adhesion in presence of sGC-deficient platelet releasate. a**. Experimental scheme: Platelets were isolated from *Pf4-Cre*$^{+}$*Gucy1b1*$^{+/LoxP}$ and *Pf4-Cre*$^{+}$*Gucy1b1*$^{LoxP/LoxP}$ mice, activated by shaking, and supernatant incubated with EC and leukocytes derived from wildtype animals. **b**. Both monocytes and neutrophils adhered more to EC when incubated with *Pf4-Cre*$^{+}$*Gucy1b1*$^{LoxP/LoxP}$ platelet supernatant. Each symbol represents one sample derived from one independent animal (n=8 per group). Two-sided unpaired t-test. Data are mean ± s.e.m. Abbreviations: *BM*, bone marrow; *PLT*, platelet; *RFU*, relative fluorescence units. Reprinted under the terms of the Creative Commons CC BY license (**b**): Figure 2a,b from reference (Mauersberger et al., 2022).

Platelet factors can target both leukocytes and EC to mediate leukocyte adhesion. Thus, to clarify which cell type was specifically affected by platelet factors in this assay, neutrophils and EC were incubated separately with sGC-deficient-platelet releasate and then added to the respective other, naïve, cell type that was not contacted with platelet factors. Compared with mutual or neutrophil-exclusive incubation, EC exposed to the platelet material strongly enhanced subsequent adhesion of neutrophils (31,383 ± 1,731 *vs.* 25,097 ± 1,709 and 22,254 ± 1,662 RFU, p_{adj}=0.04 and 0.0003, respectively, n=12 sample pairs, Figure 18a). A similar result was observed when monocytes

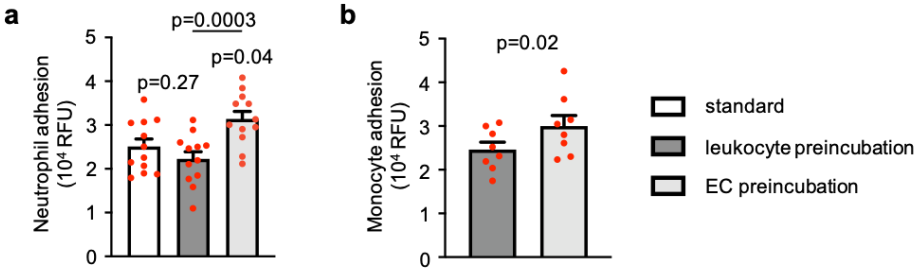

Figure 18 Leukocyte adhesion after preincubating leukocytes or EC with platelet releasate. a. Enhanced neutrophil adhesion after preincubation of ECs compared with neutrophils with supernatant of activated platelets from *Pf4-Cre*$^{+}$*Gucy1b1*$^{LoxP/LoxP}$ mice. Non-preincubation conditions with mutual incubation of both cell types with platelet material following Figure 17 were included as a standard. Each symbol represents one paired sample (each derived from n=12 independent animals). Repeated measures one-way ANOVA with Tukey test for multiple testing. **b**. Monocyte adhesion after exposing monocytes or EC to releasate of sGC-deficient platelets. Each symbol represents one paired sample (derived from n=8 independent animals). Two-sided paired t-test. Data are mean ± s.e.m. Abbreviations: *EC*, endothelial cells; *RFU*, relative fluorescence units. Reprinted under the terms of the Creative Commons CC BY license: Figure 2c and Extended Data Figure 5 from reference (Mauersberger et al., 2022).

instead of neutrophils were included in this experiment, with significantly more adherent monocytes after exclusive exposure of EC to platelet releasate than to releasate-exposed monocytes (30,007 ± 2,406 *vs.* 24,626 ± 1,683 RFU, p=0.02, n=8 sample pairs, Figure 18b).

These data indicate that sGC deficiency in platelets results in an altered release of soluble factors from platelets after activation. These factors contribute to increased adhesion of neutrophils and monocytes to EC, primarily by targeting EC.

4.3.2 Differentially released factors from sGC-deficient platelets

Next, in order to identify differentially released soluble factors from platelets lacking functional sGC, a cytokine profiling assay capable of detecting more than 100 cytokines was performed on *Pf4-Cre*$^{+}$*Gucy1b1*$^{LoxP/LoxP}$ and *Pf4-Cre*$^{+}$*Gucy1b1*$^{+/LoxP}$ platelet releasates. Thereby, two proteins with release dynamics potentially influenced by sGC were identified: Angiopoietin-1 (ANGPT1), which was found at lower levels (3.2 ± 0.4 (n=7) *vs.* 6.7 ± 0.8 (n=8) arbitrary units (AU), p=0.002), and retinol-binding protein 4 (RBP4; 4.4 ± 0.5 *vs.* 3.7 ± 0.5 AU, p=0.01, n=8 each), which was found at higher levels in sGC-deficient platelet samples (Figure 19). ANGPT1 is a glycoprotein mainly secreted by peri-endothelial cells and platelets which regulates angiogenesis and cell permeability (Milam & Parikh, 2015). RBP4 is a retinol transport protein involved in ocular physiology but also associated with CAD risk (Sun et al., 2013). Therefore, both proteins appeared to be promising candidates for further investigation.

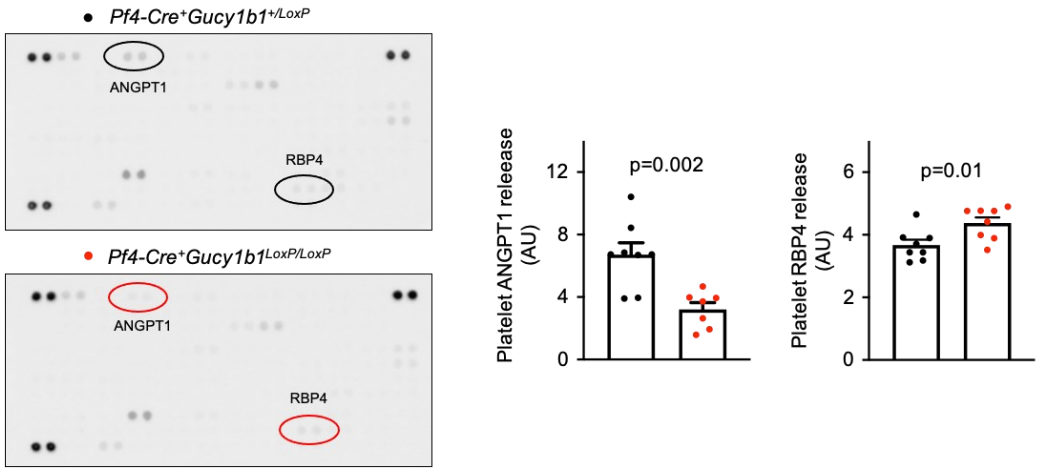

Figure 19 Differentially released soluble factors from shake-activated platelets lacking sGC. Cytokine profiling suggested decreased angiopoietin-1 and increased retinol binding protein 4 levels in *Pf4-Cre*$^{+}$*Gucy1b1*$^{LoxP/LoxP}$ compared with *Pf4-Cre*$^{+}$*Gucy1b1*$^{+/LoxP}$ platelet releasate after shaking. Each symbol represents one sample (derived from n=8 or 7 independent animals). Two-sided unpaired t-test. One outlier was removed in the analysis of ANGPT1 according to the ROUT method. Data are mean ± s.e.m. Abbreviations: *ANGPT1*, angiopoietin-1; *AU*, arbitrary units; *RBP4*, retinol binding protein 4. Reprinted under the terms of the Creative Commons CC BY license: Figure 3a from reference (Mauersberger et al., 2022).

Next, the assumption of differentially released ANGPT1 and RBP4 from sGC-deficient platelets was verified by ELISA. ANGPT1 was confirmed to be significantly less present in *Pf4-Cre*$^{+}$*Gucy1b1*$^{LoxP/LoxP}$ compared with *Pf4-Cre*$^{+}$*Gucy1b1*$^{+/LoxP}$ platelet releasate after shaking (30.4 ± 6.4 *vs.* 60.3 ± 4.7 ng/ml, p=0.004, n=6 each; Figure 20a). However, enhanced RBP4 amount in these samples could not be replicated (Figure 20b, n=5 each) and was therefore not pursued further. Additionally, a selection of other important platelet α- and dense granule factors including PF4, P-selectin, and serotonin was examined by ELISA, but none of the factors tested was found in significantly different quantities in the platelet releasate of both groups (Appendix Figure 5). In order to clarify whether differential amounts of ANGPT1 in platelet releasate are due to lower protein expression or due to altered release kinetics, ANGPT1 was quantified in quiescent platelets. As depicted in Figure 20c, ANGPT1 amount was not markedly different between control and sGC-deficient platelets (5.5 ± 0.3 *vs.* 5.2 ± 0.3 pg/10^3 platelets, p=0.52, n=6 each), indicating similar ANGPT1 expression in both groups. Likewise, ANGPT1 content in platelet-poor plasma (PPP) was not altered in mice of both genotypes (0.6 ± 0.2 (n=6) *vs.* 0.4 ± 0.1 ng/ml (n=5), p= 0.46). This renders it unlikely that ANGPT1 was released more into the circulation from sGC-deficient platelets prior to their isolation.

In summary, these data support the notion that lack of sGC in platelets inhibits ANGPT1 release from platelets upon activation.

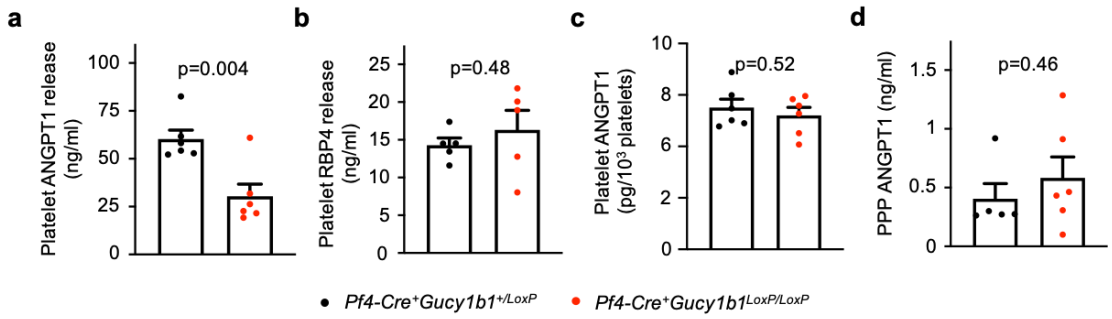

Figure 20 Differential release of ANGPT1 from shake-activated platelets lacking sGC. Protein quantification by ELISA in platelet releasate from *Pf4-Cre*$^{+}$*Gucy1b1*$^{LoxP/LoxP}$ compared with *Pf4-Cre*$^{+}$*Gucy1b1*$^{+/LoxP}$ mice (n=6 each) confirms (**a**) lower platelet ANGPT1 release from sGC-deficient platelets after shaking, whereas (**b**) RBP4 platelet releasate concentrations (n=5 each) were not significantly altered. ANGPT1 content in (**c**) unstimulated platelets and (**d**) PPP indicate no difference between samples (n=5 and 6 independent animals, respectively). Two-sided unpaired t-test. Data are mean ± s.e.m. Abbreviations: *ANGPT1*, angiopoietin-1; *PPP*, platelet-poor plasma; *RBP4*, retinol binding protein 4. Reprinted under the terms of the Creative Commons CC BY license: Figure 3c,d and Extended Data Figure 7i from reference (Mauersberger et al., 2022).

4.4 Linking platelet sGC activity and ANGPT1

4.4.1 ANGPT1 and leukocyte-endothelium adhesion

In the next step, it was tested whether ANGPT1 as the only confirmed differentially released protein from over 100 tested cytokines in sGC-deficient platelet releasate is indeed linked to the leukocyte adhesion phenotype (section 4.3.1). To this end, ANGPT1-mediated effects on EC were interrupted by using an inhibitor of the tyrosine kinase TIE2 (tyrosine kinase with immunoglobulin-like and EGF-like domains 2). TIE2 functions as the ANGPT1 receptor on EC and mediates ANGPT1-related functions via intracellular signaling (Peters et al., 2004). In this experiment, EC were therefore incubated with the TIE2-specific inhibitor BAY-826 or vehicle and subsequently, adhesion of neutrophils quantified in presence of platelet releasate. Indeed, as shown in Figure 21, neutrophil adhesion to EC increased by 17% (± 1.2%, p=0.04, n=11 sample pairs) when the ANGPT1-TIE2-axis was interrupted by the inhibitor. Since BAY-826 is specifically targeting TIE2, the only known receptor mediating ANGPT1 function in the vasculature (Schneider et al., 2017), these data suggest that less release of ANGPT1 from activated sGC-deficient platelets is associated with more adhesion of leukocytes, particularly neutrophils, to EC. Although ANGPT1 is likely not the only protein affected by sGC deficiency, these results may contribute to a better understanding of how sGC deficiency and leukocyte recruitment to EC are related *in vivo*.

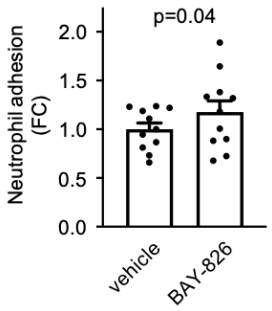

Figure 21 Neutrophil-endothelium adhesion in interrupted ANGPT1-TIE2 signaling. Wildtype neutrophils increase adhesion to EC after incubation with activated wildtype platelet releasate in presence of the Tie2 inhibitor BAY-826 (0.5 µM) compared with vehicle conditions. Two-sided paired t-test on n=11 sample pairs derived from independent animals. Data are mean ± s.e.m. Abbreviations: *FC*, fold change. Reprinted under the terms of the Creative Commons CC BY license: Figure 3e from reference (Mauersberger et al., 2022).

4.4.2 ANGPT1 and sGC expression in humans

While sGC expression in *Pf4-Cre*$^{+}$*Gucy1b1*$^{LoxP/LoxP}$ platelet progenitors is genetically reduced to near zero (Figure 9), human carriers of the rs7692387 risk variant also exhibit markedly reduced sGC

expression in whole blood samples (Kessler et al., 2017). Therefore, ANGPT1 levels in human platelet samples were quantified analogously to the murine samples as a function of *GUCY1A1* risk or non-risk genotype at the rs7692387 locus. Hence, PRP was isolated from 5 healthy subjects per genotype (non-risk: AA/AG *vs.* risk: GG) and shake-activated releasate subjected to ELISA. The baseline characteristics of the enrolled individuals are depicted in Table 30. Age, gender, presence of CAD, and intake of antiplatelet medication were all comparable in the enrolled participants. Platelet counts as measured in PRP were tendentially lower in carriers of the risk genotype, but the difference was not statistically significant.

Table 30 Baseline characteristics of individuals enrolled for investigating platelet ANGPT1 release. Unless otherwise indicated, data are mean ± s.e.m. * Unpaired t-test, † Chi-square test. Abbreviations: *PRP*, platelet-rich plasma. Reprinted under the terms of the Creative Commons CC BY license: Supplementary Table 3 from reference (Mauersberger et al., 2022).

Characteristic	AA/AG genotype	GG genotype	p-value
Age, years	37.4 ± 5.3	30.8 ± 1.8	0.27*
Female gender, n (%)	4 (80)	4 (80)	>0.99†
Presence of CAD, n (%)	0 (0)	0 (0)	>0.99†
Antiplatelet medication, n (%)	0 (0)	0 (0)	>0.99†
PRP platelet count, 10^3 platelets	365.8 ± 52.2	261.0 ± 18.2	0.09*

Platelet releasate derived from homozygous risk variant carriers indeed revealed significantly lower ANGPT1 levels compared with non-risk variant-related samples (4.5 ± 0.7 *vs.* 8.3 ± 1.4 ng/ml, p=0.04, Figure 22a). In line with the mouse data, unstimulated platelets furthermore did not exhibit differential levels of ANGPT1 prior to activation (12.3 ± 1.9 *vs.* 12.1 ± 1.6 ng/ml, p=0.94, Figure 22b). This indicates a link between sGC function and platelet ANGPT1 release under physical stress also in humans.

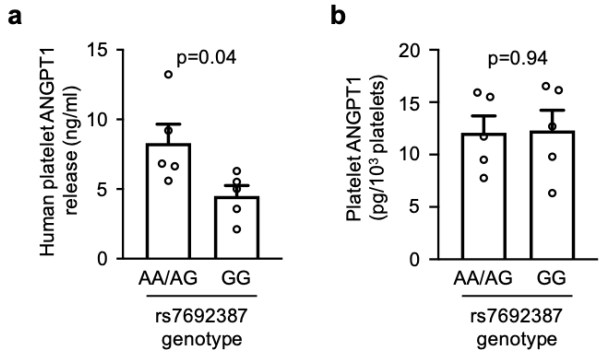

Figure 22 ANGPT1 levels in human platelet releasate and unstimulated platelets. a. ANGPT1 levels in platelet releasate of five individuals carrying the *GUCY1A1* (rs7692387) non-risk (AA, AG genotype) allele and five homozygous carriers of the risk allele (GG genotype) indicates significantly lower release from risk allele platelets as assessed by ELISA. **b**. ANGPT1 content in quiescent platelets is comparable between both groups. Each symbol represents one individual. Two-sided unpaired t-test. Data are mean ± s.e.m. Reprinted under the terms of the Creative Commons CC BY license (**a**): Figure 4f from reference (Mauersberger et al., 2022).

4.5 sGC stimulation in platelets

The above results clearly indicate that sGC deficiency decreases platelet ANGPT1 release, increases leukocyte-endothelium adhesion, and, as a suggestive consequence, promotes atherosclerotic plaque formation and vascular inflammation in mice. Next, in order to prove a biological correlation between ANGPT1 release and sGC activity, sGC was stimulated – in contrast to the previous experiments based on sGC deficiency. Apart from genetic modifications, this can be accomplished by the use of sGC stimulators or activators, a new class of drugs already approved for the treatment of PH or HFrEF (section 1.3.2). Here, the novel sGC stimulator BAY-747 with similar properties as vericiguat was used. Up to a concentration of 150 ppm, only minor hypotensive effects of BAY-747 were observed in mice (Krishnan et al., 2021). Therefore and for reasons of uniformity, a concentration of 150 ppm of BAY-747 was chosen for all experiments.

4.5.1 Functional implications

First, targeting of platelets by BAY-747 was verified by aggregometry. To this end, platelets were incubated with BAY-747 or vehicle before aggregation was induced by ADP. As shown in Figure

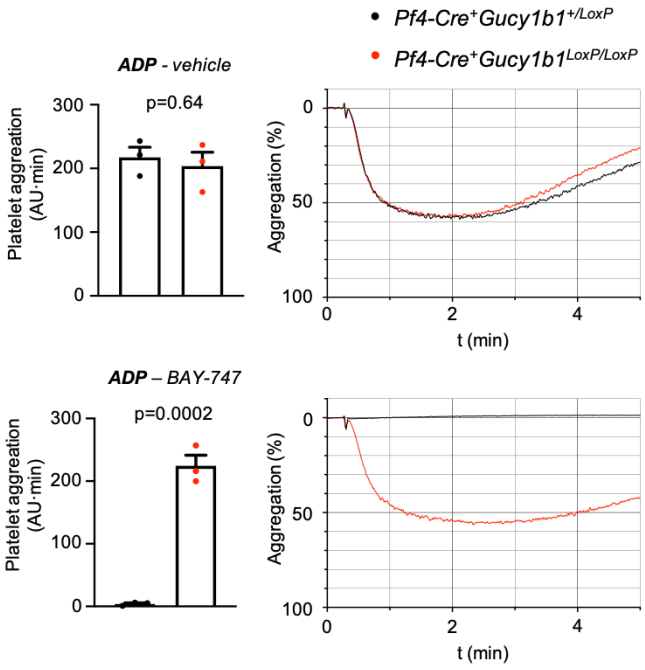

Figure 23 Platelet aggregation in presence of the sGC stimulator BAY-747. ADP-induced platelet aggregation (2 µM) in platelets (n=3 each) isolated from *Pf4-Cre*$^{+}$*Gucy1b1*$^{LoxP/LoxP}$ or *Pf4-Cre*$^{+}$*Gucy1b1*$^{+/LoxP}$ mice is similar under baseline conditions (upper panel). Upon sGC stimulation (lower panel, 150 ppm BAY-747), *Pf4-Cre*$^{+}$*Gucy1b1*$^{+/LoxP}$ platelets abolish ADP-induced aggregation whereas *Pf4-Cre*$^{+}$*Gucy1b1*$^{LoxP/LoxP}$ platelets are unaffected by BAY-747. Each symbol represents one independent animal. Aggregation tracings represent the mean values of investigated animals. Two-sided unpaired t-test. Data are mean ± s.e.m. Abbreviations: *ADP*, adenosine diphosphate, *AU·min*: arbitrary units, here depicting area under the curve over 5 min of acquisition. Reprinted under the terms of the Creative Commons CC BY license: Extended Data Figure 9 from reference (Mauersberger et al., 2022).

23, aggregation was comparable between both groups under baseline conditions (vehicle). As expected, *Pf4-Cre*$^{+}$*Gucy1b1*$^{LoxP/LoxP}$ platelets displayed the same aggregatory behavior in presence of BAY-747, whereas sGC-functional *Pf4-Cre*$^{+}$*Gucy1b1*$^{+/LoxP}$ platelets were unresponsive to ADP aggregation (224.3 ± 17.0 *vs.* 4.0 ± 1.5 AU·min, p=0.0002, n=3 animals per group).

Next, ANGPT1 release from platelets after shaking was measured in the absence and presence of 150 ppm BAY-747 in paired samples derived from 4 independent wildtype animals. In line with the previous results which indicated a positive correlation between platelet ANGPT1 release and sGC activity, sGC stimulation doubled ANGPT1 levels in platelet releasate after shake-activation (133.8 ± 6.5 ng/ml *vs.* 64.0 ± 4.3 ng/ml, p=0.002; Figure 24a). Thus, these results strengthen the hypothesis that sGC specifically stimulates the release of ANGPT1 in platelets upon activation.

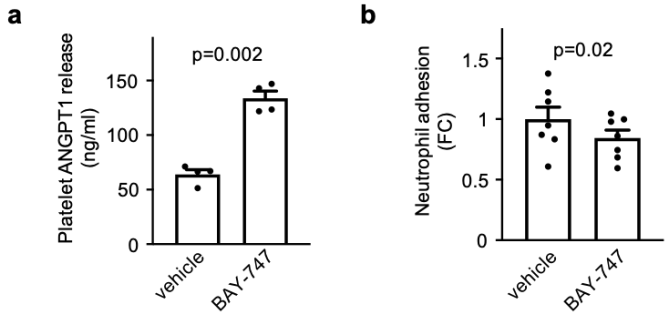

Figure 24 Effects of BAY-747 on platelet-induced ANGPT1 release and neutrophil adhesion. a. ANGPT1 release from wildtype platelets is significantly enhanced upon sGC stimulation with 150 ppm BAY-747 compared with vehicle (n=4 sample pairs from independent animals). **b**. Neutrophil adhesion to wildtype EC after incubation with supernatant from n=7 activated wildtype platelets from independent animals is decreased after preincubation with 150 ppm BAY-747. Two-sided paired t-test. Data are mean ± s.e.m. Abbreviation: *FC*: fold change. Reprinted under the terms of the Creative Commons CC BY license: Figure 4a,b from reference (Mauersberger et al., 2022).

Subsequently, the leukocyte-endothelium adhesion phenotype was again tested on sGC-stimulated platelets. For this purpose, neutrophils were isolated from the bone marrow of wildtype mice and incubated with wildtype EC as well as platelet releasate obtained from wildtype platelets after shaking. Hereby, platelets from 7 independent sample pairs were incubated either with vehicle or 150 ppm of BAY-747 prior to shaking. As displayed in Figure 24b, neutrophil adhesion to EC was found to be decreased by 15.6% (± 6.5%, p=0.02) when stimulated with releasate of platelets treated with BAY-747 instead of vehicle. These data point toward a contribution of sGC in the leukocyte recruitment process – suggestively by a mechanism that involves ANGPT1 release.

4.5.2 Signaling pathways involved

The previous results plainly indicate the involvement of ANGPT1 release in sGC-mediated functions; still, it is not clear how exactly sGC activity in platelets is mechanistically linked to

ANGPT1 release from platelet granules. The sGC pathway has numerous effector proteins and functions. One prominent protein downstream of PKG previously linked to platelet aggregation, though, is IRAG. Therefore, it was first tested, whether ANGPT1 release would also be altered in mice lacking IRAG in platelets. To this end, platelets were isolated from 6 *Pf4-Cre*$^{+}$*Irag1*$^{LoxP/LoxP}$ and 6 IRAG wildtype mice (*Pf4-Cre*$^{+}$*Irag1*$^{+/LoxP}$ or *Pf4-Cre*$^{+}$*Irag1*$^{+/+}$) and ANGPT1 quantified in shake-activated platelet supernatant by ELISA. Although *Pf4-Cre*$^{+}$*Irag1*$^{LoxP/LoxP}$ platelets indicate lower levels of ANGPT1 in platelet supernatant after shaking than controls, this difference was not statistically significant (40.8 ± 6.1 *vs.* 54.0 ± 4.7, p=0.12; Figure 25). These data suggest the involvement of other proteins in the ANGPT1-release mechanism.

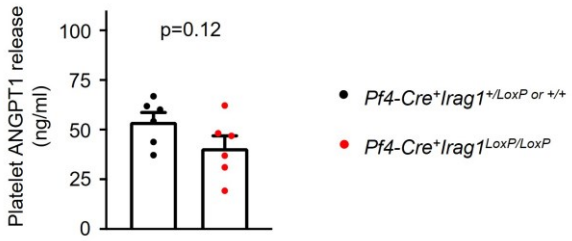

Figure 25 ANGPT1 release from shake-activated platelets lacking IRAG. No significant difference in ANGPT1 release from sGC-deficient platelets from *Pf4-Cre*$^{+}$*Irag*$^{LoxP/LoxP}$ compared with control mice (n=6 each) after shaking as assessed by ELISA. Two-sided unpaired t-test. Data are mean ± s.e.m. Abbreviations: *ANGPT1*, angiopoietin-1. Reprinted under the terms of the Creative Commons CC BY license: Extended Data Figure 8 from reference (Mauersberger et al., 2022).

Subsequently, to understand which downstream sGC-cGMP pathways rather than IRAG influence ANGPT1 release upon platelet activation by shaking, central intracellular mediators of platelet pathways were separately targeted by specific inhibitors and subsequently, ANGPT1-release from treated wildtype platelets determined (Figure 26).

Thereby, assaying literature-approved kinase inhibitors at common concentrations (see Table 21) in 6 independent platelet samples, neither cyclin-dependent kinases (CDK) 2, 5, and 9 nor Akt, extracellular signal-regulated kinases (ERK), or p38α mitogen-activated protein kinase (MAPK) were found to be directly involved in the platelet ANGPT1-release mechanism ($p \geq 0.90$ for all comparisons; Figure 26a). In contrast, both inhibitors of protein kinases C (PKC) and G significantly inhibited ANGPT1 release from platelets after shaking (-23.8 ± 2.8 ng/ml $p_{adj}=0.001$ and -21.3 ± 3.5 ng/ml $p_{adj}=0.004$, respectively; Figure 26b). PKG I is described as a central sGC-cGMP downstream mediator in platelets, thus, the observation that its inhibition also attenuates ANGPT1 release is highly suggestive. The PKC family, on the other hand, comprises many different isoforms and is known as a key mediator of platelet granule secretion (Harper & Poole, 2010). Therefore, it tends to exert an opposite role to PKG in terms of platelet activation, although its link to cGMP-signaling is not completely understood.

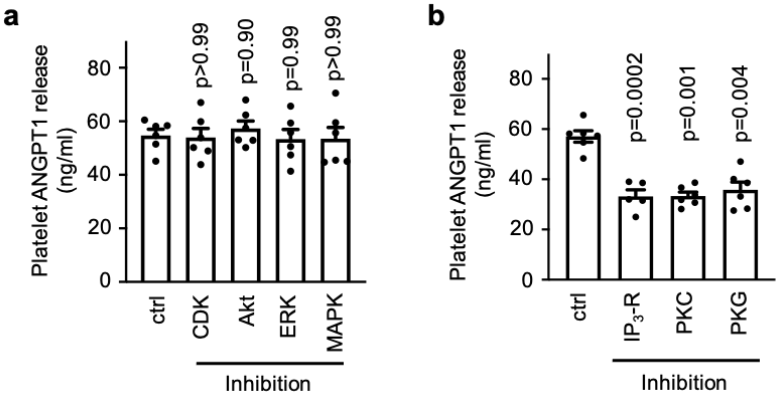

Figure 26 ANGPT1 levels in platelet releasate following incubation with different inhibitors. a. Pharmacological inhibition of MAPK (10 μM VX-702), CDK 2/5/9 (100 nM Dinaciclib), ERK (10 μM Ravoxertinib), and Akt kinase (1 μM MK-2206) does not result in diminished ANGPT1 release from wildtype platelets after shaking as determined by ELISA (n=6). **b**. Significantly attenuated ANGPT1 levels in wildtype platelet releasate after shaking from IP_3-R- (10 μM 2-APB), PKC- (5 μM Ro 32-0432), and PKG- (10 μM KT-5823) treated platelets (n=6). One outlier was removed from the PKG group (n=5) according to the ROUT's test. Each symbol represents paired samples derived from independent animals. Mixed-effects analysis (ANOVA with Dunnett's multiple comparison test). Data are mean ± s.e.m. Abbreviations: *CDK*, cyclin-dependent kinase 2/5/9; *ERK*, extracellular signal-regulated kinase; *IP_3-R*, inositol 1,4,5-trisphosphate receptor; *MAPK*, mitogen-activated protein kinase; *PKC*, protein kinase C; *PKG*, protein kinase G. Reprinted under the terms of the Creative Commons CC BY license: Figure 4c,d from reference (Mauersberger et al., 2022).

Additionally, inhibiting the inositol 1,4,5-trisphosphate receptor (IP_3-R) led to significantly decreased ANGPT1 levels in platelet releasate after shaking (-23.9 ± 1.4 ng/ml p_{adj}=0.0002, Figure 26b). IP_3-R is directly associated with IRAG and PKG I and functions as a Ca^{2+} channel in the endoplasmic reticulum. In contrast to IRAG, its activation favors platelet activation and granule secretion (Schlossmann & Desch, 2011) and therefore, may contribute to the understanding of how sGC, a platelet-silencing mediator *per se*, may be associated with ANGPT1 release.

In order to verify the implicated involvement of the kinases not only in ANGPT1 release but also in sGC activation processes within platelets, additionally, serine/threonine kinase profiling was performed on sGC-stimulated wildtype platelets (n=6 independent samples) treated with BAY-747, which was technically operated by Dr. Emiel van der Vorst (RWTH Aachen, Germany). As displayed in Figure 27, sGC stimulation indeed led to a marked increase in the activity of kinases from the AGC group (encircled), which comprises the PKC and PKG family and thus confirms their involvement in both ANGPT1 release and NO signaling downstream of sGC. A full list of the differentially active kinases following sGC stimulation can be found in Appendix Table 1. The results of the underlying phosphorylation of specific peptide sequences used to assign the kinases are listed in Appendix Table 2.

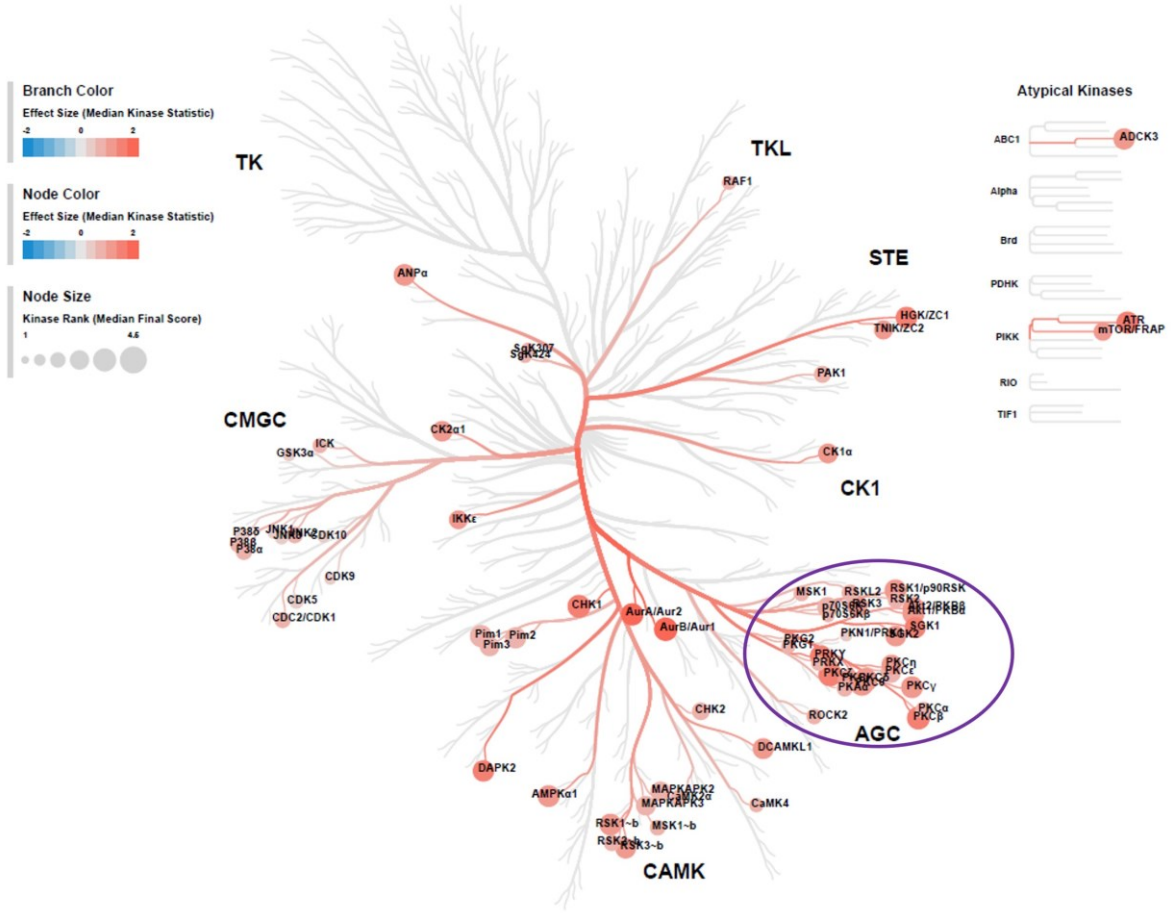

Figure 27 Serine/threonine kinase profiling in platelets stimulated with BAY-747. The CORAL kinome tree represents kinases with differential activity in wildtype platelets upon treatment with 150 ppm of BAY-747 (n=6 samples per group, each derived from one independent animal). Activity is particularly increased in the protein kinase A, G, and C family (AGC, encircled). Effect size and directionality is encoded in branch and node color (red: increased activity; blue; decreased activity in BAY-747 *vs.* vehicle treated platelets), while node size provides the computed kinase rank order. A median final score >1.2 was set as cut-off value. Abbreviations: *AGC*, A, G, and C kinases; *CAMK*, Ca^{2+}/calmodulin-dependent protein kinases; *CK1*, casein kinase 1; *CMGC*, CDK, MAP, GSK, and CDK-like kinases; *STE*, serine/threonine-specific protein kinases; *TK*, thymidine kinase; *TKL*, tyrosine kinase-like kinases. Measurement and analysis were conducted by Dr. Emiel van der Vorst (RWTH Aachen, Germany).

Taken together, kinase and inhibitor screenings confirmed a role for PKG, the direct downstream target of cGMP signaling, but also PKC and IP_3-R in sGC-mediated ANGPT1 release, while another important mediator of cGMP functions, IRAG, was not significantly associated with ANGPT1 release.

4.6 sGC stimulation in atherosclerosis

The above *in vitro* data show that sGC stimulation increases ANGPT1 release from platelets and inhibits leukocyte endothelium adhesion in an inverse manner to sGC deficiency in platelets. Therefore, the ultimate step was to investigate whether sGC stimulation could, consistently, attenuate atherogenesis *in vivo*. To this end, atherosclerosis-prone *Ldlr*$^{-/-}$ mice were fed a Western

diet for 10 weeks, containing either 0 or 150 ppm of the sGC stimulator BAY-747. Plasma concentrations of BAY-747 in these mice were measured by Dr. Lisa Dietz (Bayer AG, Wuppertal, Germany) and can be appreciated in Appendix Figure 6.

4.6.1 Basic characteristics of sGC-stimulated mice

Mice were analyzed for baseline parameters comprising plasma cholesterol, platelet count, and body weight following the 10 weeks Western diet and BAY-747 treatment. As depicted in Figure 28, all of the above characteristics were found to be unaltered in BAY-747 compared with vehicle-treated animals (n=8-12 mice per group). These results indicate no relevant influence of sGC stimulation on lipid metabolism or blood platelet numbers in this model.

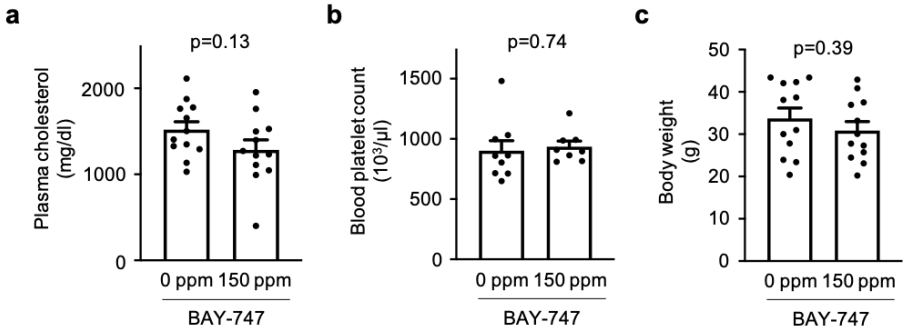

Figure 28 Mouse blood characteristics and body weight following BAY-747 treatment. No significant differences between sGC stimulator- and control-fed mice regarding (**a**) plasma cholesterol levels (n=12), (**b**) blood platelet numbers (n=9 in treatment, n=8 in control group), or (**c**) body weight after ten weeks of Western diet (n=12). Each symbol represents one animal. Data are mean ± s.e.m. Unpaired t-test. Reprinted under the terms of the Creative Commons CC BY license: Figure 10a-d from reference (Mauersberger et al., 2022).

Next, to exclude the possibility that plaque formation might be affected by differential availability of leukocytes in the blood – the central pool of leukocytes for recruitment into atherosclerotic plaques – leukocyte populations were quantified in the blood of both vehicle and sGC stimulator treated *Ldlr*$^{-/-}$ mice (n=12 independent animals per group) by flow cytometry after 10 weeks of Western diet. As depicted in Figure 29, no quantitative differences in total leukocytes, neutrophils, and pro-inflammatory Ly6C^{high} or anti-inflammatory Ly6C^{low} monocytes were found between the two groups, indicating no influence of sGC stimulation on leukocyte supply from the circulation.

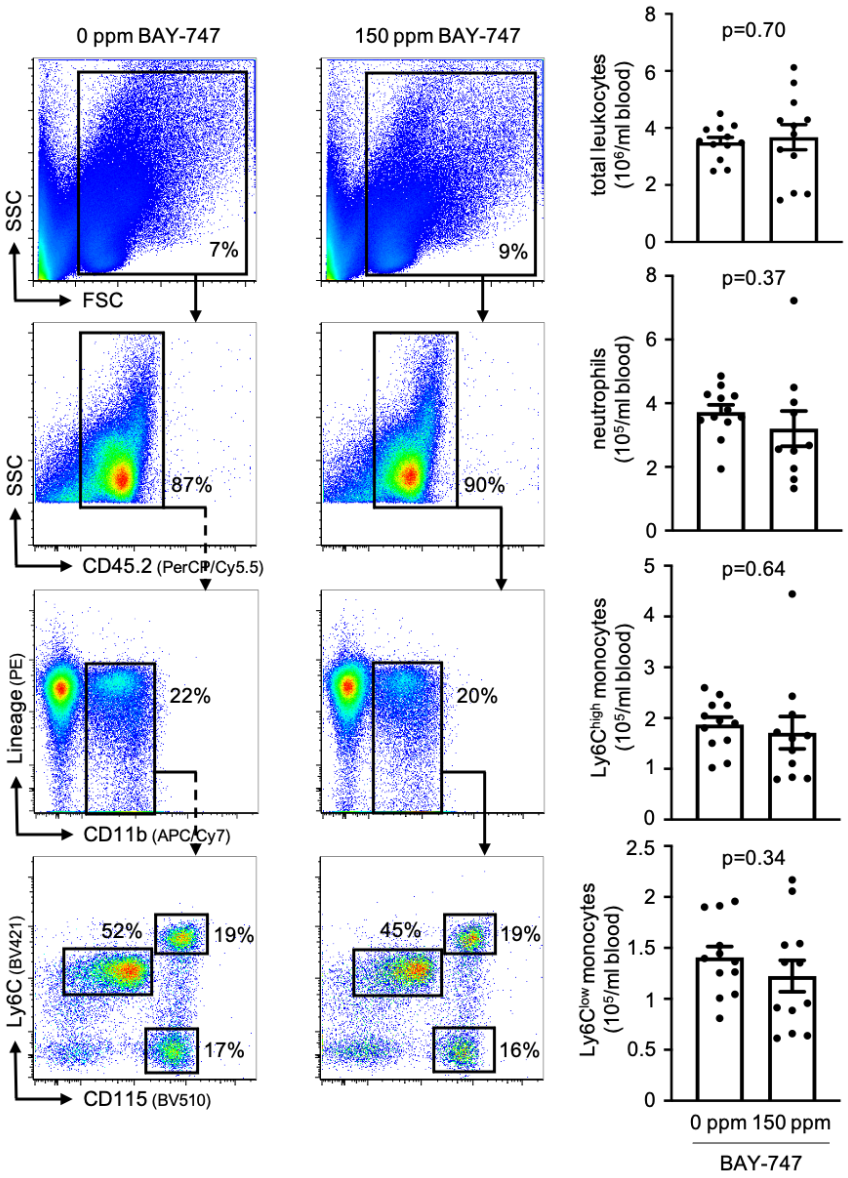

Figure 29 Blood leukocyte numbers and subsets in sGC-stimulated *Ldlr*$^{-/-}$ mice. Flow cytometry reveals no significant quantitative differences in total leukocyte, neutrophil, and monocyte levels. Each symbol represents one independent animal (n=12). Two-sided unpaired t-test. Two outliers were removed in the analysis of neutrophils (150 ppm group; n=10) and Ly6C^{high} monocytes (150 ppm group; n=11) according to the ROUT method. Data are mean ± s.e.m. Reprinted under the terms of the Creative Commons CC BY license: Extended Data Figure 10f from reference (Mauersberger et al., 2022).

4.6.2 Atherosclerotic plaque formation and vascular inflammation

To clarify whether sGC stimulation can retard atherosclerotic plaque formation, first, aortic roots were isolated from *Ldlr*$^{-/-}$ mice fed a 10-weeks Western diet with or without the sGC stimulator BAY-747 and subjected to histology. Subsequently, plaques were visualized by Masson's trichrome staining. Thereby, collagen, a main component of vessel walls and the fibrous cap of atherosclerotic lesions, is stained blue, whereas cytoplasm and muscle tissue display a red color. Nuclei, in contrast, are visible as dark spots. As depicted in Figure 30a, *Ldlr*$^{-/-}$ mice treated with

BAY-747 exhibited significantly smaller atherosclerotic lesions in aortic roots than *Ldlr*$^{-/-}$ mice of the control group which were fed the Western diet without the sGC stimulator (62.5 ± 16.1 (n=7) *vs.* 123.1 ± 18.6 ×10^3 µm^2 (n=9), p=0.03). Furthermore, myeloid cell accumulation as determined by CD11b$^+$ area of aortic root plaques was found to be significantly lower in mice from the treatment group (30.3 ± 5.8% (n=8) versus 50.5 ± 6.3% (n=11) of plaque area, p=0.04).

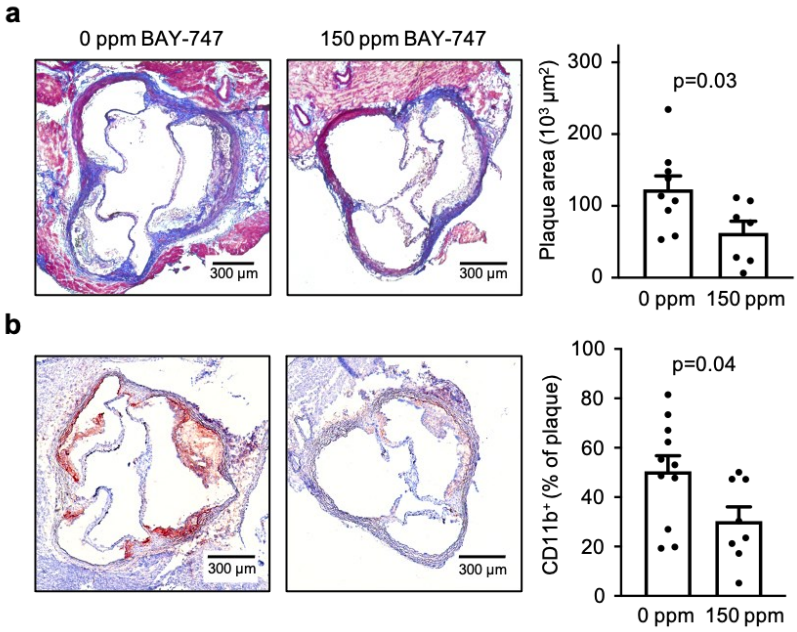

Figure 30 Atherosclerotic plaque formation in mice after pharmacological sGC stimulation. a. Aortic root atherosclerotic plaques were significantly larger in *Ldlr*$^{-/-}$ mice fed a 150 ppm BAY-747 enriched Western diet for 10 weeks (n=7) than in the control group (n=9), which was fed the same diet without the sGC stimulator. **b**. Immunohistology reveals significant higher accumulation of CD11b$^+$ cells in the aortic roots of mice from the treatment group (n=8) compared with controls (n=11). Each symbol represents one independent mouse. Two-sided unpaired t-test. Data are mean ± s.e.m. Reprinted under the terms of the Creative Commons CC BY license: Figure 5b,c from reference (Mauersberger et al., 2022).

Subsequently, aortae of *Ldlr*$^{-/-}$ mice subjected to the same treatment as stated above were analyzed by flow cytometry. Compared with control mice, BAY-747-treated mice harbored significantly lower numbers of neutrophils (1,201 ± 192 (n=11) *vs.* 1,885 ± 232 (n=12), p=0.04) and macrophages (13,915 ± 1,550 *vs.* 22,156 ± 2,737, n=12 each) in the aortae after 10 weeks of Western diet (Figure 31). Ly6C^{high} monocytes follow the same trend, with a p-value close to the significance threshold (1,485 ± 348 *vs.* 2,688 ± 531, n=12 each, p=0.07). A higher quantity of leukocytes within the aortae indicates larger atherosclerotic plaques and/or higher leukocyte density within plaques, both factors of which are correlated to a higher risk of plaque rupture or erosion. To conclude, BAY-747 significantly attenuated plaque formation and leukocyte accumulation in aortic roots and whole aortae, respectively, in atherosclerosis-prone mice.

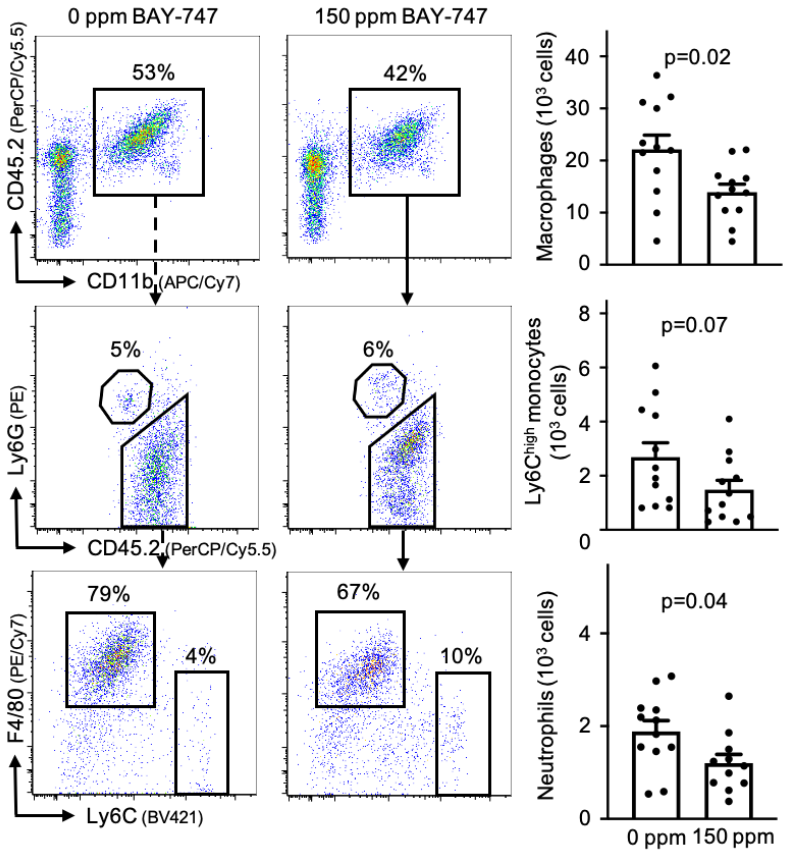

Figure 31 Vascular inflammation in mice after pharmacological sGC stimulation. Aortic cell suspensions of *Ldlr*$^{-/-}$ mice that were fed a 150 ppm BAY-747 enriched Western diet for 10 weeks contained significantly fewer macrophages and neutrophils compared with respective controls (n=12 each), as analyzed by flow cytometry. Each symbol represents one independent mouse. Two-sided unpaired t-test. Data are the mean ± s.e.m. One outlier was removed in the analysis of neutrophils (150 ppm; n=11) according to the ROUT test. Reprinted under the terms of the Creative Commons CC BY license: Figure 5d from reference (Mauersberger et al., 2022).

4.6.3 *In vivo* leukocyte recruitment

Ultimately, it was investigated whether decreased lesion formation and reduced leukocyte accumulation within aortic plaques in sGC-stimulated mice were due to diminished recruitment of leukocytes from the blood – as suggested by the *in vitro* results. To this end, *Ldlr*$^{-/-}$ mice were again fed a Western diet containing either 0 ppm (control group) or 150 ppm BAY-747. In order to investigate early atherogenesis, in this experiment mice were only fed the Western diet together with the sGC stimulator for 6 weeks instead of 10. The experimental scheme is illustrated in Figure 32 (top). After 6 weeks, each mouse was injected intravenously with equal numbers of monocytes and neutrophils. These cells were freshly isolated from the bone marrow of ubiquitous GFP^{+} reporter mice – as a result, injected cells could be distinguished from the endogenous cells afterward. 24 hours later, taking into account the relatively short lifespan of leukocytes in the circulation (Patel et al., 2021), aortae were subjected to flow cytometry and the amount of GFP^{+} – *i.e.*, recruited – cells was determined. Indeed, mice treated with 150 ppm of the sGC stimulator

exhibited significantly fewer GFP$^+$ myeloid cells in aortic cell suspensions than untreated mice (21.4 ± 3.3 *vs.* 42.8 ± 6.9 cells, n=8 each, p=0.01, Figure 32). Thus, it can be concluded that BAY-747 treatment significantly reduces aortic leukocyte recruitment in atherosclerotic mice.

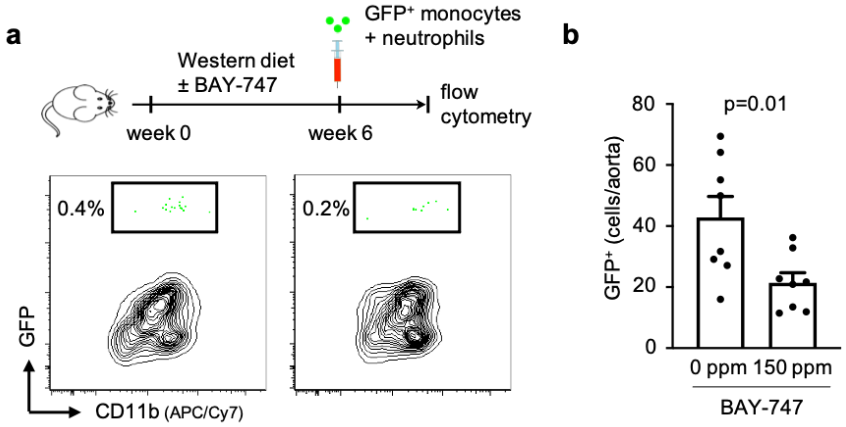

Figure 32 Leukocyte recruitment in mice after pharmacological sGC stimulation. a. Study scheme depicting the experimental setup of GFP$^+$ monocyte and neutrophil adoptive transfer in *Ldlr*$^{-/-}$ mice following a 6-weeks Western diet enriched with 0 or 150 ppm of BAY-747. The panel below shows a representative flow cytometry plot of GFP$^+$ cells retrieved in the aortae 24 hours later. **b**. Significantly lower numbers of GFP$^+$ cells in aortic suspensions of 150 ppm BAY-747 compared with vehicle-treated mice (n=8 independent animals). Two-sided unpaired t-test. Data are the mean ± s.e.m. Abbreviations: *GFP*, green fluorescent protein. Reprinted under the terms of the Creative Commons CC BY license: Figure 5a from reference (Mauersberger et al., 2022).

5 Discussion

When Robert F. Furchgott, Louis J. Ignarro, and Ferid Murad deciphered the nitric oxide (NO) signaling pathway in the 1980s, they could not have anticipated that it not only significantly influences blood pressure and hemostasis, but is also associated with one of the leading causes of death worldwide: coronary artery disease (CAD). This association was established only in the last decades, particularly by means of genome-wide association (CARDIoGRAMplusC4D Consortium, 2013; Nelson et al., 2017; Nikpay, 2015; Webb, 2017) and exome sequencing studies (Dang et al., 2021; Emdin et al., 2018; Erdmann et al., 2013) that linked the occurrence of several polymorphisms in genes tightly involved in the formation, the fate, or downstream functions of the NO signaling pathway to a significantly higher risk of CAD and myocardial infarction (MI). Although the soluble guanylyl cyclase (sGC) and other proteins of this pathway are expressed in almost all tissues, the key functions of NO signaling, regulation of vascular tone and platelet activation, particularly affect vascular smooth muscle cells (SMC) and platelets. In line, functional studies investigating the risk variant rs7692387 in *GUCY1A1*, the sGC-subunit α_1 encoding gene, found significantly less sGC expression in SMC and platelets of risk-allele carriers (Kessler et al., 2017). Importantly, the actual impact of the rs7692387 *GUCY1A1* non-risk variant on CAD incidence is reported to be significantly greater than expected from its effect on blood pressure alone (Emdin et al., 2018) – a function which is mainly mediated by SMC. Thus, investigations of sGC signaling beyond its blood pressure-lowering effects in the context of CAD have been intensified with a particular focus on platelets – bearing in mind the direct effects of sGC on platelets and a recent study correlating the common rs7692387 locus sGC risk variant with the benefit of aspirin, a widely used antiplatelet treatment, in secondary prevention of cardiovascular events in CAD patients (Hall et al., 2019).

Therefore, in a series of *in vivo* and *in vitro* experiments, a long-neglected cell type and a signaling pathway of unprecedented importance in atherogenesis research until a few years ago were jointly put into focus here: Platelets, and their contribution to sGC-mediated effects on atherosclerosis. In short, it was revealed that lack of platelet sGC promotes, while pharmacologically stimulating sGC activity mitigates atherosclerosis. Thereby, leukocyte recruitment into atherosclerotic plaques was indicated as a causally involved mechanism in both scenarios. As one potentially effect-mediating protein, angiopoietin-1 (ANGPT1) was consistently identified as a differentially released platelet factor in both sGC-deficient and sGC-stimulated murine, as well as sGC-reduced human platelets. Each of these aspects will be separately discussed in detail below.

5.1 Platelet sGC influences atherosclerotic plaque formation in mice

By investigating atherosclerotic plaque formation and vascular inflammation in this thesis, mice lacking platelet sGC indeed presented with i) larger atherosclerotic plaques and ii) enhanced aortic leukocyte accumulation compared with sGC wildtype mice following a Western diet – two major indicative signs of atherosclerosis. As a possible mechanistic hint, platelet sGC-deficient mice were shown to increase leukocyte adhesion to plaque-prone carotid arteries *in vivo*, which favors increased leukocyte recruitment into aortic plaques. In line, the presence of shake-activated releasate from sGC-deficient platelets increased leukocyte adhesion to endothelial cells (EC) *in vitro*. In addition to the above-mentioned genetic association studies, this is in broad agreement with the literature: *E.g.*, a previous study on ubiquitous *Nos3*-deficient mice linked impaired NO-sGC signaling with enhanced leukocyte adhesion to atherosclerotic plaques (Ahluwalia et al., 2004) as well as increased atherosclerosis (Kuhlencordt et al., 2001). Moreover, genetic variants associated with reduced *Gucy1a1*-expression were likewise associated with enlarged aortic atherosclerotic lesions in mice (Bennett et al., 2015; Kessler et al., 2017). *Vice versa*, further evidence for a crucial influence of sGC activity on atherosclerosis may come from another study that showed reduced neointimal formation after genetic upregulation of $\alpha_1\beta_1$-sGC in mice (Sinnaeve et al., 2001). In contrast, though, globally *Gucy1a1*-deficient mice on a pro-atherosclerotic background revealed reduced atherosclerotic plaque formation compared with α_1-sGC-competent mice (Segura-Puimedon et al., 2016). However, it has been suggested that this contradictory result may be due to a compensatory upregulation of α_2-sGC, which can indeed form a functional sGC enzyme with the β_1-subunit in SMC (Mergia et al., 2006). Platelets do not express relevant amounts of α_2- or β_2-sGC (Burkhart et al., 2012), which was confirmed by gene expression studies on megakaryocytes here. Therefore, a possible compensatory effect of α_2-sGC can be excluded for the mouse model used in this thesis.

Further, to interpret the results, it is important to consider the nature of the platelet-specific knockout, which is based on the introduction of a Cre-encoding construct into the *Pf4*-promoter. This leads to the exclusive activity of Cre in *Pf4*-expressing cells, *i.e.*, cells of the megakaryocyte lineage. However, it was reported that *Pf4* may also be expressed in certain leukocyte populations (Schaffner et al., 2005). By using specific reporter mice, one publication even found a 15-60% activation of myeloid and lymphoid lineages (Calaminus et al., 2012), suggesting the *Pf4-Cre* model to be not specific for the megakaryocyte lineage. sGC deficiency not only in platelets but also in leukocytes would indeed confound the results of the *in vivo* experiments in this study. It is not clear, though, how abundantly circulating leukocytes express *Pf4* in general, and it apparently varies

widely depending on environmental factors and the specific model used. For instance, another group reported *Pf4-Cre* expression in less than 1% of the CD45-positive cells (Pertuy et al., 2015), while further publications reported their *Pf4-Cre*-based knockout model to be restricted to the megakaryocytic lineage (Rudolph et al., 2019; Tiedt et al., 2006). Therefore, as i) protein expression of β_1-sGC in PBMCs was not found to be visibly altered in sGC-deficient compared with wildtype mice in our model and ii), the confirmatory *in vitro* data in this project were gathered on isolated platelets from this mouse model only, it appears unlikely that sGC deficiency in leukocytes substantially influenced the results of this research project. Further evidence may also come from the observation, that – in contrast to sGC-deficient platelet releasate used to stimulate wildtype leukocytes – leukocytes derived from platelet-specific sGC-deficient mice did not increase adhesion after incubation with wildtype platelet releasates and therefore, do not have a substantial impact on the adhesion phenotype observed in mice with sGC-deficient platelets here. Nevertheless, to completely rule out off-target effects of sGC depletion in leukocytes in this mouse model, it would be necessary to quantify β_1-sGC expression in circulating leukocytes after Western diet, or to verify the *in vivo* findings using a different platelet-specific mouse model. Such an alternative might be the *Cp1ba-Cre* model, though, it is paralleled by other disadvantages such as Cre-recombination within the native *Gp1ba* gene, likely affecting platelet biology and offering only minor experimental experience on basis of this model so far (Gollomp & Poncz, 2019).

Besides, genetic modifications always bear the risk of undesired effects, which is also true for the introduction of Cre in the mouse model. For instance, it has been reported in the literature that off-site Cre activity may impair angiogenesis or affect the numbers and functions of hematopoietic cells (Rashbrook et al., 2022). Therefore, to control for potential toxic influences of Cre-expression in the *Pf4-Cre* mouse model, single-floxed littermate controls that likewise express *Pf4-Cre* were used, contrary to the common use of homozygously floxed, but *Cre*-lacking controls (Pertuy et al., 2015). This strategy is also suitable to meet further model-related confounding effects such as those related to the mouse bacterial artificial chromosome (BAC) clone which was used to introduce *Cre* in the mouse genome.

Lastly, it is important to reflect that this work provides results from *in vitro* and mouse *in vivo* studies that cannot fully resemble human physiology. Despite the large overlap with the human transcriptome, mouse models differ from the human organism in many respects, making their findings only partially transferable. Nevertheless, the vast majority of CAD-associated human risk genes studied showed consistent results in mice (von Scheidt et al., 2017), rendering mouse models a valuable tool to gain insight into the disease and particularly into its development, as they offer

the unique possibility of studying atherosclerosis in a much smaller time frame while allowing for multiple genetic manipulations (Gisterå et al., 2022). Further, in addition to the concordant findings from the genetic studies discussed above, consistent results in *in vitro* studies regarding decreased platelet ANGPT1 release from sGC-lacking murine as well as sGC-α_1-reduced human platelets discussed below support a possible translation.

5.2 Platelet sGC positively influences ANGPT1 release

The idea of sGC as an endogenous brake of platelet aggregation, as recently described (Wen et al., 2018) and confirmed by previous results in sGC-deficient mice *in vivo* (Dangel et al., 2010; Erdmann et al., 2013), is clearly reflected in the literature. Also, the results on atherosclerosis formation and leukocyte recruitment in this thesis point toward a higher pro-inflammatory activity in platelets lacking sGC. Likewise, the inhibitory role of the NO donor SNP or the sGC stimulator BAY-747 in platelet aggregation in response to diverse platelet agonists *in vitro* clearly indicates a platelet-silencing effect of sGC, which is absent in platelets lacking sGC. Unexpectedly, however, it was also found that upon physical shaking, platelet sGC positively influences the release of the α-granule component ANGPT1 – a process usually linked to platelet activation, as mirrored by enhanced ANGPT1 release from platelets upon thrombin stimulation (Li et al., 2001). In fact, the concept that the sGC pathway uniquely and exclusively silences platelets has also been challenged by other findings: *E.g.*, it was shown that the major cGMP effector kinase PKG downstream of sGC-signaling plays an important stimulatory role in both platelet activation and secretion (Li et al., 2003; Li et al., 2004; Vogel et al., 2015; Yin et al., 2008). This is also reflected by another study performed on platelet sGC-deficient mice which indicates a stimulatory rather than an inhibitory role of sGC in platelet aggregation (Zhang et al., 2011) as well as the finding, that a rare loss-of-function mutation in *GUCY1A1* leads to platelet stimulation (Hervé et al., 2014). As a possible explanation, a biphasic role of sGC/cGMP signaling was proposed, consisting of an initial stimulatory response that promotes platelet activation and aggregation, followed by an inhibitory response that is partially sGC-independent and inhibits excessive platelet aggregation (Li et al., 2003; Zhang et al., 2011), in line with the abovementioned data.

Although it needs to be acknowledged that ANGPT1 is likely not the only mediator of sGC effects in atherosclerosis, it can nevertheless be regarded as a substantial finding with implications also in human platelets. As such, decreased sGC availability in human platelets of the CAD-associated risk variant rs7692387 was consistently associated with reduced ANGPT1 release upon shaking.

Importantly, this positive correlation of sGC availability and ANGPT1 release was independent of the total ANGPT1 content, which was equal in wildtype platelets and platelets with depleted or impaired sGC availability in mice and men, respectively. This suggests a direct influence of sGC availability on ANGPT1 release rather than translational processes, consistent with the fact that release can already be observed shortly after incubation of platelets with the sGC stimulator. Additionally, a transcriptomic sub-analysis querying *ANGPT1* expression in tissues of CAD patients in the STARNET database (Franzén et al., 2016), which contains RNA-Seq data from cardiometabolic tissues of patients undergoing coronary artery bypass graft surgery, renders a common pathway of ANGPT1 and platelet sGC likely (Figure 33). Specifically, *ANGPT1* – which is mainly expressed in platelets and peri-endothelial cells but was detected in seven co-expression modules of atherosclerosis-relevant tissues including aorta, blood, and skeletal muscle – was co-expressed with both *GUCY1A1* and *GUCY1B1*, along with enrichment for genes involved in platelet activation in 6 of 7 tissues.

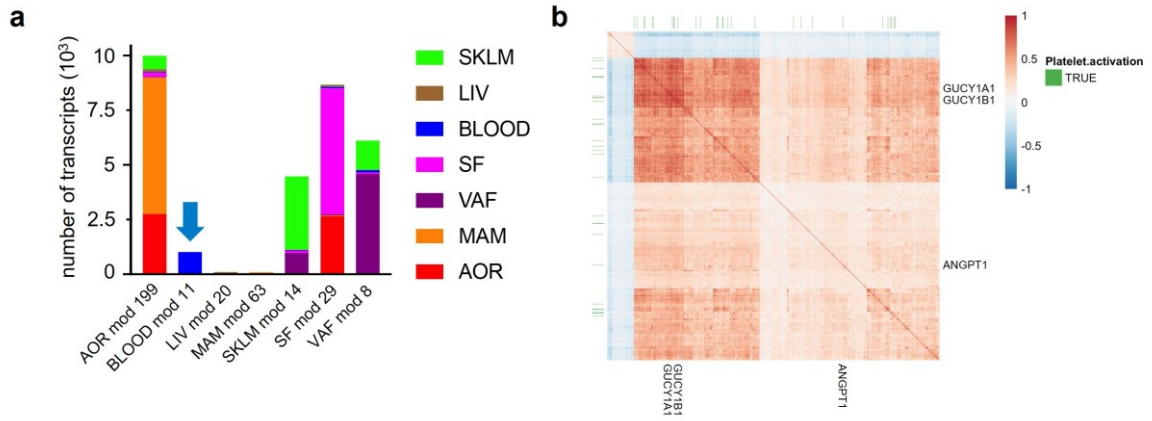

Figure 33 *ANGPT1* expression in different tissues from CAD patients. a. *ANGPT1* is expressed in different STARNET co-expression modules from multi-tissue RNA-Seq of approximately 600 CAD patients. The arrow denotes co-expression module 11 from whole-blood samples (BLOOD). **b**. Heatmap of Pearson's correlation coefficients of genes in co-expression module 11, showing positive correlation of *ANGPT1*, *GUCY1A1*, and *GUCY1B1* and enrichment for platelet activation genes (false discovery rate = 6.863×10^{-13}, Enrichr). Abbreviations: *AOR*, aorta; *LIV*, liver; *MAM*, mammary artery; *SF*, subcutaneous fat; *SKLM*, skeletal muscle; *VAF*, visceral fat. Reprinted under the terms of the Creative Commons CC BY license: Figure 3f,g,h from reference (Mauersberger et al., 2022). Analysis was conducted by Simon Koplev (University of Cambridge, UK).

ANGPT1, on the other hand, is an important pro-angiogenic factor that, by binding the TIE2 receptor on EC, promotes endothelial integrity and inhibits vascular inflammation (Brindle et al., 2006; Gamble et al., 2000). This clearly implies anti-atherogenic functions of ANGPT1 regarding leukocyte recruitment, which has been confirmed by several studies that specifically described ANGPT1 as an opponent of inflammatory or VEGF-mediated leukocyte transmigration (Alfieri et al., 2014; Ismail et al., 2012; Kim et al., 2001; Pizurki et al., 2003; Wang et al., 2004). Accordingly, ANGPT1 was shown to protect from the development of cardiac allograft atherosclerosis

(Nykanen et al., 2003) and was described as an important factor in preventing plasma leakage during leukocyte diapedesis (Braun et al., 2020) with *in vivo* implications, *e.g.*, in endotoxin-induced septic shock (Witzenbichler et al., 2005). Yet, other studies have found opposite effects of ANGPT1 on atherosclerosis, in particular by promoting monocyte and neutrophil migration and atherosclerotic plaque formation (Ahmad et al., 2010; Burnett et al., 2017; Fujisawa et al., 2017). Revisiting the above hypothesis of a biphasic role of sGC in platelet aggregation, it could be speculated that the observed pro-inflammatory functions of ANGPT1 specifically appear in emergency events of excessive platelet activation such as atherothrombosis in MI, which subsequently requires massive leukocyte recruitment into the affected tissues (Moggio et al., 2022). This might be triggered by peak levels of ANGPT1 that outbalance its protective effects on EC by pro-atherogenic functions on leukocytes. Indeed, plasma or *in vitro* concentrations of ANGPT1 in the above-mentioned studies, respectively, exceeded by far physiological levels – levels *in vivo* most likely only reached by pro-thrombotic platelet stimuli such as thrombin. This is supported by the fact that in contrast to agonist-induced release, shaking (Alard et al., 2015) is a relatively mild form of shear stress-induced activation that does not lead to platelet aggregation, and therefore, rather resembles early phases of atherogenesis unrelated to atherothrombosis. Consequently, following the hypothesis of a biphasic role of sGC and ANGPT1 in atherosclerosis, the results obtained from this thesis resemble sGC and ANGPT1 functions during development rather than acute complications of atherosclerosis, and thereby support a beneficial, disease-mitigating effect of both factors.

5.3 ANGPT1 release might be linked to sGC signaling via protein kinases G and C

Since the correlation of ANGPT1 release with sGC activity can thus be considered experimentally well established, the question immediately arises as to how exactly sGC mechanistically influences the release of ANGPT1. Apart from a potential ANGPT1/TIE2/NO pathway in endothelial target cells, no such axis is described in the literature within platelets so far. Downstream of sGC and its effector protein cGMP, the protein kinase G (PKG) and its two main target proteins IRAG and VASP are among the most famous mediators of NO signaling. IRAG was described as a central mediator of cGMP-dependent inhibition of platelet aggregation (Schinner et al., 2011) and was therefore the first intuitive target of further research in an effort to pin down a potential activation route that connects sGC activity to ANGPT1 release. IRAG is a direct binding partner of PKG and the inositol 1,4,5-trisphospate receptor (IP_3-R) and inhibits IP_3-R-induced Ca^{2+}-

release from intracellular stores (Schlossmann et al., 2000). After shake-activating platelets from wildtype mice and mice that genetically lack IRAG, though, ANGPT1 release was not significantly altered – excluding IRAG as a central mediator in the sGC-ANGPT1 release axis. Although this finding may be surprising, considering the crucial involvement of IRAG in platelet physiology, it is in line with the phenotype of enhanced ANGPT1 release following sGC activation – a function *per se* requiring platelet activation.

Next, two complementary approaches, involving kinase and inhibitor screening assays, were employed. On one hand, serine/threonine kinase profiling was utilized as an unbiased tool to identify kinases that are significantly involved in sGC stimulation, while on the other hand, by incubating platelets with specific small molecule inhibitors prior to physical activation, selected important intracellular mediators implicated in NO signaling, but also other pathways were investigated for their direct effect on ANGPT1 release. Thereby, PKG but also protein kinase C (PKC) were identified as significantly involved proteins in both sGC stimulation and ANGPT1 release. The involvement of PKG is not surprising, as it is the key downstream target of cGMP signaling, thus contributing to most sGC-mediated functions (Makhoul et al., 2018). Even more, the finding that this kinase is also involved in ANGPT1 release once again confirms the correlation between ANGPT1 and sGC. Conversely, PKC is not traditionally linked to sGC signaling. It was rather described as an upstream activator of PKG (Hou et al., 2003; Lopes-Pires et al., 2015), but also suggested as a mediator of PKG-induced ischemic preconditioning, a phenomenon that leads to cardioprotection following brief ischemia (Costa et al., 2005). However, PKC is well known for its crucial involvement in platelet secretion. Platelet agonists, by binding to specific receptors on the platelet surface, intracellularly activate phospholipases and their two messenger proteins inositol 1,4,5-trisphosphate (IP_3) as well as 1,2-diacylglycerol. While IP_3 acts via the IP_3 receptor (IP_3-R), 1,2-diacylglycerol activates PKC, which is particularly involved in granule secretion (Offermanns, 2006). Thereby, different PKC isoforms fulfill specific functions in granule secretion with sometimes divergent effects (Harper & Poole, 2010). In the kinase screening performed, several isoforms of PKC were found to be involved in ANGPT1 release, while for the inhibitor screening assay, a broad-spectrum PKC inhibitor was used. Therefore, further experiments are necessary to clearly identify the PKC subtypes involved in the sGC-ANGPT1 signaling pathway. Nevertheless, the finding that NO-sGC signaling – known for its platelet silencing effects – is also correlated with platelet secretion, is very intriguing. It can only be speculated whether the downstream PKC effects are targeted, *i.e.*, ANGPT1-specific, or a sign of general platelet activation following sGC activation. Therefore, further studies are warranted to better understand how PKG and particularly, PKC are involved in sGC stimulation and ANGPT1 release. Besides, it also has

to be taken into account that PKG and PKC might fulfill distinct, non-related functions following sGC stimulation. Yet, a recent study screening for PKG substrates using human recombinant PKG I and II also found PKC, specifically PKCα, as a top target of PKG-mediated phosphorylation, indicating a direct link between both kinases (Roy et al., 2021).

Additionally, IP_3-R as the third binding partner in the trimeric complex of PKG I and IRAG was also identified as a mediator of ANGPT1 release following platelet activation by shaking. In contrast to IRAG, IP_3-R is associated with Ca^{2+} release and platelet activation and might therefore explain ANGPT1 release in sGC-stimulated platelets following activation – although no direct activation of IP_3-R by PKG in platelets has been described in the literature so far. Such direct activation by PKG I, though, has been described for the neuronal splice form of IP_3-R (Wagner et al., 2003). It remains to be seen whether a similar, alternative pathway of IP_3-R activation via PKG I might also be active in platelets.

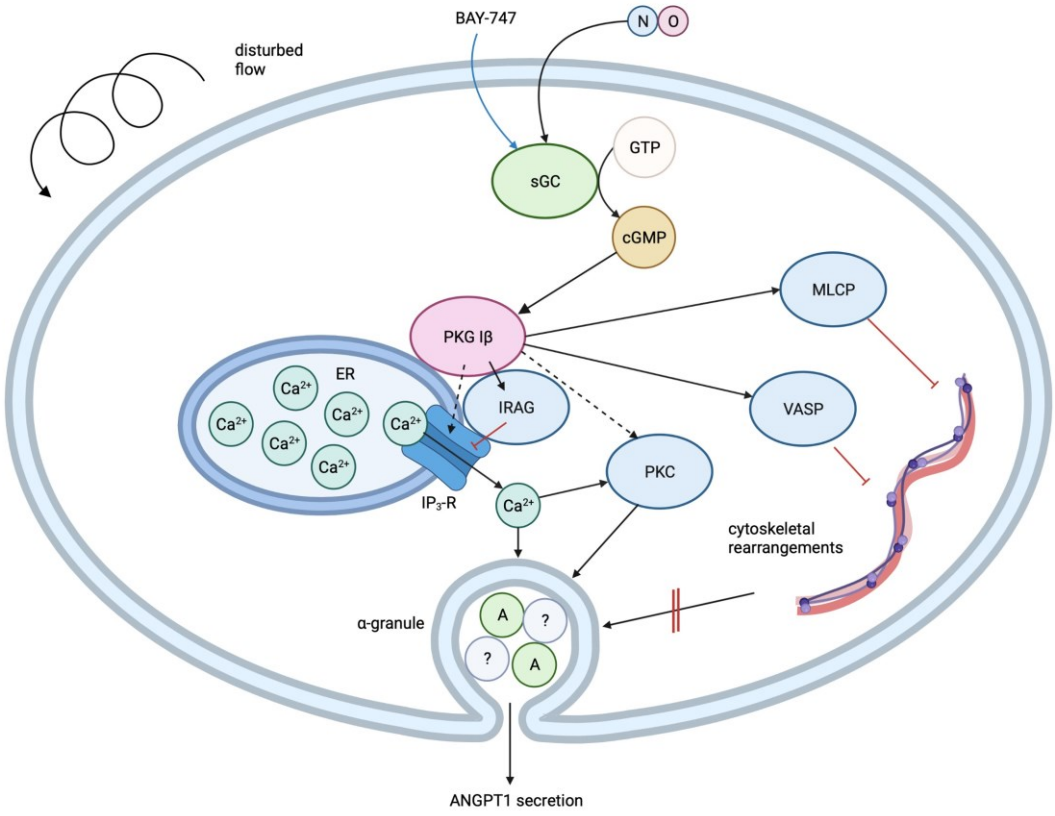

Figure 34 Schematic representation of hypothetical ANGPT1 release from activated platelets. ANGPT1 release from α-granules is increased in sGC-functional or BAY-747-stimulated platelets under shear stress, suggestibly via increased downstream PKG, PKC, and IP_3-R activity and subsequent Ca^{2+} release from the ER. Simultaneously, in a finely modulated manner, PKG inhibits excessive platelet activation via IRAG, VASP, and MLCP which attenuate Ca^{2+} release and cytoskeletal rearrangements important for granule release. Abbreviations: *ANGPT1*, angiopoietin-1, *cGMP*, cyclic guanosine-3',5'-monophosphate; *ER*, endoplasmic reticulum; *GTP*, guanosine 5'-triphosphate; *IP_3-R*, inositol 1,4,5-trisphosphate receptor; *IRAG*, IP_3R-associated cGMP-kinase substrate; *MLCP*, myosin light chain phosphatase; *NO*, nitric oxide; *PKC*, protein kinase C; *PKG*, protein kinase G; *sGC*, soluble guanylyl cyclase; *VASP*, vasodilator-stimulated phosphoprotein. Created with BioRender.com.

At the same time, the identity of the differentially phosphorylated peptides, which were used to infer protein kinase activity in the comparison of vehicle- versus sGC-stimulated platelets, may also be informative when considered separately. There, with VASP and phosphodiesterase 5A, peptides emerged that are well known for their involvement in NO signaling. Notably, several of the phosphorylated peptides overlap with the PKG I and II substrates identified in the above-mentioned study (Roy et al., 2021). This highlights the central, downstream role of PKG in sGC stimulation. However, this approach also has certain limitations. For instance, impurities such as traces of erythrocytes and blood leukocytes in the platelet lysates, which also contain several active kinases, may confound the results. Moreover, indirect identification of kinases via phosphorylated proteins and *in silico* prediction using databases also carries some risk of erroneous conclusions.

Taken together and as schematically depicted in Figure 34, the results from this thesis indicate that PKG, PKC, and IP_3-R are involved in ANGPT1 release from platelets – the former being associated with platelet silencing, and the latter two being rather associated with platelet activation. Release of ANGPT1 by both sGC- and shake-activated platelets – a counterintuitive finding given the generally accepted role of sGC signaling as a platelet inhibitor – seems to be regulated by PKC and IP_3-R activation rather than IRAG. The latter could explain how ANGPT1 is released downstream, but it remains unclear how PKG or upstream mediators of sGC signaling may stimulate – rather than inhibit – IP_3-R as well as PKC. Yet, evidence from studies revealing involvement of NO signaling in angiogenesis or ANGPT1-mediated effects raises hope for future studies that may elucidate the here proposed link between sGC and ANGPT1 (Babaei et al., 2003; Gomes de Almeida Schirmer et al., 2020).

Lastly, in this context, the question arises as to how exactly platelets are able to regulate the particular release of ANGPT1, since ANGPT1 was the only one of several proteins investigated found to be differentially released from sGC-deficient or sGC-stimulated platelets, respectively. This question is further accentuated by the fact that among the plethora of platelet-derived factors, often factors with opposing functions reside within the same granules in platelets (Coppinger et al., 2004). It can already be anticipated that there is no definite answer to this question so far, owing to the fact that due to their high reactivity and rapid morphogenetic changes, the molecular investigation of platelets is particularly challenging. One obvious solution proposed by the literature, though, is the existence of functionally distinct subpopulations of α-granules, thus allowing for the selective release of cargo by different stimuli (Battinelli et al., 2019; Chatterjee et al., 2011; Italiano et al., 2008; Sehgal & Storrie, 2007). The authors specifically found distinct localization of pro- and anti-angiogenic factors within α-granules, that were released differentially

by different thrombin receptor agonists, but also by ADP and thromboxane (Battinelli et al., 2011; Ma et al., 2005). Of note, a similar observation was made in neutrophils regarding the storage of ANGPT1 and VEGF (Neagoe et al., 2009). This broad evidence indeed supports the hypothesis of a stimulus-dependent release of pro- and antiangiogenic factors including ANGPT1 from platelets, which would allow for a finely targeted platelet response. On the other hand, although confirming a clustered rather than a homogenous cargo distribution within these granules, other studies challenged the notion of platelets as smart just-in-time suppliers of selected molecules and rather discovered random, non-thematic sorting of granule cargo (Jonnalagadda et al., 2012; Kamykowski et al., 2011). (Heijnen & van der Sluijs, 2015; Yadav & Storrie, 2017) – and ANGPT1 in particular. Therefore, despite the central importance of platelet granule secretion in the organism, further studies are needed to understand if and how platelets regulate the differential release of specific granule components.

5.4 sGC stimulators attenuate atherosclerotic plaque formation in mice

sGC signaling in platelets was clearly indicated as a decelerator of murine atherosclerosis progression in the here presented results, but the translation of observations from knockout models onto therapeutical effects is often difficult. Therefore, the ultimate goal of this study was to directly query the potential therapeutic effect of sGC stimulation on atherosclerosis. Hereby, it was shown that oral administration of the sGC stimulator BAY-747 in mice attenuates atherosclerotic plaque formation and vascular inflammation. Moreover, it was indicated by adoptive transfer experiments, that this phenotype involves decreased leukocyte recruitment into aortic atherosclerotic lesions in line with the previous observations in mice lacking platelet sGC. These results are in accordance with other studies that showed decreased leukocyte rolling and adhesion in mice following administration of the sGC activator BAY 41-2272 (Ahluwalia et al., 2004) and decreased aortic atherosclerotic plaque size in atherosclerotic mice treated with the sGC activator YC-1 (Tsou et al., 2014).

While data on the efficiency of sGC stimulation or activation in human atherosclerotic patients are so far lacking, several human trials investigated the effect of nitrates such as nitroglycerin, isosorbide-mononitrate (ISDN), or -dinitrate (ISMN) in CAD patients. These substances act by releasing NO into the circulation and thereby stimulate the sGC signaling cascade with subsequent vasodilation, reduced cardiac workload, and decreased oxygen demand by the heart (Münzel & Gori, 2013). Therefore, they are commonly applied for treating angina pectoris (Knuuti et al., 2019)

and are among the oldest synthetic drugs in use today. However, while nitrates are a useful tool to fight acute ischemic symptoms, they scarcely showed beneficial long-term effects in this context in clinical studies (Divakaran & Loscalzo, 2017). This might be due to several negative effects of NO donors following long-term intake, including nitrate tolerance, oxidative stress, and endothelial dysfunction (Daiber & Münzel, 2015) – phenomena not intrinsically related to sGC stimulators or activators (Jabs et al., 2015; Stasch et al., 2002). Similarly, clinical studies proving the efficiency of sildenafil, an inhibitor of phosphodiesterase 5A, in CAD are lacking. Yet, the observation that CAD patients treated with sildenafil for erectile dysfunction show a reduced risk of all-cause mortality and myocardial infarction compared with men treated with the alternative drug alprostadil (Andersson et al., 2021) encourages further investigations. Meanwhile, sGC stimulators, which directly activate sGC either in synergy with or independently of NO, have emerged as new therapeutic agents in different cardiovascular diseases including pulmonary hypertension (Ghofrani et al., 2013) and heart failure with reduced ejection fraction (Armstrong et al., 2020). sGC stimulators were already proven safe in patients with chronic coronary syndromes in combination with nitroglycerin and ISMN (Boettcher, Düngen, et al., 2022; Boettcher, Mikus, et al., 2022). Overall, although clinical data are lacking to date, enhancing NO signaling in CAD patients represents a promising therapeutic target and the results of this thesis may aid in stimulating future clinical trials in atherosclerosis patients.

It needs to be considered, though, that orally administered sGC stimulators are unspecific in their cellular target, and their effects reported in the above studies thus most likely exceed effects mediated by platelet sGC alone. For instance, hypertension is a common risk factor for atherosclerosis, and the known anti-hypertensive effects of sGC stimulators mediated via smooth muscle cells might lead to an overestimation of the effect of sGC stimulators in *in vivo* experiments. Nevertheless, it can at least be considered a nice coincidence that the platelet factor ANGPT1, which directly correlated with sGC activity in this thesis, also showed beneficial effects on experimental pulmonary hypertension, one of the approved indications for sGC stimulators (Zhao et al., 2003). Still, an *in vitro* study indicated that functional antiplatelet effects of riociguat require higher concentrations than those usually reached in patients (Reiss et al., 2015). Indeed, the plasma concentration of BAY-747 determined in the orally treated mice in this research project was significantly lower than the concentration used for the *in vitro* experiments. Yet, the correlation of ANGPT1 release with sGC activity was consistent also in the scenario of physiological sGC deficiency in platelets. Eventually, how strongly platelet sGC really contributes to the beneficial effects of sGC stimulation in atherosclerosis can only be clarified by further studies.

5.5 Conclusion

The results obtained in this thesis allow for several conclusions, which are summarized in Figure 35. Firstly, lack of sGC in platelets promotes atherosclerotic plaque formation and vascular inflammation in mice, in line with previously reported results from sGC-deficient or -stimulated rodents *in vivo* and human genetic studies. Secondly, this phenotype is particularly driven by increased adhesion and subsequent recruitment of leukocytes from the circulation, which was indicated both by *in vivo* microscopy and *in vitro* cell adhesion studies. Thirdly, one factor potentially involved in this phenotype is the glycoprotein ANGPT1. It was released less both by murine and human platelets with genetically reduced sGC availability following moderate physical activation and, conversely, released more by sGC-stimulated platelets. Albeit being controversially discussed for its impact on atherosclerosis, ANGPT1 is generally described as a guardian of vascular barrier function in the literature and was, accordingly, implied to negatively impact leukocyte adhesion to EC *in vitro*. This protein could well serve as a link between the observed *in vitro* effects and possible functional effects of platelet sGC in atherosclerosis. Yet, further studies are necessary to decipher the precise molecular mechanism linking sGC and ANGPT1 release – and to comprehend whether ANGPT1 is indeed causally involved in the mechanism by which sGC activity retards atherosclerosis *in vivo*. Finally, sGC is a druggable target and sGC stimulators significantly attenuate the progression of atherosclerosis in mice. They could therefore be a promising therapeutic strategy to contain atherosclerosis also in humans.

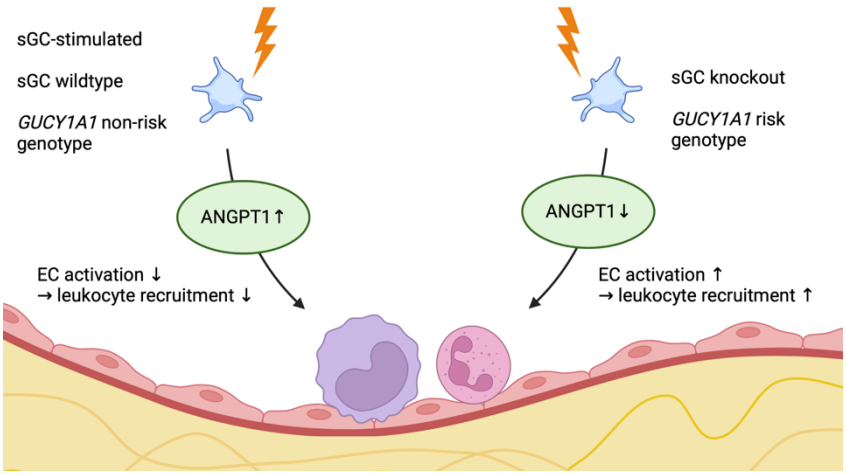

Figure 35 Schematic summary of sGC-mediated effects in platelets. Depending on the endogenous availability/activity of sGC, more or less ANGPT1 is released from platelets. ANGPT1 is involved in reduced endothelial activation and subsequently reduced leukocyte recruitment of monocytes and neutrophils into atherosclerotic plaques in mice. Abbreviations: *ANGPT1*, angiopoietin-1; *EC*, endothelial cell; *sGC*, soluble guanylyl cyclase. Created with BioRender.com.

Essentially, the results of this work emphasize the crucial role of platelets and, foremost, their enzyme sGC in the pathology of atherosclerosis. The here performed *in vivo* studies in mice and complementary *in vitro* studies using human and murine biospecimens particularly indicate an endogenous inhibitory role of platelet sGC on EC-mediated leukocyte recruitment. Beyond the effect of sGC signaling in platelets, therapeutic targeting of sGC using modern sGC-modulating drugs may be a promising strategy to combat the residual risk of atherosclerosis-related complications in cardiovascular diseases – the leading cause of death worldwide.

6 Bibliography

Ahluwalia, A., Foster, P., Scotland, R. S., McLean, P. G., Mathur, A., Perretti, M., Moncada, S., & Hobbs, A. J. (2004). Antiinflammatory activity of soluble guanylate cyclase: cGMP-dependent down-regulation of P-selectin expression and leukocyte recruitment. *Proc Natl Acad Sci U S A*, *101*(5), 1386-1391. https://doi.org/10.1073/pnas.0304264101

Ahmad, S., Cudmore, M. J., Wang, K., Hewett, P., Potluri, R., Fujisawa, T., & Ahmed, A. (2010). Angiopoietin-1 induces migration of monocytes in a tie-2 and integrin-independent manner. *Hypertension*, *56*(3), 477-483. https://doi.org/10.1161/HYPERTENSIONAHA.110.155556

Ahrens, I., Habersberger, J., Baumlin, N., Qian, H., Smith, B. K., Stasch, J. P., Bode, C., Schmidt, H. H., & Peter, K. (2011). Measuring oxidative burden and predicting pharmacological response in coronary artery disease patients with a novel direct activator of haem-free/oxidised sGC. *Atherosclerosis*, *218*(2), 431-434. https://doi.org/10.1016/j.atherosclerosis.2011.06.042

Alard, J. E., Ortega-Gomez, A., Wichapong, K., Bongiovanni, D., Horckmans, M., Megens, R. T., Leoni, G., Ferraro, B., Rossaint, J., Paulin, N., Ng, J., Ippel, H., Suylen, D., Hinkel, R., Blanchet, X., Gaillard, F., D'Amico, M., von Hundelshausen, P., Zarbock, A., Scheiermann, C., Hackeng, T. M., Steffens, S., Kupatt, C., Nicolaes, G. A., Weber, C., & Soehnlein, O. (2015). Recruitment of classical monocytes can be inhibited by disturbing heteromers of neutrophil HNP1 and platelet CCL5. *Sci Transl Med*, *7*(317), 317ra196. https://doi.org/10.1126/scitranslmed.aad5330

Alfieri, A., Ong, A. C., Kammerer, R. A., Solanky, T., Bate, S., Tasab, M., Brown, N. J., & Brookes, Z. L. (2014). Angiopoietin-1 regulates microvascular reactivity and protects the microcirculation during acute endothelial dysfunction: role of eNOS and VE-cadherin. *Pharmacol Res*, *80*, 43-51. https://doi.org/10.1016/j.phrs.2013.12.008

Anderson, J. L. & Morrow, D. A. (2017). Acute Myocardial Infarction. *N Engl J Med*, *376*(21), 2053-2064. https://doi.org/10.1056/NEJMra1606915

Andersson, D. P., Landucci, L., Lagerros, Y. T., Grotta, A., Bellocco, R., Lehtihet, M., & Holzmann, M. J. (2021). Association of Phosphodiesterase-5 Inhibitors Versus Alprostadil With Survival in Men With Coronary Artery Disease. *J Am Coll Cardiol*, *77*(12), 1535-1550. https://doi.org/10.1016/j.jacc.2021.01.045

Armstrong, P. W., Pieske, B., Anstrom, K. J., Ezekowitz, J., Hernandez, A. F., Butler, J., Lam, C. S. P., Ponikowski, P., Voors, A. A., Jia, G., McNulty, S. E., Patel, M. J., Roessig, L., Koglin, J., O'Connor, C. M., & VICTORIA Study Group. (2020). Vericiguat in Patients with Heart Failure and Reduced Ejection Fraction. *N Engl J Med*. https://doi.org/10.1056/NEJMoa1915928

Ashley, E. A. (2016). Towards precision medicine. *Nat Rev Genet*, *17*(9), 507-522. https://doi.org/10.1038/nrg.2016.86

Aszódi, A., Pfeifer, A., Ahmad, M., Glauner, M., Zhou, X. H., Ny, L., Andersson, K. E., Kehrel, B., Offermanns, S., & Fässler, R. (1999). The vasodilator-stimulated phosphoprotein (VASP) is involved in cGMP- and cAMP-mediated inhibition of agonist-induced platelet aggregation, but

is dispensable for smooth muscle function. *EMBO J*, *18*(1), 37-48. https://doi.org/10.1093/emboj/18.1.37

Babaei, S., Teichert-Kuliszewska, K., Zhang, Q., Jones, N., Dumont, D. J., & Stewart, D. J. (2003). Angiogenic actions of angiopoietin-1 require endothelium-derived nitric oxide. *Am J Pathol*, *162*(6), 1927-1936. https://doi.org/10.1016/S0002-9440(10)64326-X

Badrnya, S., Schrottmaier, W. C., Kral, J. B., Yaiw, K. C., Volf, I., Schabbauer, G., Söderberg-Nauclér, C., & Assinger, A. (2014). Platelets mediate oxidized low-density lipoprotein-induced monocyte extravasation and foam cell formation. *Arterioscler Thromb Vasc Biol*, *34*(3), 571-580. https://doi.org/10.1161/atvbaha.113.302919

Baigent, C., Blackwell, L., Emberson, J., Holland, L. E., Reith, C., Bhala, N., Peto, R., Barnes, E. H., Keech, A., Simes, J., & Collins, R. (2010). Efficacy and safety of more intensive lowering of LDL cholesterol: a meta-analysis of data from 170,000 participants in 26 randomised trials. *Lancet*, *376*(9753), 1670-1681. https://doi.org/10.1016/s0140-6736(10)61350-5

Bakogiannis, C., Sachse, M., Stamatelopoulos, K., & Stellos, K. (2019). Platelet-derived chemokines in inflammation and atherosclerosis. *Cytokine*, *122*, 154157. https://doi.org/10.1016/j.cyto.2017.09.013

Barrett, T. J., Schlegel, M., Zhou, F., Gorenchtein, M., Bolstorff, J., Moore, K. J., Fisher, E. A., & Berger, J. S. (2019). Platelet regulation of myeloid suppressor of cytokine signaling 3 accelerates atherosclerosis. *Sci Transl Med*, *11*(517). https://doi.org/10.1126/scitranslmed.aax0481

Battinelli, E. M., Markens, B. A., & Italiano, J. E., Jr. (2011). Release of angiogenesis regulatory proteins from platelet alpha granules: modulation of physiologic and pathologic angiogenesis. *Blood*, *118*(5), 1359-1369. https://doi.org/10.1182/blood-2011-02-334524

Battinelli, E. M., Thon, J. N., Okazaki, R., Peters, C. G., Vijey, P., Wilkie, A. R., Noetzli, L. J., Flaumenhaft, R., & Italiano, J. E. (2019). Megakaryocytes package contents into separate alpha-granules that are differentially distributed in platelets. *Blood Adv*, *3*(20), 3092-3098. https://doi.org/10.1182/bloodadvances.2018020834

Bennett, B. J., Davis, R. C., Civelek, M., Orozco, L., Wu, J., Qi, H., Pan, C., Packard, R. R., Eskin, E., Yan, M., Kirchgessner, T., Wang, Z., Li, X., Gregory, J. C., Hazen, S. L., Gargalovic, P. S., & Lusis, A. J. (2015). Genetic Architecture of Atherosclerosis in Mice: A Systems Genetics Analysis of Common Inbred Strains. *PLoS Genet*, *11*(12), e1005711. https://doi.org/10.1371/journal.pgen.1005711

Berenson, G. S., Srinivasan, S. R., Bao, W., Newman, W. P., 3rd, Tracy, R. E., & Wattigney, W. A. (1998). Association between multiple cardiovascular risk factors and atherosclerosis in children and young adults. The Bogalusa Heart Study. *N Engl J Med*, *338*(23), 1650-1656. https://doi.org/10.1056/nejm199806043382302

Bhatt, D. L., Steg, P. G., Miller, M., Brinton, E. A., Jacobson, T. A., Ketchum, S. B., Doyle, R. T., Jr., Juliano, R. A., Jiao, L., Granowitz, C., Tardif, J. C., & Ballantyne, C. M. (2019).

Cardiovascular Risk Reduction with Icosapent Ethyl for Hypertriglyceridemia. *N Engl J Med*, *380*(1), 11-22. https://doi.org/10.1056/NEJMoa1812792

Blair, A., Shaul, P. W., Yuhanna, I. S., Conrad, P. A., & Smart, E. J. (1999). Oxidized low density lipoprotein displaces endothelial nitric-oxide synthase (eNOS) from plasmalemmal caveolae and impairs eNOS activation. *J Biol Chem*, *274*(45), 32512-32519. https://doi.org/10.1074/jbc.274.45.32512

Boettcher, M., Düngen, H. D., Donath, F., Mikus, G., Werner, N., Thuermann, P. A., Karakas, M., Besche, N., Koch, T., Gurniak, M., & Becker, C. (2022). Vericiguat in Combination with Short-Acting Nitroglycerin in Patients With Chronic Coronary Syndromes: The Randomized, Phase Ib, VENICE Study. *Clin Pharmacol Ther*, *111*(6), 1239-1247. https://doi.org/10.1002/cpt.2574

Boettcher, M., Mikus, G., Trenk, D., Düngen, H. D., Donath, F., Werner, N., Karakas, M., Besche, N., Schulz-Burck, D., Gerrits, M., Hung, J., & Becker, C. (2022). Vericiguat in combination with isosorbide mononitrate in patients with chronic coronary syndromes: The randomized, phase Ib, VISOR study. *Clin Transl Sci*, *15*(5), 1204-1214. https://doi.org/10.1111/cts.13238

Borén, J., Chapman, M. J., Krauss, R. M., Packard, C. J., Bentzon, J. F., Binder, C. J., Daemen, M. J., Demer, L. L., Hegele, R. A., Nicholls, S. J., Nordestgaard, B. G., Watts, G. F., Bruckert, E., Fazio, S., Ference, B. A., Graham, I., Horton, J. D., Landmesser, U., Laufs, U., Masana, L., Pasterkamp, G., Raal, F. J., Ray, K. K., Schunkert, H., Taskinen, M. R., van de Sluis, B., Wiklund, O., Tokgozoglu, L., Catapano, A. L., & Ginsberg, H. N. (2020). Low-density lipoproteins cause atherosclerotic cardiovascular disease: pathophysiological, genetic, and therapeutic insights: a consensus statement from the European Atherosclerosis Society Consensus Panel. *Eur Heart J*, *41*(24), 2313-2330. https://doi.org/10.1093/eurheartj/ehz962

Braun, L. J., Stegmeyer, R. I., Schafer, K., Volkery, S., Currie, S. M., Kempe, B., Nottebaum, A. F., & Vestweber, D. (2020). Platelets docking to VWF prevent leaks during leukocyte extravasation by stimulating Tie-2. *Blood*, *136*(5), 627-639. https://doi.org/10.1182/blood.2019003442

Brindle, N. P., Saharinen, P., & Alitalo, K. (2006). Signaling and functions of angiopoietin-1 in vascular protection. *Circ Res*, *98*(8), 1014-1023. https://doi.org/10.1161/01.RES.0000218275.54089.12

Burger, P. C. & Wagner, D. D. (2003). Platelet P-selectin facilitates atherosclerotic lesion development. *Blood*, *101*(7), 2661-2666. https://doi.org/10.1182/blood-2002-07-2209

Burkhart, J. M., Vaudel, M., Gambaryan, S., Radau, S., Walter, U., Martens, L., Geiger, J., Sickmann, A., & Zahedi, R. P. (2012). The first comprehensive and quantitative analysis of human platelet protein composition allows the comparative analysis of structural and functional pathways. *Blood*, *120*(15), e73-82. https://doi.org/10.1182/blood-2012-04-416594

Burnett, A., Gomez, I., De Leon, D. D., Ariaans, M., Progias, P., Kammerer, R. A., Velasco, G., Marron, M., Hellewell, P., & Ridger, V. (2017). Angiopoietin-1 enhances neutrophil chemotaxis in vitro and migration in vivo through interaction with CD18 and release of CCL4. *Sci Rep*, *7*(1), 2332. https://doi.org/10.1038/s41598-017-02216-y

Calaminus, S. D., Guitart, A. V., Sinclair, A., Schachtner, H., Watson, S. P., Holyoake, T. L., Kranc, K. R., & Machesky, L. M. (2012). Lineage tracing of Pf4-Cre marks hematopoietic stem cells and their progeny. *PLoS One*, *7*(12), e51361. https://doi.org/10.1371/journal.pone.0051361

Campbell, B. C. V. & Khatri, P. (2020). Stroke. *Lancet*, *396*(10244), 129-142. https://doi.org/10.1016/S0140-6736(20)31179-X

CARDIoGRAMplusC4D Consortium, D., P., Kanoni, S., Willenborg, C., Farrall, M., Assimes, T. L., Thompson, J. R., Ingelsson, E., Saleheen, D., Erdmann, J., Goldstein, B. A., Stirrups, K., König, I. R., Cazier, J. B., Johansson, A., Hall, A. S., Lee, J. Y., Willer, C. J., Chambers, J. C., Esko, T., Folkersen, L., Goel, A., Grundberg, E., Havulinna, A. S., Ho, W. K., Hopewell, J. C., Eriksson, N., Kleber, M. E., Kristiansson, K., Lundmark, P., Lyytikainen, L. P., Rafelt, S., Shungin, D., Strawbridge, R. J., Thorleifsson, G., Tikkanen, E., Van Zuydam, N., Voight, B. F., Waite, L. L., Zhang, W., Ziegler, A., Absher, D., Altshuler, D., Balmforth, A. J., Barroso, I., Braund, P. S., Burgdorf, C., Claudi-Boehm, S., Cox, D., Dimitriou, M., Do, R., DIAGRAM Consortium, CARDIOGENICS Consortium, Doney, A. S., El Mokhtari, N., Eriksson, P., Fischer, K., Fontanillas, P., Franco-Cereceda, A., Gigante, B., Groop, L., Gustafsson, S., Hager, J., Hallmans, G., Han, B. G., Hunt, S. E., Kang, H. M., Illig, T., Kessler, T., Knowles, J. W., Kolovou, G., Kuusisto, J., Langenberg, C., Langford, C., Leander, K., Lokki, M. L., Lundmark, A., McCarthy, M. I., Meisinger, C., Melander, O., Mihailov, E., Maouche, S., Morris, A. D., Müller-Nurasyid, M., MuTHER Consortium, Nikus, K., Peden, J. F., Rayner, N. W., Rasheed, A., Rosinger, S., Rubin, D., Rumpf, M. P., Schäfer, A., Sivananthan, M., Song, C., Stewart, A. F., Tan, S. T., Thorgeirsson, G., van der Schoot, C. E., Wagner, P. J., Wellcome Trust Case Control Consortium, Wells, G. A., Wild, P. S., Yang, T. P., Amouyel, P., Arveiler, D., Basart, H., Boehnke, M., Boerwinkle, E., Brambilla, P., Cambien, F., Cupples, A. L., de Faire, U., Dehghan, A., Diemert, P., Epstein, S. E., Evans, A. Ferrario, M. M. Ferrieres, J., Gauguier, D., Go, A. S., Goodall, A. H., Gudnason, V., Hazen, S. L., Holm, H., Iribarren, C., Jang, Y., Kahonen, M., Kee, F., Kim, H. S., Klopp, N., Koenig, W., Kratzer, W., Kuulasmaa, K., Laakso, M., Laaksonen, R., Lee, J. Y., Lind, L., Ouwehand, W. H., Parish, S., Park, J. E., Pedersen, N. L., Peters, A., Quertermous, T., Rader, D. J., Salomaa, V., Schadt, E., Shah, S. H., Sinisalo, J., Stark, K., Stefansson, K., Tregouet, D. A., Virtamo, J., Wallentin, L., Wareham, N., Zimmermann, M. E., Nieminen, M. S., Hengstenberg, C., Sandhu, M. S., Pastinen, T., Syvanen, A. C., Hovingh, G. K., Dedoussis, G., Franks, P. W., Lehtimaki, T., Metspalu, A., Zalloua, P. A., Siegbahn, A., Schreiber, S., Ripatti, S., Blankenberg, S. S., Perola, M., Clarke, R., Boehm, B. O., O'Donnell, C., Reilly, M. P., März, W., Collins, R., Kathiresan, S., Hamsten, A., Kooner, J. S., Thorsteinsdottir, U., Danesh, J., Palmer, C. N., Roberts, R., Watkins, H., Schunkert, H., Samani, N. J. (2013). Large-scale association analysis identifies new risk loci for coronary artery disease. *Nat Genet*, *45*(1), 25-33. https://doi.org/10.1038/ng.2480

Chatterjee, M., Huang, Z., Zhang, W., Jiang, L., Hultenby, K., Zhu, L., Hu, H., Nilsson, G. P., & Li, N. (2011). Distinct platelet packaging, release, and surface expression of proangiogenic and antiangiogenic factors on different platelet stimuli. *Blood*, *117*(14), 3907-3911. https://doi.org/10.1182/blood-2010-12-327007

Chen, Z. & Schunkert, H. (2021). Genetics of coronary artery disease in the post-GWAS era. *J Intern Med*, *290*(5), 980-992. https://doi.org/10.1111/joim.13362

Coenen, D. M., Heinzmann, A. C. A., Karel, M. F. A., Cosemans, J. M. E. M., & Koenen, R. R. (2021). The multifaceted contribution of platelets in the emergence and aftermath of acute

cardiovascular events. *Atherosclerosis*, *319*, 132-141. https://doi.org/https://doi.org/10.1016/j.atherosclerosis.2020.12.017

Coppinger, J. A., Cagney, G., Toomey, S., Kislinger, T., Belton, O., McRedmond, J. P., Cahill, D. J., Emili, A., Fitzgerald, D. J., & Maguire, P. B. (2004). Characterization of the proteins released from activated platelets leads to localization of novel platelet proteins in human atherosclerotic lesions. *Blood*, *103*(6), 2096-2104. https://doi.org/10.1182/blood-2003-08-2804

Costa, A. D., Garlid, K. D., West, I. C., Lincoln, T. M., Downey, J. M., Cohen, M. V., & Critz, S. D. (2005). Protein kinase G transmits the cardioprotective signal from cytosol to mitochondria. *Circ Res*, *97*(4), 329-336. https://doi.org/10.1161/01.RES.0000178451.08719.5b

Daiber, A. & Münzel, T. (2015). Organic Nitrate Therapy, Nitrate Tolerance, and Nitrate-Induced Endothelial Dysfunction: Emphasis on Redox Biology and Oxidative Stress. *Antioxid Redox Signal*, *23*(11), 899-942. https://doi.org/10.1089/ars.2015.6376

Dang, T. A., Kessler, T., Wobst, J., Wierer, M., Braenne, I., Strom, T. M., Tennstedt, S., Sager, H. B., Meitinger, T., Erdmann, J., & Schunkert, H. (2021). Identification of a Functional PDE5A Variant at the Chromosome 4q27 Coronary Artery Disease Locus in an Extended Myocardial Infarction Family. *Circulation*, *144*(8), 662-665. https://doi.org/10.1161/circulationaha.120.052975

Dang, T. A., Schunkert, H., & Kessler, T. (2020). cGMP Signaling in Cardiovascular Diseases: Linking Genotype and Phenotype. *J Cardiovasc Pharmacol*, *75*(6), 516-525. https://doi.org/10.1097/FJC.0000000000000744

Dangel, O., Mergia, E., Karlisch, K., Groneberg, D., Koesling, D., & Friebe, A. (2010). Nitric oxide-sensitive guanylyl cyclase is the only nitric oxide receptor mediating platelet inhibition. *J Thromb Haemost*, *8*(6), 1343-1352. https://doi.org/10.1111/j.1538-7836.2010.03806.x

Davì, G. & Patrono, C. (2007). Platelet activation and atherothrombosis. *N Engl J Med*, *357*(24), 2482-2494. https://doi.org/10.1056/NEJMra071014

Davis, M. E., Grumbach, I. M., Fukai, T., Cutchins, A., & Harrison, D. G. (2004). Shear stress regulates endothelial nitric-oxide synthase promoter activity through nuclear factor kappaB binding. *J Biol Chem*, *279*(1), 163-168. https://doi.org/10.1074/jbc.M307528200

Delporte, C., Boudjeltia, K. Z., Noyon, C., Furtmüller, P. G., Nuyens, V., Slomianny, M. C., Madhoun, P., Desmet, J. M., Raynal, P., Dufour, D., Koyani, C. N., Reyé, F., Rousseau, A., Vanhaeverbeek, M., Ducobu, J., Michalski, J. C., Nève, J., Vanhamme, L., Obinger, C., Malle, E., & Van Antwerpen, P. (2014). Impact of myeloperoxidase-LDL interactions on enzyme activity and subsequent posttranslational oxidative modifications of apoB-100. *J Lipid Res*, *55*(4), 747-757. https://doi.org/10.1194/jlr.M047449

Denis, M. M., Tolley, N. D., Bunting, M., Schwertz, H., Jiang, H., Lindemann, S., Yost, C. C., Rubner, F. J., Albertine, K. H., Swoboda, K. J., Fratto, C. M., Tolley, E., Kraiss, L. W., McIntyre, T. M., Zimmerman, G. A., & Weyrich, A. S. (2005). Escaping the nuclear confines: signal-

dependent pre-mRNA splicing in anucleate platelets. *Cell*, *122*(3), 379-391. https://doi.org/10.1016/j.cell.2005.06.015

Desch, M., Sigl, K., Hieke, B., Salb, K., Kees, F., Bernhard, D., Jochim, A., Spiessberger, B., Hocherl, K., Feil, R., Feil, S., Lukowski, R., Wegener, J. W., Hofmann, F., & Schlossmann, J. (2010). IRAG determines nitric oxide- and atrial natriuretic peptide-mediated smooth muscle relaxation. *Cardiovasc Res*, *86*(3), 496-505. https://doi.org/10.1093/cvr/cvq008

Divakaran, S. & Loscalzo, J. (2017). The Role of Nitroglycerin and Other Nitrogen Oxides in Cardiovascular Therapeutics. *J Am Coll Cardiol*, *70*(19), 2393-2410. https://doi.org/10.1016/j.jacc.2017.09.1064

Drachman, J. G., Sabath, D. F., Fox, N. E., & Kaushansky, K. (1997). Thrombopoietin signal transduction in purified murine megakaryocytes. *Blood*, *89*(2), 483-492. https://www.ncbi.nlm.nih.gov/pubmed/9002950

Emdin, C. A., Khera, A. V., Klarin, D., Natarajan, P., Zekavat, S. M., Nomura, A., Haas, M., Aragam, K., Ardissino, D., Wilson, J. G., Schunkert, H., McPherson, R., Watkins, H., Elosua, R., Bown, M. J., Samani, N. J., Baber, U., Erdmann, J., Gormley, P., Palotie, A., Stitziel, N. O., Gupta, N., Danesh, J., Saleheen, D., Gabriel, S., & Kathiresan, S. (2018). Phenotypic Consequences of a Genetic Predisposition to Enhanced Nitric Oxide Signaling. *Circulation*, *137*(3), 222-232. https://doi.org/10.1161/CIRCULATIONAHA.117.028021

Erbel, C., Tyka, M., Helmes, C. M., Akhavanpoor, M., Rupp, G., Domschke, G., Linden, F., Wolf, A., Doesch, A., Lasitschka, F., Katus, H. A., & Gleissner, C. A. (2015). CXCL4-induced plaque macrophages can be specifically identified by co-expression of MMP7+S100A8+ in vitro and in vivo. *Innate Immun*, *21*(3), 255-265. https://doi.org/10.1177/1753425914526461

Erdmann, J., Stark, K., Esslinger, U. B., Rumpf, P. M., Koesling, D., de Wit, C., Kaiser, F. J., Braunholz, D., Medack, A., Fischer, M., Zimmermann, M. E., Tennstedt, S., Graf, E., Eck, S., Aherrahrou, Z., Nahrstaedt, J., Willenborg, C., Bruse, P., Braenne, I., Nothen, M. M., Hofmann, P., Braund, P. S., Mergia, E., Reinhard, W., Burgdorf, C., Schreiber, S., Balmforth, A. J., Hall, A. S., Bertram, L., Steinhagen-Thiessen, E., Li, S. C., Marz, W., Reilly, M., Kathiresan, S., McPherson, R., Walter, U., CardioGram, Ott, J., Samani, N. J., Strom, T. M., Meitinger, T., Hengstenberg, C., & Schunkert, H. (2013). Dysfunctional nitric oxide signalling increases risk of myocardial infarction. *Nature*, *504*(7480), 432-436. https://doi.org/10.1038/nature12722

Feil, R. & Kemp-Harper, B. (2006). cGMP signalling: from bench to bedside. Conference on cGMP generators, effectors and therapeutic implications. *EMBO Rep*, *7*(2), 149-153. https://doi.org/10.1038/sj.embor.7400627

Fiolet, A. T. L., Opstal, T. S. J., Mosterd, A., Eikelboom, J. W., Jolly, S. S., Keech, A. C., Kelly, P., Tong, D. C., Layland, J., Nidorf, S. M., Thompson, P. L., Budgeon, C., Tijssen, J. G. P., & Cornel, J. H. (2021). Efficacy and safety of low-dose colchicine in patients with coronary disease: a systematic review and meta-analysis of randomized trials. *Eur Heart J*, *42*(28), 2765-2775. https://doi.org/10.1093/eurheartj/ehab115

Förstermann, U., Xia, N., & Li, H. (2017). Roles of Vascular Oxidative Stress and Nitric Oxide in

the Pathogenesis of Atherosclerosis. *Circ Res*, *120*(4), 713-735. https://doi.org/10.1161/CIRCRESAHA.116.309326

Francis, S. H., Busch, J. L., Corbin, J. D., & Sibley, D. (2010). cGMP-dependent protein kinases and cGMP phosphodiesterases in nitric oxide and cGMP action. *Pharmacol Rev*, *62*(3), 525-563. https://doi.org/10.1124/pr.110.002907

Franzén, O., Ermel, R., Cohain, A., Akers, N. K., Di Narzo, A., Talukdar, H. A., Foroughi-Asl, H., Giambartolomei, C., Fullard, J. F., Sukhavasi, K., Köks, S., Gan, L. M., Giannarelli, C., Kovacic, J. C., Betsholtz, C., Losic, B., Michoel, T., Hao, K., Roussos, P., Skogsberg, J., Ruusalepp, A., Schadt, E. E., & Björkegren, J. L. (2016). Cardiometabolic risk loci share downstream cis- and trans-gene regulation across tissues and diseases. *Science*, *353*(6301), 827-830. https://doi.org/10.1126/science.aad6970

Friebe, A., Mergia, E., Dangel, O., Lange, A., & Koesling, D. (2007). Fatal gastrointestinal obstruction and hypertension in mice lacking nitric oxide-sensitive guanylyl cyclase. *Proc Natl Acad Sci U S A*, *104*(18), 7699-7704. https://doi.org/10.1073/pnas.0609778104

Fujisawa, T., Wang, K., Niu, X. L., Egginton, S., Ahmad, S., Hewett, P., Kontos, C. D., & Ahmed, A. (2017). Angiopoietin-1 promotes atherosclerosis by increasing the proportion of circulating Gr1+ monocytes. *Cardiovasc Res*, *113*(1), 81-89. https://doi.org/10.1093/cvr/cvw223

Furchgott, R. F. & Zawadzki, J. V. (1980). The obligatory role of endothelial cells in the relaxation of arterial smooth muscle by acetylcholine. *Nature*, *288*(5789), 373-376. https://doi.org/10.1038/288373a0

Gamble, J. R., Drew, J., Trezise, L., Underwood, A., Parsons, M., Kasminkas, L., Rudge, J., Yancopoulos, G., & Vadas, M. A. (2000). Angiopoietin-1 is an antipermeability and anti-inflammatory agent in vitro and targets cell junctions. *Circ Res*, *87*(7), 603-607. https://doi.org/10.1161/01.res.87.7.603

Gerhardt, T. & Ley, K. (2015). Monocyte trafficking across the vessel wall. *Cardiovasc Res*, *107*(3), 321-330. https://doi.org/10.1093/cvr/cvv147

Gerrity, R. G. (1981). The role of the monocyte in atherogenesis: I. Transition of blood-borne monocytes into foam cells in fatty lesions. *Am J Pathol*, *103*(2), 181-190. https://www.ncbi.nlm.nih.gov/pubmed/7234961

Ghofrani, H. A., Galiè, N., Grimminger, F., Grünig, E., Humbert, M., Jing, Z. C., Keogh, A. M., Langleben, D., Kilama, M. O., Fritsch, A., Neuser, D., & Rubin, L. J. (2013). Riociguat for the treatment of pulmonary arterial hypertension. *N Engl J Med*, *369*(4), 330-340. https://doi.org/10.1056/NEJMoa1209655

Gisterå, A., Ketelhuth, D. F. J., Malin, S. G., & Hansson, G. K. (2022). Animal Models of Atherosclerosis-Supportive Notes and Tricks of the Trade. *Circ Res*, *130*(12), 1869-1887. https://doi.org/10.1161/circresaha.122.320263

Gleissner, C. A., Shaked, I., Erbel, C., Bockler, D., Katus, H. A., & Ley, K. (2010). CXCL4 downregulates the atheroprotective hemoglobin receptor CD163 in human macrophages. *Circ Res*, *106*(1), 203-211. https://doi.org/10.1161/CIRCRESAHA.109.199505

Gollomp, K. & Poncz, M. (2019). Gp1ba-Cre or Pf4-Cre: pick your poison. *Blood*, *133*(4), 287-288. https://doi.org/10.1182/blood-2018-11-887513

Gomes de Almeida Schirmer, B., Crucet, M., Stivala, S., Vucicevic, G., da Silva Barcelos, L., Vanhoutte, P. M., Pellegrini, G., Camici, G. G., Seebeck, P., Pfundstein, S., Stein, S., Paneni, F., Luscher, T. F., & Simic, B. (2020). The NO-donor MPC-1011 stimulates angiogenesis and arteriogenesis and improves hindlimb ischemia via a cGMP-dependent pathway involving VEGF and SDF-1alpha. *Atherosclerosis*, *304*, 30-38. https://doi.org/10.1016/j.atherosclerosis.2020.05.012

Gros, A., Ollivier, V., & Ho-Tin-Noé, B. (2014). Platelets in inflammation: regulation of leukocyte activities and vascular repair. *Front Immunol*, *5*, 678.

Guedeney, P., Giustino, G., Sorrentino, S., Claessen, B. E., Camaj, A., Kalkman, D. N., Vogel, B., Sartori, S., De Rosa, S., Baber, U., Indolfi, C., Montalescot, G., Dangas, G. D., Rosenson, R. S., Pocock, S. J., & Mehran, R. (2019). Efficacy and safety of alirocumab and evolocumab: a systematic review and meta-analysis of randomized controlled trials. *Eur Heart J*. https://doi.org/10.1093/eurheartj/ehz430

Hall, K. T., Kessler, T., Buring, J. E., Passow, D., Sesso, H. D., Zee, R. Y. L., Ridker, P. M., Chasman, D. I., & Schunkert, H. (2019). Genetic variation at the coronary artery disease risk locus GUCY1A3 modifies cardiovascular disease prevention effects of aspirin. *Eur Heart J*, *40*(41), 3385-3392. https://doi.org/10.1093/eurheartj/ehz384

Harper, M. T. & Poole, A. W. (2010). Diverse functions of protein kinase C isoforms in platelet activation and thrombus formation. *J Thromb Haemost*, *8*(3), 454-462. https://doi.org/https://doi.org/10.1111/j.1538-7836.2009.03722.x

Heib, T., Gross, C., Muller, M. L., Stegner, D., & Pleines, I. (2021). Isolation of murine bone marrow by centrifugation or flushing for the analysis of hematopoietic cells - a comparative study. *Platelets*, *32*(5), 601-607. https://doi.org/10.1080/09537104.2020.1797323

Heidt, T., Sager, H. B., Courties, G., Dutta, P., Iwamoto, Y., Zaltsman, A., von Zur Muhlen, C., Bode, C., Fricchione, G. L., Denninger, J., Lin, C. P., Vinegoni, C., Libby, P., Swirski, F. K., Weissleder, R., & Nahrendorf, M. (2014). Chronic variable stress activates hematopoietic stem cells. *Nat Med*, *20*(7), 754-758. https://doi.org/10.1038/nm.3589

Heijnen, H. F. G. & Korporaal, S. J. A. (2017). Platelet Morphology and Ultrastructure. In P. Gresele, N. S. Kleiman, J. A. Lopez, & C. P. Page (Eds.), *Platelets in Thrombotic and Non-Thrombotic Disorders: Pathophysiology, Pharmacology and Therapeutics: an Update* (pp. 21-37). Springer International Publishing. https://doi.org/10.1007/978-3-319-47462-5_3

Heijnen, H. F. G. & van der Sluijs, P. (2015). Platelet secretory behaviour: as diverse as the granules

... or not? *J Thromb Haemost*, *13*(12), 2141-2151. https://doi.org/10.1111/jth.13147

Henn, V., Slupsky, J. R., Gräfe, M., Anagnostopoulos, I., Förster, R., Müller-Berghaus, G., & Kroczek, R. A. (1998). CD40 ligand on activated platelets triggers an inflammatory reaction of endothelial cells. *Nature*, *391*(6667), 591-594. https://doi.org/10.1038/35393

Hervé, D., Philippi, A., Belbouab, R., Zerah, M., Chabrier, S., Collardeau-Frachon, S., Bergametti, F., Essongue, A., Berrou, E., Krivosic, V., Sainte-Rose, C., Houdart, E., Adam, F., Billiemaz, K., Lebret, M., Roman, S., Passemard, S., Boulday, G., Delaforge, A., Guey, S., Dray, X., Chabriat, H., Brouckaert, P., Bryckaert, M., & Tournier-Lasserve, E. (2014). Loss of α1β1 soluble guanylate cyclase, the major nitric oxide receptor, leads to moyamoya and achalasia. *Am J Hum Genet*, *94*(3), 385-394. https://doi.org/10.1016/j.ajhg.2014.01.018

Hou, Y., Lascola, J., Dulin, N. O., Ye, R. D., & Browning, D. D. (2003). Activation of cGMP-dependent Protein Kinase by Protein Kinase C*. *J Biol Chem*, *278*(19), 16706-16712. https://doi.org/https://doi.org/10.1074/jbc.M300045200

Howson, J. M. M., Zhao, W., Barnes, D. R., Ho, W. K., Young, R., Paul, D. S., Waite, L. L., Freitag, D. F., Fauman, E. B., Salfati, E. L., Sun, B. B., Eicher, J. D., Johnson, A. D., Sheu, W. H. H., Nielsen, S. F., Lin, W. Y., Surendran, P., Malarstig, A., Wilk, J. B., Tybjaerg-Hansen, A., Rasmussen, K. L., Kamstrup, P. R., Deloukas, P., Erdmann, J., Kathiresan, S., Samani, N. J., Schunkert, H., Watkins, H., CardioGramplusC4D, Do, R., Rader, D. J., Johnson, J. A., Hazen, S. L., Quyyumi, A. A., Spertus, J. A., Pepine, C. J., Franceschini, N., Justice, A., Reiner, A. P., Buyske, S., Hindorff, L. A., Carty, C. L., North, K. E., Kooperberg, C., Boerwinkle, E., Young, K., Graff, M., Peters, U., Absher, D., Hsiung, C. A., Lee, W. J., Taylor, K. D., Chen, Y. H., Lee, I. T., Guo, X., Chung, R. H., Hung, Y. J., Rotter, J. I., Juang, J. J., Quertermous, T., Wang, T. D., Rasheed, A., Frossard, P., Alam, D. S., Majumder, A. A. S., Di Angelantonio, E., Chowdhury, R., Epic, C. V. D., Chen, Y. I., Nordestgaard, B. G., Assimes, T. L., Danesh, J., Butterworth, A. S., & Saleheen, D. (2017). Fifteen new risk loci for coronary artery disease highlight arterial-wall-specific mechanisms. *Nat Genet*, *49*(7), 1113-1119. https://doi.org/10.1038/ng.3874

Ignarro, L. J., Buga, G. M., Wood, K. S., Byrns, R. E., & Chaudhuri, G. (1987). Endothelium-derived relaxing factor produced and released from artery and vein is nitric oxide. *Proc Natl Acad Sci U S A*, *84*(24), 9265-9269. https://doi.org/10.1073/pnas.84.24.9265

Ismail, H., Mofarrahi, M., Echavarria, R., Harel, S., Verdin, E., Lim, H. W., Jin, Z. G., Sun, J., Zeng, H., & Hussain, S. N. (2012). Angiopoietin-1 and vascular endothelial growth factor regulation of leukocyte adhesion to endothelial cells: role of nuclear receptor-77. *Arterioscler Thromb Vasc Biol*, *32*(7), 1707-1716. https://doi.org/10.1161/atvbaha.112.251546

Italiano, J. E., Jr., Richardson, J. L., Patel-Hett, S., Battinelli, E., Zaslavsky, A., Short, S., Ryeom, S., Folkman, J., & Klement, G. L. (2008). Angiogenesis is regulated by a novel mechanism: pro- and antiangiogenic proteins are organized into separate platelet alpha granules and differentially released. *Blood*, *111*(3), 1227-1233. https://doi.org/10.1182/blood-2007-09-113837

Jabs, A., Oelze, M., Mikhed, Y., Stamm, P., Kröller-Schön, S., Welschof, P., Jansen, T., Hausding, M., Kopp, M., Steven, S., Schulz, E., Stasch, J. P., Münzel, T., & Daiber, A. (2015). Effect of

soluble guanylyl cyclase activator and stimulator therapy on nitroglycerin-induced nitrate tolerance in rats. *Vascul Pharmacol*, *71*, 181-191. https://doi.org/10.1016/j.vph.2015.03.007

Jonnalagadda, D., Izu, L. T., & Whiteheart, S. W. (2012). Platelet secretion is kinetically heterogeneous in an agonist-responsive manner. *Blood*, *120*(26), 5209-5216. https://doi.org/10.1182/blood-2012-07-445080

Joshi, P. H. & de Lemos, J. A. (2021). Diagnosis and Management of Stable Angina: A Review. *JAMA*, *325*(17), 1765-1778. https://doi.org/10.1001/jama.2021.1527

Kamykowski, J., Carlton, P., Sehgal, S., & Storrie, B. (2011). Quantitative immunofluorescence mapping reveals little functional coclustering of proteins within platelet α-granules. *Blood*, *118*(5), 1370-1373. https://doi.org/10.1182/blood-2011-01-330910

Kang, Y., Liu, R., Wu, J.-X., & Chen, L. (2019). Structural insights into the mechanism of human soluble guanylate cyclase. *Nature*, *574*(7777), 206-210. https://doi.org/10.1038/s41586-019-1584-6

Kessler, T., Wobst, J., Wolf, B., Eckhold, J., Vilne, B., Hollstein, R., von Ameln, S., Dang, T. A., Sager, H. B., Moritz Rumpf, P., Aherrahrou, R., Kastrati, A., Björkegren, J. L. M., Erdmann, J., Lusis, A. J., Civelek, M., Kaiser, F. J., & Schunkert, H. (2017). Functional Characterization of the GUCY1A3 Coronary Artery Disease Risk Locus. *Circulation*, *136*(5), 476-489. https://doi.org/10.1161/circulationaha.116.024152

Khera, A. V., Emdin, C. A., Drake, I., Natarajan, P., Bick, A. G., Cook, N. R., Chasman, D. I., Baber, U., Mehran, R., Rader, D. J., Fuster, V., Boerwinkle, E., Melander, O., Orho-Melander, M., Ridker, P. M., & Kathiresan, S. (2016). Genetic Risk, Adherence to a Healthy Lifestyle, and Coronary Disease. *N Engl J Med*, *375*(24), 2349-2358. https://doi.org/10.1056/NEJMoa1605086

Kim, I., Moon, S. O., Park, S. K., Chae, S. W., & Koh, G. Y. (2001). Angiopoietin-1 reduces VEGF-stimulated leukocyte adhesion to endothelial cells by reducing ICAM-1, VCAM-1, and E-selectin expression. *Circ Res*, *89*(6), 477-479. https://doi.org/10.1161/hh1801.097034

Kim, K., Shim, D., Lee, J. S., Zaitsev, K., Williams, J. W., Kim, K. W., Jang, M. Y., Seok Jang, H., Yun, T. J., Lee, S. H., Yoon, W. K., Prat, A., Seidah, N. G., Choi, J., Lee, S. P., Yoon, S. H., Nam, J. W., Seong, J. K., Oh, G. T., Randolph, G. J., Artyomov, M. N., Cheong, C., & Choi, J. H. (2018). Transcriptome Analysis Reveals Nonfoamy Rather Than Foamy Plaque Macrophages Are Proinflammatory in Atherosclerotic Murine Models. *Circ Res*, *123*(10), 1127-1142. https://doi.org/10.1161/circresaha.118.312804

Kinexus Bioinformatics Corporation. (2019). *PhosphoNET*. Retrieved July 1, 2022 from http://www.phosphonet.ca

Klarin, D., Zhu, Q. M., Emdin, C. A., Chaffin, M., Horner, S., McMillan, B. J., Leed, A., Weale, M. E., Spencer, C. C. A., Aguet, F., Segre, A. V., Ardlie, K. G., Khera, A. V., Kaushik, V. K., Natarajan, P., CARDIoGRAMplusC4D Consortium, & Kathiresan, S. (2017). Genetic analysis

in UK Biobank links insulin resistance and transendothelial migration pathways to coronary artery disease. *Nat Genet*, *49*(9), 1392-1397. https://doi.org/10.1038/ng.3914

Knuuti, J., Wijns, W., Saraste, A., Capodanno, D., Barbato, E., Funck-Brentano, C., Prescott, E., Storey, R. F., Deaton, C., Cuisset, T., Agewall, S., Dickstein, K., Edvardsen, T., Escaned, J., Gersh, B. J., Svitil, P., Gilard, M., Hasdai, D., Hatala, R., Mahfoud, F., Masip, J., Muneretto, C., Valgimigli, M., Achenbach, S., Bax, J. J., & ESC Scientific Document Group. (2019). 2019 ESC Guidelines for the diagnosis and management of chronic coronary syndromes: The Task Force for the diagnosis and management of chronic coronary syndromes of the European Society of Cardiology (ESC). *Eur Heart J*, *41*(3), 407-477. https://doi.org/10.1093/eurheartj/ehz425

Konkoth, A., Saraswat, R., Dubrou, C., Sabatier, F., Leroyer, A. S., Lacroix, R., Duchez, A.-C., & Dignat-George, F. (2021). Multifaceted role of extracellular vesicles in atherosclerosis. *Atherosclerosis*, *319*, 121-131. https://doi.org/https://doi.org/10.1016/j.atherosclerosis.2020.11.006

Kraehling, J. R. & Sessa, W. C. (2017). Contemporary Approaches to Modulating the Nitric Oxide-cGMP Pathway in Cardiovascular Disease. *Circ Res*, *120*(7), 1174-1182. https://doi.org/10.1161/circresaha.117.303776

Krishnan, S. M., Nordlohne, J., Dietz, L., Vakalopoulos, A., Haning, P., Hartmann, E., Seifert, R., Hüser, J., Mathar, I., & Sandner, P. (2021). Assessing the Use of the sGC Stimulator BAY-747, as a Potential Treatment for Duchenne Muscular Dystrophy. *Int J Mol Sci*, *22*(15). https://doi.org/10.3390/ijms22158016

Kuhlencordt, P. J., Gyurko, R., Han, F., Scherrer-Crosbie, M., Aretz, T. H., Hajjar, R., Picard, M. H., & Huang, P. L. (2001). Accelerated atherosclerosis, aortic aneurysm formation, and ischemic heart disease in apolipoprotein E/endothelial nitric oxide synthase double-knockout mice. *Circulation*, *104*(4), 448-454. https://doi.org/10.1161/hc2901.091399

Ley, K., Laudanna, C., Cybulsky, M. I., & Nourshargh, S. (2007). Getting to the site of inflammation: the leukocyte adhesion cascade updated. *Nat Rev Immunol*, *7*(9), 678-689. https://doi.org/10.1038/nri2156

Li, J. J., Huang, Y. Q., Basch, R., & Karpatkin, S. (2001). Thrombin induces the release of angiopoietin-1 from platelets. *Thromb Haemost*, *85*(2), 204-206. https://www.ncbi.nlm.nih.gov/pubmed/11246533

Li, N., Hu, H., Lindqvist, M., Wikström-Jonsson, E., Goodall, A. H., & Hjemdahl, P. (2000). Platelet-leukocyte cross talk in whole blood. *Arterioscler Thromb Vasc Biol*, *20*(12), 2702-2708. https://doi.org/10.1161/01.atv.20.12.2702

Li, Z., Xi, X., Gu, M., Feil, R., Ye, R. D., Eigenthaler, M., Hofmann, F., & Du, X. (2003). A stimulatory role for cGMP-dependent protein kinase in platelet activation. *Cell*, *112*(1), 77-86. https://doi.org/10.1016/s0092-8674(02)01254-0

Li, Z., Zhang, G., Marjanovic, J. A., Ruan, C., & Du, X. (2004). A platelet secretion pathway

mediated by cGMP-dependent protein kinase. *J Biol Chem*, *279*(41), 42469-42475. https://doi.org/10.1074/jbc.M401532200

Libby, P. (2021). Inflammation during the life cycle of the atherosclerotic plaque. *Cardiovasc Res*, *117*(13), 2525-2536. https://doi.org/10.1093/cvr/cvab303

Libby, P., Pasterkamp, G., Crea, F., & Jang, I. K. (2019). Reassessing the Mechanisms of Acute Coronary Syndromes. *Circ Res*, *124*(1), 150-160. https://doi.org/10.1161/circresaha.118.311098

Lincoln, T. M. (2007). Myosin phosphatase regulatory pathways: different functions or redundant functions? *Circ Res*, *100*(1), 10-12. https://doi.org/10.1161/01.Res.0000255894.25293.82

Liu, R., Kang, Y., & Chen, L. (2021). Activation mechanism of human soluble guanylate cyclase by stimulators and activators. *Nat Commun*, *12*(1), 5492. https://doi.org/10.1038/s41467-021-25617-0

Lopes-Pires, M. E., Naime, A. C., Almeida Cardelli, N. J., Anjos, D. J., Antunes, E., & Marcondes, S. (2015). PKC and AKT Modulate cGMP/PKG Signaling Pathway on Platelet Aggregation in Experimental Sepsis. *PLoS One*, *10*(9), e0137901. https://doi.org/10.1371/journal.pone.0137901

Lu, X. & Kassab, G. S. (2004). Nitric oxide is significantly reduced in ex vivo porcine arteries during reverse flow because of increased superoxide production. *J Physiol*, *561*(Pt 2), 575-582. https://doi.org/10.1113/jphysiol.2004.075218

Ludwig, N., Hilger, A., Zarbock, A., & Rossaint, J. (2022). Platelets at the Crossroads of Pro-Inflammatory and Resolution Pathways during Inflammation. *Cells*, *11*(12). https://doi.org/10.3390/cells11121957

Ma, L., Perini, R., McKnight, W., Dicay, M., Klein, A., Hollenberg, M. D., & Wallace, J. L. (2005). Proteinase-activated receptors 1 and 4 counter-regulate endostatin and VEGF release from human platelets. *Proc Natl Acad Sci U S A*, *102*(1), 216-220. https://doi.org/10.1073/pnas.0406682102

Magwenzi, S., Woodward, C., Wraith, K. S., Aburima, A., Raslan, Z., Jones, H., McNeil, C., Wheatcroft, S., Yuldasheva, N., Febbriao, M., Kearney, M., & Naseem, K. M. (2015). Oxidized LDL activates blood platelets through CD36/NOX2-mediated inhibition of the cGMP/protein kinase G signaling cascade. *Blood*, *125*(17), 2693-2703. https://doi.org/10.1182/blood-2014-05-574491

Makhoul, S., Walter, E., Pagel, O., Walter, U., Sickmann, A., Gambaryan, S., Smolenski, A., Zahedi, R. P., & Jurk, K. (2018). Effects of the NO/soluble guanylate cyclase/cGMP system on the functions of human platelets. *Nitric Oxide*, *76*, 71-80. https://doi.org/10.1016/j.niox.2018.03.008

Marchini, T., Mitre, L. S., & Wolf, D. (2021). Inflammatory Cell Recruitment in Cardiovascular

Disease. *Front Cell Dev Biol*, *9*, 635527. https://doi.org/10.3389/fcell.2021.635527

Marx, N., Husain, M., Lehrke, M., Verma, S., & Sattar, N. (2022). GLP-1 Receptor Agonists for the Reduction of Atherosclerotic Cardiovascular Risk in Patients With Type 2 Diabetes. *Circulation*, *146*(24), 1882-1894. https://doi.org/doi:10.1161/CIRCULATIONAHA.122.059595

Massberg, S., Brand, K., Grüner, S., Page, S., Müller, E., Müller, I., Bergmeier, W., Richter, T., Lorenz, M., Konrad, I., Nieswandt, B., & Gawaz, M. (2002). A critical role of platelet adhesion in the initiation of atherosclerotic lesion formation. *J Exp Med*, *196*(7), 887-896. https://doi.org/10.1084/jem.20012044

Mauersberger, C., Sager, H. B., Wobst, J., Dang, T. A., Lambrecht, L., Koplev, S., Stroth, M., Bettaga, N., Schlossmann, J., Wunder, F., Friebe, A., Björkegren, J. L. M., Dietz, L., Maas, S. L., van der Vorst, E. P. C., Sandner, P., Soehnlein, O., Schunkert, H., & Kessler, T. (2022). Loss of soluble guanylyl cyclase in platelets contributes to atherosclerotic plaque formation and vascular inflammation. *Nat Cardiovasc Res*, *1*(12), 1174-1186. https://doi.org/10.1038/s44161-022-00175-w

May, A. E., Kälsch, T., Massberg, S., Herouy, Y., Schmidt, R., & Gawaz, M. (2002). Engagement of glycoprotein IIb/IIIa (alpha(IIb)beta3) on platelets upregulates CD40L and triggers CD40L-dependent matrix degradation by endothelial cells. *Circulation*, *106*(16), 2111-2117. https://doi.org/10.1161/01.cir.0000033597.45947.0f

Maynard, D. M., Heijnen, H. F., Horne, M. K., White, J. G., & Gahl, W. A. (2007). Proteomic analysis of platelet alpha-granules using mass spectrometry. *J Thromb Haemost*, *5*(9), 1945-1955. https://doi.org/10.1111/j.1538-7836.2007.02690.x

Mergia, E., Friebe, A., Dangel, O., Russwurm, M., & Koesling, D. (2006). Spare guanylyl cyclase NO receptors ensure high NO sensitivity in the vascular system. *J Clin Invest*, *116*(6), 1731-1737. https://doi.org/10.1172/jci27657

Milam, K. E. & Parikh, S. M. (2015). The angiopoietin-Tie2 signaling axis in the vascular leakage of systemic inflammation. *Tissue Barriers*, *3*(1-2), e957508. https://doi.org/10.4161/21688362.2014.957508

Moggio, A., Schunkert, H., Kessler, T., & Sager, H. (2022). Quo Vadis? Immunodynamics of Myeloid Cells after Myocardial Infarction. *Int J Mol Sci*, *23*(24), 15814. https://doi.org/10.3390/ijms232415814

Mullis, K., Faloona, F., Scharf, S., Saiki, R., Horn, G., & Erlich, H. (1986). Specific enzymatic amplification of DNA in vitro: the polymerase chain reaction. *Cold Spring Harb Symp Quant Biol*, *51 Pt 1*, 263-273. https://doi.org/10.1101/sqb.1986.051.01.032

Münzel, T. & Gori, T. (2013). Nitrate therapy and nitrate tolerance in patients with coronary artery disease. *Curr Opin Pharmacol*, *13*(2), 251-259. https://doi.org/https://doi.org/10.1016/j.coph.2012.12.008

Neagoe, P. E., Brkovic, A., Hajjar, F., & Sirois, M. G. (2009). Expression and release of angiopoietin-1 from human neutrophils: intracellular mechanisms. *Growth Factors*, *27*(6), 335-344. https://doi.org/10.3109/08977190903155043

Nelson, C. P., Goel, A., Butterworth, A. S., Kanoni, S., Webb, T. R., Marouli, E., Zeng, L., Ntalla, I., Lai, F. Y., Hopewell, J. C., Giannakopoulou, O., Jiang, T., Hamby, S. E., Di Angelantonio, E., Assimes, T. L., Bottinger, E. P., Chambers, J. C., Clarke, R., Palmer, C. N. A., Cubbon, R. M., Ellinor, P., Ermel, R., Evangelou, E., Franks, P. W., Grace, C., Gu, D., Hingorani, A. D., Howson, J. M. M., Ingelsson, E., Kastrati, A., Kessler, T., Kyriakou, T., Lehtimaki, T., Lu, X., Lu, Y., März, W., McPherson, R., Metspalu, A., Pujades-Rodriguez, M., Ruusalepp, A., Schadt, E. E., Schmidt, A. F., Sweeting, M. J., Zalloua, P. A., AlGhalayini, K., Keavney, B. D., Kooner, J. S., Loos, R. J. F., Patel, R. S., Rutter, M. K., Tomaszewski, M., Tzoulaki, I., Zeggini, E., Erdmann, J., Dedoussis, G., Björkegren, J. L. M., EPIC-CVD Consortium, CARDIoGRAMplusC4D, The UK Biobank CardioMetabolic Consortium CHD working group, Schunkert, H., Farrall, M., Danesh, J., Samani, N. J., Watkins, H., & Deloukas, P. (2017). Association analyses based on false discovery rate implicate new loci for coronary artery disease. *Nat Genet*, *49*(9), 1385-1391. https://doi.org/10.1038/ng.3913

Nieswandt, B., Varga-Szabo, D., & Elvers, M. (2009). Integrins in platelet activation. *J Thromb Haemost*, *7 Suppl 1*, 206-209. https://doi.org/10.1111/j.1538-7836.2009.03370.x

Nikpay, M., Goel, A., Won, H. H., Hall, L. M., Willenborg, C., Kanoni, S., Saleheen, D., Kyriakou, T., Nelson, C. P., Hopewell, J. C., Webb, T. R., Zeng, L., Dehghan, A., Alver, M., Armasu, S. M., Auro, K., Bjonnes, A., Chasman, D. I., Chen, S., Ford, I., Franceschini, N., Gieger, C., Grace, C., Gustafsson, S., Huang, J., Hwang, S. J., Kim, Y. K., Kleber, M. E., Lau, K. W., Lu, X., Lu, Y., Lyytikainen, L. P., Mihailov, E., Morrison, A. C., Pervjakova, N., Qu, L., Rose, L. M., Salfati, E., Saxena, R., Scholz, M., Smith, A. V., Tikkanen, E., Uitterlinden, A., Yang, X., Zhang, W., Zhao, W., de Andrade, M., de Vries, P. S., van Zuydam, N. R., Anand, S. S., Bertram, L., Beutner, F., Dedoussis, G., Frossard, P., Gauguier, D., Goodall, A. H., Gottesman, O., Haber, M., Han, B. G., Huang, J., Jalilzadeh, S., Kessler, T., König, I. R., Lannfelt, L., Lieb, W., Lind, L., Lindgren, C. M., Lokki, M. L., Magnusson, P. K., Mallick, N. H., Mehra, N., Meitinger, T., Memon, F. U., Morris, A. P., Nieminen, M. S., Pedersen, N. L., Peters, A., Rallidis, L. S., Rasheed, A., Samuel, M., Shah, S. H., Sinisalo, J., Stirrups, K. E., Trompet, S., Wang, L., Zaman, K. S., Ardissino, D., Boerwinkle, E., Borecki, I. B., Bottinger, E. P., Buring, J. E., Chambers, J. C., Collins, R., Cupples, L. A., Danesh, J., Demuth, I., Elosua, R., Epstein, S. E., Esko, T., Feitosa, M. F., Franco, O. H., Franzosi, M. G., Granger, C. B., Gu, D., Gudnason, V., Hall, A. S., Hamsten, A., Harris, T. B., Hazen, S. L., Hengstenberg, C., Hofman, A., Ingelsson, E., Iribarren, C., Jukema, J. W., Karhunen, P. J., Kim, B. J., Kooner, J. S., Kullo, I. J., Lehtimaki, T., Loos, R. J. F., Melander, O., Metspalu, A., Marz, W., Palmer, C. N., Perola, M., Quertermous, T., Rader, D. J., Ridker, P. M., Ripatti, S., Roberts, R., Salomaa, V., Sanghera, D. K., Schwartz, S. M., Seedorf, U., Stewart, A. F., Stott, D. J., Thiery, J., Zalloua, P. A., O'Donnell, C. J., Reilly, M. P., Assimes, T. L., Thompson, J. R., Erdmann, J., Clarke, R., Watkins, H., Kathiresan, S., McPherson, R., Deloukas, P., Schunkert, H., Samani, N. J., Farrall, M. (2015). A comprehensive 1,000 Genomes-based genome-wide association meta-analysis of coronary artery disease. *Nat Genet*, *47*(10), 1121-1130. https://doi.org/10.1038/ng.3396

Nordestgaard, B. G. (2016). Triglyceride-Rich Lipoproteins and Atherosclerotic Cardiovascular Disease. *Circ Res*, *118*(4), 547-563. https://doi.org/doi:10.1161/CIRCRESAHA.115.306249

Nykanen, A. I., Krebs, R., Saaristo, A., Turunen, P., Alitalo, K., Yla-Herttuala, S., Koskinen, P. K., & Lemstrom, K. B. (2003). Angiopoietin-1 protects against the development of cardiac allograft arteriosclerosis. *Circulation*, *107*(9), 1308-1314. https://doi.org/10.1161/01.cir.0000054623.35669.3f

Oesterle, A., Laufs, U., & Liao, J. K. (2017). Pleiotropic Effects of Statins on the Cardiovascular System. *Circ Res*, *120*(1), 229-243. https://doi.org/10.1161/circresaha.116.308537

Offermanns, S. (2006). Activation of platelet function through G protein-coupled receptors. *Circ Res*, *99*(12), 1293-1304. https://doi.org/10.1161/01.Res.0000251742.71301.16

Orban, P. C., Chui, D., & Marth, J. D. (1992). Tissue- and site-specific DNA recombination in transgenic mice. *Proc Natl Acad Sci U S A*, *89*(15), 6861-6865. https://doi.org/10.1073/pnas.89.15.6861

Ortega-Gomez, A., Salvermoser, M., Rossaint, J., Pick, R., Brauner, J., Lemnitzer, P., Tilgner, J., de Jong, R. J., Megens, R. T., Jamasbi, J., Doring, Y., Pham, C. T., Scheiermann, C., Siess, W., Drechsler, M., Weber, C., Grommes, J., Zarbock, A., Walzog, B., & Soehnlein, O. (2016). Cathepsin G Controls Arterial But Not Venular Myeloid Cell Recruitment. *Circulation*, *134*(16), 1176-1188. https://doi.org/10.1161/CIRCULATIONAHA.116.024790

Pagel, O., Walter, E., Jurk, K., & Zahedi, R. P. (2017). Taking the stock of granule cargo: Platelet releasate proteomics. *Platelets*, *28*(2), 119-128. https://doi.org/10.1080/09537104.2016.1254762

Panigrahi, S., Ma, Y., Hong, L., Gao, D., West, X. Z., Salomon, R. G., Byzova, T. V., & Podrez, E. A. (2013). Engagement of platelet toll-like receptor 9 by novel endogenous ligands promotes platelet hyperreactivity and thrombosis. *Circ Res*, *112*(1), 103-112. https://doi.org/10.1161/circresaha.112.274241

Patel, A. A., Ginhoux, F., & Yona, S. (2021). Monocytes, macrophages, dendritic cells and neutrophils: an update on lifespan kinetics in health and disease. *Immunology*, *163*(3), 250-261. https://doi.org/10.1111/imm.13320

Patel, S. R., Hartwig, J. H., & Italiano, J. E., Jr. (2005). The biogenesis of platelets from megakaryocyte proplatelets. *J Clin Invest*, *115*(12), 3348-3354. https://doi.org/10.1172/jci26891

Pertuy, F., Aguilar, A., Strassel, C., Eckly, A., Freund, J. N., Duluc, I., Gachet, C., Lanza, F., & Leon, C. (2015). Broader expression of the mouse platelet factor 4-cre transgene beyond the megakaryocyte lineage. *J Thromb Haemost*, *13*(1), 115-125. https://doi.org/10.1111/jth.12784

Peters, K. G., Kontos, C. D., Lin, P. C., Wong, A. L., Rao, P., Huang, L., Dewhirst, M. W., & Sankar, S. (2004). Functional significance of Tie2 signaling in the adult vasculature. *Recent Prog Horm Res*, *59*, 51-71. https://doi.org/10.1210/rp.59.1.51

Peters, L. J. F., Baaten, C., Maas, S. L., Lu, C., Nagy, M., Jooss, N. J., Bidzhekov, K., Santovito, D., Moreno-Andrés, D., Jankowski, J., Biessen, E. A. L., Döring, Y., Heemskerk, J. W. M.,

Weber, C., Kuijpers, M. J. E., & van der Vorst, E. P. C. (2022). MicroRNA-26b Attenuates Platelet Adhesion and Aggregation in Mice. *Biomedicines*, *10*(5). https://doi.org/10.3390/biomedicines10050983

Pizurki, L., Zhou, Z., Glynos, K., Roussos, C., & Papapetropoulos, A. (2003). Angiopoietin-1 inhibits endothelial permeability, neutrophil adherence and IL-8 production. *Br J Pharmacol*, *139*(2), 329-336. https://doi.org/10.1038/sj.bjp.0705259

Podrez, E. A., Byzova, T. V., Febbraio, M., Salomon, R. G., Ma, Y., Valiyaveettil, M., Poliakov, E., Sun, M., Finton, P. J., Curtis, B. R., Chen, J., Zhang, R., Silverstein, R. L., & Hazen, S. L. (2007). Platelet CD36 links hyperlipidemia, oxidant stress and a prothrombotic phenotype. *Nat Med*, *13*(9), 1086-1095. https://doi.org/10.1038/nm1626

Poznyak, A. V., Nikiforov, N. G., Markin, A. M., Kashirskikh, D. A., Myasoedova, V. A., Gerasimova, E. V., & Orekhov, A. N. (2020). Overview of OxLDL and Its Impact on Cardiovascular Health: Focus on Atherosclerosis. *Front Pharmacol*, *11*, 613780. https://doi.org/10.3389/fphar.2020.613780

Quintar, A., McArdle, S., Wolf, D., Marki, A., Ehinger, E., Vassallo, M., Miller, J., Mikulski, Z., Ley, K., & Buscher, K. (2017). Endothelial Protective Monocyte Patrolling in Large Arteries Intensified by Western Diet and Atherosclerosis. *Circ Res*, *120*(11), 1789-1799. https://doi.org/10.1161/CIRCRESAHA.117.310739

Raitakari, O., Pahkala, K., & Magnussen, C. G. (2022). Prevention of atherosclerosis from childhood. *Nat Rev Cardiol*. https://doi.org/10.1038/s41569-021-00647-9

Rana, A., Westein, E., Niego, B., & Hagemeyer, C. E. (2019). Shear-Dependent Platelet Aggregation: Mechanisms and Therapeutic Opportunities. *Front Cardiovasc Med*, *6*, 141. https://doi.org/10.3389/fcvm.2019.00141

Rashbrook, V. S., Brash, J. T., & Ruhrberg, C. (2022). Cre toxicity in mouse models of cardiovascular physiology and disease. *Nat Cardiovasc Res*, *1*(9), 806-816. https://doi.org/10.1038/s44161-022-00125-6

Reiss, C., Mindukshev, I., Bischoff, V., Subramanian, H., Kehrer, L., Friebe, A., Stasch, J. P., Gambaryan, S., & Walter, U. (2015). The sGC stimulator riociguat inhibits platelet function in washed platelets but not in whole blood. *Br J Pharmacol*, *172*(21), 5199-5210. https://doi.org/10.1111/bph.13286

Ridker, P. M. (2017). How Common Is Residual Inflammatory Risk? *Circ Res*, *120*(4), 617-619. https://doi.org/10.1161/circresaha.116.310527

Ridker, P. M. (2018). Should Aspirin Be Used for Primary Prevention in the Post-Statin Era? *N Engl J Med*, *379*(16), 1572-1574. https://doi.org/10.1056/NEJMe1812000

Ridker, P. M., Everett, B. M., Thuren, T., MacFadyen, J. G., Chang, W. H., Ballantyne, C., Fonseca, F., Nicolau, J., Koenig, W., Anker, S. D., Kastelein, J. J. P., Cornel, J. H., Pais, P., Pella, D.,

Genest, J., Cifkova, R., Lorenzatti, A., Forster, T., Kobalava, Z., Vida-Simiti, L., Flather, M., Shimokawa, H., Ogawa, H., Dellborg, M., Rossi, P. R. F., Troquay, R. P. T., Libby, P., Glynn, R. J., & CANTOS Trial Group. (2017). Antiinflammatory Therapy with Canakinumab for Atherosclerotic Disease. *N Engl J Med*, *377*(12), 1119-1131. https://doi.org/10.1056/NEJMoa1707914

Rink, T. J. & Sage, S. O. (1990). Calcium signaling in human platelets. *Annu Rev Physiol*, *52*, 431-449. https://doi.org/10.1146/annurev.ph.52.030190.002243

Roth, G. A., Mensah, G. A., Johnson, C. O., Addolorato, G., Ammirati, E., Baddour, L. M., Barengo, N. C., Beaton, A. Z., Benjamin, E. J., Benziger, C. P., Bonny, A., Brauer, M., Brodmann, M., Cahill, T. J., Carapetis, J., Catapano, A. L., Chugh, S. S., Cooper, L. T., Coresh, J., Criqui, M., DeCleene, N., Eagle, K. A., Emmons-Bell, S., Feigin, V. L., Fernández-Solà, J., Fowkes, G., Gakidou, E., Grundy, S. M., He, F. J., Howard, G., Hu, F., Inker, L., Karthikeyan, G., Kassebaum, N., Koroshetz, W., Lavie, C., Lloyd-Jones, D., Lu, H. S., Mirijello, A., Temesgen, A. M., Mokdad, A., Moran, A. E., Muntner, P., Narula, J., Neal, B., Ntsekhe, M., Moraes de Oliveira, G., Otto, C., Owolabi, M., Pratt, M., Rajagopalan, S., Reitsma, M., Ribeiro, A. L. P., Rigotti, N., Rodgers, A., Sable, C., Shakil, S., Sliwa-Hahnle, K., Stark, B., Sundström, J., Timpel, P., Tleyjeh, I. M., Valgimigli, M., Vos, T., Whelton, P. K., Yacoub, M., Zuhlke, L., Murray, C., & Fuster, V. (2020). Global Burden of Cardiovascular Diseases and Risk Factors, 1990-2019: Update From the GBD 2019 Study. *J Am Coll Cardiol*, *76*(25), 2982-3021. https://doi.org/10.1016/j.jacc.2020.11.010

Roy, A., Groten, J., Marigo, V., Tomar, T., & Hilhorst, R. (2021). Identification of Novel Substrates for cGMP Dependent Protein Kinase (PKG) through Kinase Activity Profiling to Understand Its Putative Role in Inherited Retinal Degeneration. *Int J Mol Sci*, *22*(3). https://doi.org/10.3390/ijms22031180

Rudolph, J. M., Guttek, K., Weitz, G., Meinke, C. A., Kliche, S., Reinhold, D., Schraven, B., & Reinhold, A. (2019). Characterization of Mice with a Platelet-Specific Deletion of the Adapter Molecule ADAP. *Mol Cell Biol*, *39*(9). https://doi.org/10.1128/mcb.00365-18

Rukoyatkina, N., Walter, U., Friebe, A., & Gambaryan, S. (2011). Differentiation of cGMP-dependent and -independent nitric oxide effects on platelet apoptosis and reactive oxygen species production using platelets lacking soluble guanylyl cyclase. *Thromb Haemost*, *106*(5), 922-933. https://doi.org/10.1160/th11-05-0319

Saigusa, R., Winkels, H., & Ley, K. (2020). T cell subsets and functions in atherosclerosis. *Nat Rev Cardiol*, *17*(7), 387-401. https://doi.org/10.1038/s41569-020-0352-5

Samani, N. J., Erdmann, J., Hall, A. S., Hengstenberg, C., Mangino, M., Mayer, B., Dixon, R. J., Meitinger, T., Braund, P., Wichmann, H. E., Barrett, J. H., König, I. R., Stevens, S. E., Szymczak, S., Tregouet, D. A., Iles, M. M., Pahlke, F., Pollard, H., Lieb, W., Cambien, F., Fischer, M., Ouwehand, W., Blankenberg, S., Balmforth, A. J., Baessler, A., Ball, S. G., Strom, T. M., Braenne, I., Gieger, C., Deloukas, P., Tobin, M. D., Ziegler, A., Thompson, J. R., & Schunkert, H. (2007). Genomewide association analysis of coronary artery disease. *N Engl J Med*, *357*(5), 443-453. https://doi.org/10.1056/NEJMoa072366

Sandner, P., Zimmer, D. P., Milne, G. T., Follmann, M., Hobbs, A., & Stasch, J.-P. (2021). Soluble Guanylate Cyclase Stimulators and Activators. In H. H. H. W. Schmidt, P. Ghezzi, & A. Cuadrado (Eds.), *Reactive Oxygen Species: Network Pharmacology and Therapeutic Applications* (pp. 355-394). Springer International Publishing. https://doi.org/10.1007/164_2018_197

Schaffner, A., Rhyn, P., Schoedon, G., & Schaer, D. J. (2005). Regulated expression of platelet factor 4 in human monocytes--role of PARs as a quantitatively important monocyte activation pathway. *J Leukoc Biol*, *78*(1), 202-209. https://doi.org/10.1189/jlb.0105024

Schinner, E., Salb, K., & Schlossmann, J. (2011). Signaling via IRAG is essential for NO/cGMP-dependent inhibition of platelet activation. *Platelets*, *22*(3), 217-227. https://doi.org/10.3109/09537104.2010.544151

Schlossmann, J., Ammendola, A., Ashman, K., Zong, X., Huber, A., Neubauer, G., Wang, G. X., Allescher, H. D., Korth, M., Wilm, M., Hofmann, F., & Ruth, P. (2000). Regulation of intracellular calcium by a signalling complex of IRAG, IP3 receptor and cGMP kinase Ibeta. *Nature*, *404*(6774), 197-201. https://doi.org/10.1038/35004606

Schlossmann, J. & Desch, M. (2011). IRAG and novel PKG targeting in the cardiovascular system. *Am J Physiol Heart Circ Physiol*, *301*(3), H672-682. https://doi.org/10.1152/ajpheart.00198.2011

Schmidt, H. H., Lohmann, S. M., & Walter, U. (1993). The nitric oxide and cGMP signal transduction system: regulation and mechanism of action. *Biochim Biophys Acta*, *1178*(2), 153-175. https://doi.org/10.1016/0167-4889(93)90006-b

Schneider, H., Szabo, E., Machado, R. A., Broggini-Tenzer, A., Walter, A., Lobell, M., Heldmann, D., Sussmeier, F., Grunewald, S., & Weller, M. (2017). Novel TIE-2 inhibitor BAY-826 displays in vivo efficacy in experimental syngeneic murine glioma models. *J Neurochem*, *140*(1), 170-182. https://doi.org/10.1111/jnc.13877

Schober, A., Manka, D., von Hundelshausen, P., Huo, Y., Hanrath, P., Sarembock, I. J., Ley, K., & Weber, C. (2002). Deposition of platelet RANTES triggering monocyte recruitment requires P-selectin and is involved in neointima formation after arterial injury. *Circulation*, *106*(12), 1523-1529. https://doi.org/10.1161/01.cir.0000028590.02477.6f

Segura-Puimedon, M., Mergia, E., Al-Hasani, J., Aherrahrou, R., Stoelting, S., Kremer, F., Freyer, J., Koesling, D., Erdmann, J., Schunkert, H., de Wit, C., & Aherrahrou, Z. (2016). Proatherosclerotic Effect of the alpha1-Subunit of Soluble Guanylyl Cyclase by Promoting Smooth Muscle Phenotypic Switching. *Am J Pathol*, *186*(8), 2220-2231. https://doi.org/10.1016/j.ajpath.2016.04.010

Sehgal, S. & Storrie, B. (2007). Evidence that differential packaging of the major platelet granule proteins von Willebrand factor and fibrinogen can support their differential release. *J Thromb Haemost*, *5*(10), 2009-2016. https://doi.org/10.1111/j.1538-7836.2007.02698.x

Shankman, L. S., Gomez, D., Cherepanova, O. A., Salmon, M., Alencar, G. F., Haskins, R. M., Swiatlowska, P., Newman, A. A., Greene, E. S., Straub, A. C., Isakson, B., Randolph, G. J., &

Owens, G. K. (2015). KLF4-dependent phenotypic modulation of smooth muscle cells has a key role in atherosclerotic plaque pathogenesis. *Nat Med*, *21*(6), 628-637. https://doi.org/10.1038/nm.3866

Silvestre-Roig, C., Braster, Q., Ortega-Gomez, A., & Soehnlein, O. (2020). Neutrophils as regulators of cardiovascular inflammation. *Nat Rev Cardiol*, *17*(6), 327-340. https://doi.org/10.1038/s41569-019-0326-7

Sinnaeve, P., Chiche, J. D., Nong, Z., Varenne, O., Van Pelt, N., Gillijns, H., Collen, D., Bloch, K. D., & Janssens, S. (2001). Soluble guanylate cyclase alpha(1) and beta(1) gene transfer increases NO responsiveness and reduces neointima formation after balloon injury in rats via antiproliferative and antimigratory effects. *Circ Res*, *88*(1), 103-109. https://www.ncbi.nlm.nih.gov/pubmed/11139481

https://www.ahajournals.org/doi/pdf/10.1161/01.RES.88.1.103

Soehnlein, O., Kai-Larsen, Y., Frithiof, R., Sorensen, O. E., Kenne, E., Scharffetter-Kochanek, K., Eriksson, E. E., Herwald, H., Agerberth, B., & Lindbom, L. (2008). Neutrophil primary granule proteins HBP and HNP1-3 boost bacterial phagocytosis by human and murine macrophages. *J Clin Invest*, *118*(10), 3491-3502. https://doi.org/10.1172/jci35740

Stasch, J. P., Dembowsky, K., Perzborn, E., Stahl, E., & Schramm, M. (2002). Cardiovascular actions of a novel NO-independent guanylyl cyclase stimulator, BAY 41-8543: in vivo studies. *Br J Pharmacol*, *135*(2), 344-355. https://doi.org/10.1038/sj.bjp.0704483

Stasch, J. P., Schmidt, P. M., Nedvetsky, P. I., Nedvetskaya, T. Y., H, S. A., Meurer, S., Deile, M., Taye, A., Knorr, A., Lapp, H., Müller, H., Turgay, Y., Rothkegel, C., Tersteegen, A., Kemp-Harper, B., Müller-Esterl, W., & Schmidt, H. H. (2006). Targeting the heme-oxidized nitric oxide receptor for selective vasodilatation of diseased blood vessels. *J Clin Invest*, *116*(9), 2552-2561. https://doi.org/10.1172/jci28371

Statistisches Bundesamt (Destatis). (2021). *Gestorbene: Deutschland, Jahre, Todesursachen, Geschlecht 2020*. Retrieved November 28, 2022 from https://www-genesis.destatis.de/genesis/online?sequenz=tabelleErgebnis&selectionname=23211-0002#abreadcrumb

Sternberg, N. & Hamilton, D. (1981). Bacteriophage P1 site-specific recombination. I. Recombination between loxP sites. *J Mol Biol*, *150*(4), 467-486. https://doi.org/10.1016/0022-2836(81)90375-2

Stroth, M. (2022). *Dissertation: Einfluss des thrombozytenspezifischen Knockouts der löslichen Guanylatzyklase auf die Ausbildung atherosklerotischer Plaques* [Technical University of Munich]. https://mediatum.ub.tum.de/node?id=1638187

Sun, Q., Kiernan, U. A., Shi, L., Phillips, D. A., Kahn, B. B., Hu, F. B., Manson, J. E., Albert, C. M., & Rexrode, K. M. (2013). Plasma retinol-binding protein 4 (RBP4) levels and risk of coronary heart disease: a prospective analysis among women in the nurses' health study. *Circulation*, *127*(19), 1938-1947. https://doi.org/10.1161/circulationaha.113.002073

Supernat, A., Popęda, M., Pastuszak, K., Best, M. G., Grešner, P., Veld, S. I. t., Siek, B., Bednarz-Knoll, N., Rondina, M. T., Stokowy, T., Wurdinger, T., Jassem, J., & Żaczek, A. J. (2021). Transcriptomic landscape of blood platelets in healthy donors. *Sci Rep*, *11*(1), 15679. https://doi.org/10.1038/s41598-021-94003-z

Tacke, F., Alvarez, D., Kaplan, T. J., Jakubzick, C., Spanbroek, R., Llodra, J., Garin, A., Liu, J., Mack, M., van Rooijen, N., Lira, S. A., Habenicht, A. J., & Randolph, G. J. (2007). Monocyte subsets differentially employ CCR2, CCR5, and CX3CR1 to accumulate within atherosclerotic plaques. *J Clin Invest*, *117*(1), 185-194. https://doi.org/10.1172/JCI28549

Tersteeg, C., Heijnen, H. F., Eckly, A., Pasterkamp, G., Urbanus, R. T., Maas, C., Hoefer, I. E., Nieuwland, R., Farndale, R. W., Gachet, C., de Groot, P. G., & Roest, M. (2014). FLow-induced PRotrusions (FLIPRs): a platelet-derived platform for the retrieval of microparticles by monocytes and neutrophils. *Circ Res*, *114*(5), 780-791. https://doi.org/10.1161/CIRCRESAHA.114.302361

Thoonen, R., Cauwels, A., Decaluwe, K., Geschka, S., Tainsh, R. E., Delanghe, J., Hochepied, T., De Cauwer, L., Rogge, E., Voet, S., Sips, P., Karas, R. H., Bloch, K. D., Vuylsteke, M., Stasch, J.-P., Van de Voorde, J., Buys, E. S., & Brouckaert, P. (2015). Cardiovascular and pharmacological implications of haem-deficient NO-unresponsive soluble guanylate cyclase knock-in mice. *Nat Commun*, *6*(1), 8482. https://doi.org/10.1038/ncomms9482

Tiedt, R., Schomber, T., Hao-Shen, H., & Skoda, R. C. (2006). Pf4-Cre transgenic mice allow the generation of lineage-restricted gene knockouts for studying megakaryocyte and platelet function in vivo. *Blood*, *109*(4), 1503-1506. https://doi.org/10.1182/blood-2006-04-020362

Timmis, A., Vardas, P., Townsend, N., Torbica, A., Katus, H., De Smedt, D., Gale, C. P., Maggioni, A. P., Petersen, S. E., Huculeci, R., Kazakiewicz, D., de Benito Rubio, V., Ignatiuk, B., Raisi-Estabragh, Z., Pawlak, A., Karagiannidis, E., Treskes, R., Gaita, D., Beltrame, J. F., McConnachie, A., Bardinet, I., Graham, I., Flather, M., Elliott, P., Mossialos, E. A., Weidinger, F., Achenbach, S., & Atlas Writing Group, E. S. o. C. (2022). European Society of Cardiology: cardiovascular disease statistics 2021. *Eur Heart J*, *43*(8), 716-799. https://doi.org/10.1093/eurheartj/ehab892

Tsou, C. Y., Chen, C. Y., Zhao, J. F., Su, K. H., Lee, H. T., Lin, S. J., Shyue, S. K., Hsiao, S. H., & Lee, T. S. (2014). Activation of soluble guanylyl cyclase prevents foam cell formation and atherosclerosis. *Acta Physiol (Oxf)*, *210*(4), 799-810. https://doi.org/10.1111/apha.12210

Tzima, E., Irani-Tehrani, M., Kiosses, W. B., Dejana, E., Schultz, D. A., Engelhardt, B., Cao, G., DeLisser, H., & Schwartz, M. A. (2005). A mechanosensory complex that mediates the endothelial cell response to fluid shear stress. *Nature*, *437*(7057), 426-431. https://doi.org/10.1038/nature03952

Vaduganathan, M., Docherty, K. F., Claggett, B. L., Jhund, P. S., de Boer, R. A., Hernandez, A. F., Inzucchi, S.E., Kosiborod, M. N., Lam, C. S. P., Martinez, F., Shah, S. J., Desai A. S., McMurray, J. J. V., Solomon, S.D. (2022). SGLT-2 inhibitors in patients with heart failure: a comprehensive meta-analysis of five randomised controlled trials. *Lancet*, *400*(10354):757-767. https://doi.org/10.1016/S0140-6736(22)01429-5

Varga-Szabo, D., Braun, A., & Nieswandt, B. (2009). Calcium signaling in platelets. *J Thromb Haemost*, *7*(7), 1057-1066. https://doi.org/10.1111/j.1538-7836.2009.03455.x

Veillard, N. R., Kwak, B., Pelli, G., Mulhaupt, F., James, R. W., Proudfoot, A. E., & Mach, F. (2004). Antagonism of RANTES receptors reduces atherosclerotic plaque formation in mice. *Circ Res*, *94*(2), 253-261. https://doi.org/10.1161/01.RES.0000109793.17591.4E

Virani, S. S. (2022). The Fibrates Story - A Tepid End to a PROMINENT Drug. *N Engl J Med*, *387*(21), 1991-1992. https://doi.org/10.1056/NEJMe2213208

Visseren, F. L. J., Mach, F., Smulders, Y. M., Carballo, D., Koskinas, K. C., Back, M., Benetos, A., Biffi, A., Boavida, J. M., Capodanno, D., Cosyns, B., Crawford, C., Davos, C. H., Desormais, I., Di Angelantonio, E., Franco, O. H., Halvorsen, S., Hobbs, F. D. R., Hollander, M., Jankowska, E. A., Michal, M., Sacco, S., Sattar, N., Tokgozoglu, L., Tonstad, S., Tsioufis, K. P., van Dis, I., van Gelder, I. C., Wanner, C., Williams, B., Societies, E. S. C. N. C., & Group, E. S. C. S. D. (2021). 2021 ESC Guidelines on cardiovascular disease prevention in clinical practice. *Eur Heart J*, *42*(34), 3227-3337. https://doi.org/10.1093/eurheartj/ehab484

Vogel, B., Claessen, B. E., Arnold, S. V., Chan, D., Cohen, D. J., Giannitsis, E., Gibson, C. M., Goto, S., Katus, H. A., Kerneis, M., Kimura, T., Kunadian, V., Pinto, D. S., Shiomi, H., Spertus, J. A., Steg, P. G., & Mehran, R. (2019). ST-segment elevation myocardial infarction. *Nat Rev Dis Primers*, *5*(1), 39. https://doi.org/10.1038/s41572-019-0090-3

Vogel, S., Bodenstein, R., Chen, Q., Feil, S., Feil, R., Rheinlaender, J., Schäffer, T. E., Bohn, E., Frick, J. S., Borst, O., Münzer, P., Walker, B., Markel, J., Csanyi, G., Pagano, P. J., Loughran, P., Jessup, M. E., Watkins, S. C., Bullock, G. C., Sperry, J. L., Zuckerbraun, B. S., Billiar, T. R., Lotze, M. T., Gawaz, M., & Neal, M. D. (2015). Platelet-derived HMGB1 is a critical mediator of thrombosis. *J Clin Invest*, *125*(12), 4638-4654. https://doi.org/10.1172/jci81660

von Hundelshausen, P., Weber, K. S., Huo, Y., Proudfoot, A. E., Nelson, P. J., Ley, K., & Weber, C. (2001). RANTES deposition by platelets triggers monocyte arrest on inflamed and atherosclerotic endothelium. *Circulation*, *103*(13), 1772-1777. https://doi.org/10.1161/01.cir.103.13.1772

von Scheidt, M., Zhao, Y., Kurt, Z., Pan, C., Zeng, L., Yang, X., Schunkert, H., & Lusis, A. J. (2017). Applications and Limitations of Mouse Models for Understanding Human Atherosclerosis. *Cell Metab*, *25*(2), 248-261. https://doi.org/10.1016/j.cmet.2016.11.001

Wagner, L. E., 2nd, Li, W. H., & Yule, D. I. (2003). Phosphorylation of type-1 inositol 1,4,5-trisphosphate receptors by cyclic nucleotide-dependent protein kinases: a mutational analysis of the functionally important sites in the S2+ and S2- splice variants. *J Biol Chem*, *278*(46), 45811-45817. https://doi.org/10.1074/jbc.M306270200

Wang, Y., Pampou, S., Fujikawa, K., & Varticovski, L. (2004). Opposing effect of angiopoietin-1 on VEGF-mediated disruption of endothelial cell-cell interactions requires activation of PKC beta. *J Cell Physiol*, *198*(1), 53-61. https://doi.org/10.1002/jcp.10386

Warnatsch, A., Ioannou, M., Wang, Q., & Papayannopoulos, V. (2015). Neutrophil extracellular traps license macrophages for cytokine production in atherosclerosis. *Science*, *349*(6245), 316-320. https://doi.org/doi:10.1126/science.aaa8064

Warner, T. D., Mitchell, J. A., Sheng, H., & Murad, F. (1994). Effects of cyclic GMP on smooth muscle relaxation. *Adv Pharmacol*, *26*, 171-194. https://doi.org/10.1016/s1054-3589(08)60054-x

Webb, T. R., Erdmann, J., Stirrups, K. E., Stitziel, N. O., Masca, N. G., Jansen, H., Kanoni, S., Nelson, C. P., Ferrario, P. G., König, I. R., Eicher, J. D., Johnson, A. D., Hamby, S. E., Betsholtz, C., Ruusalepp, A., Franzén, O., Schadt, E. E., Björkegren, J. L., Weeke, P. E., Auer, P. L., Schick, U. M., Lu, Y., Zhang, H., Dube, M. P., Goel, A., Farrall, M., Peloso, G. M., Won, H. H., Do, R., van Iperen, E., Kruppa, J., Mahajan, A., Scott, R. A., Willenborg, C., Braund, P. S., van Capelleveen, J. C., Doney, A. S., Donnelly, L. A., Asselta, R., Merlini, P. A., Duga, S., Marziliano, N., Denny, J. C., Shaffer, C., El-Mokhtari, N. E., Franke, A., Heilmann, S., Hengstenberg, C., Hoffmann, P., Holmen, O. L., Hveem, K., Jansson, J. H., Jöckel, K. H., Kessler, T., Kriebel, J., Laugwitz, K. L., Marouli, E., Martinelli, N., McCarthy, M. I., Van Zuydam, N. R., Meisinger, C., Esko, T., Mihailov, E., Escher, S. A., Alver, M., Moebus, S., Morris, A. D., Virtamo, J., Nikpay, M., Olivieri, O., Provost, S., AlQarawi, A., Robertson, N. R., Akinsansya, K. O., Reilly, D. F., Vogt, T. F., Yin, W., Asselbergs, F. W., Kooperberg, C., Jackson, R. D., Stahl, E., Müller-Nurasyid, M., Strauch, K., Varga, T. V., Waldenberger, M., Zeng, L., Chowdhury, R., Salomaa, V., Ford, I., Jukema, J. W., Amouyel, P., Kontto, J., Nordestgaard, B. G., Ferrières, J., Saleheen, D., Sattar, N., Surendran, P., Wagner, A., Young, R., Howson, J. M., Butterworth, A. S., Danesh, J., Ardissino, D., Bottinger, E. P., Erbel, R., Franks, P. W., Girelli, D., Hall, A. S., Hovingh, G. K., Kastrati, A., Lieb, W., Meitinger, T., Kraus, W. E., Shah, S. H., McPherson, R., Orho-Melander, M., Melander, O., Metspalu, A., Palmer, C. N., Peters, A., Rader, D. J., Reilly, M. P., Loos, R. J., Reiner, A. P., Roden, D. M., Tardif, J. C., Thompson, J. R., Wareham, N. J., Watkins, H., Willer, C. J., Samani, N. J., Schunkert, H., Deloukas, P., Kathiresan, S. (2017). Systematic Evaluation of Pleiotropy Identifies 6 Further Loci Associated With Coronary Artery Disease. *J Am Coll Cardiol*, *69*(7), 823-836. https://doi.org/10.1016/j.jacc.2016.11.056

Wen, L., Feil, S., Wolters, M., Thunemann, M., Regler, F., Schmidt, K., Friebe, A., Olbrich, M., Langer, H., Gawaz, M., de Wit, C., & Feil, R. (2018). A shear-dependent NO-cGMP-cGKI cascade in platelets acts as an auto-regulatory brake of thrombosis. *Nat Commun*, *9*(1). https://doi.org/10.1038/s41467-018-06638-8

Williams, J. W., Zaitsev, K., Kim, K. W., Ivanov, S., Saunders, B. T., Schrank, P. R., Kim, K., Elvington, A., Kim, S. H., Tucker, C. G., Wohltmann, M., Fife, B. T., Epelman, S., Artyomov, M. N., Lavine, K. J., Zinselmeyer, B. H., Choi, J. H., & Randolph, G. J. (2020). Limited proliferation capacity of aortic intima resident macrophages requires monocyte recruitment for atherosclerotic plaque progression. *Nat Immunol*, *21*(10), 1194-1204. https://doi.org/10.1038/s41590-020-0768-4

Winter, C., Silvestre-Roig, C., Ortega-Gomez, A., Lemnitzer, P., Poelman, H., Schumski, A., Winter, J., Drechsler, M., de Jong, R., Immler, R., Sperandio, M., Hristov, M., Zeller, T., Nicolaes, G. A. F., Weber, C., Viola, J. R., Hidalgo, A., Scheiermann, C., & Soehnlein, O. (2018). Chrono-pharmacological Targeting of the CCL2-CCR2 Axis Ameliorates Atherosclerosis. *Cell Metab*, *28*(1), 175-182.e175. https://doi.org/10.1016/j.cmet.2018.05.002

Witzenbichler, B., Westermann, D., Knueppel, S., Schultheiss, H. P., & Tschope, C. (2005). Protective role of angiopoietin-1 in endotoxic shock. *Circulation*, *111*(1), 97-105. https://doi.org/10.1161/01.Cir.0000151287.08202.8e

Wobst, J., Schunkert, H., & Kessler, T. (2018). Genetic alterations in the NO-cGMP pathway and cardiovascular risk. *Nitric Oxide*. https://doi.org/10.1016/j.niox.2018.03.019

World Health Organisation. (2021). *Cardiovascular diseases (CVDs)*. Retrieved December 3, 2022 from https://www.who.int/news-room/fact-sheets/detail/the-top-10-causes-of-death

Yadav, S. & Storrie, B. (2017). The cellular basis of platelet secretion: Emerging structure/function relationships. *Platelets*, *28*(2), 108-118. https://doi.org/10.1080/09537104.2016.1257786

Yin, H., Liu, J., Li, Z., Berndt, M. C., Lowell, C. A., & Du, X. (2008). Src family tyrosine kinase Lyn mediates VWF/GPIb-IX-induced platelet activation via the cGMP signaling pathway. *Blood*, *112*(4), 1139-1146. https://doi.org/10.1182/blood-2008-02-140970

Yu, D. & Liao, J. K. (2022). Emerging views of statin pleiotropy and cholesterol lowering. *Cardiovasc Res*, *118*(2), 413-423. https://doi.org/10.1093/cvr/cvab032

Zhang, G., Xiang, B., Dong, A., Skoda, R. C., Daugherty, A., Smyth, S. S., Du, X., & Li, Z. (2011). Biphasic roles for soluble guanylyl cyclase (sGC) in platelet activation. *Blood*, *118*(13), 3670-3679. https://doi.org/10.1182/blood-2011-03-341107

Zhao, Y. D., Campbell, A. I., Robb, M., Ng, D., & Stewart, D. J. (2003). Protective role of angiopoietin-1 in experimental pulmonary hypertension. *Circ Res*, *92*(9), 984-991. https://doi.org/10.1161/01.Res.0000070587.79937.F0

Zhou, J., Li, Y. S., & Chien, S. (2014). Shear stress-initiated signaling and its regulation of endothelial function. *Arterioscler Thromb Vasc Biol*, *34*(10), 2191-2198. https://doi.org/10.1161/atvbaha.114.303422

Ziegler-Heitbrock, L., Ancuta, P., Crowe, S., Dalod, M., Grau, V., Hart, D. N., Leenen, P. J., Liu, Y. J., MacPherson, G., Randolph, G. J., Scherberich, J., Schmitz, J., Shortman, K., Sozzani, S., Strobl, H., Zembala, M., Austyn, J. M., & Lutz, M. B. (2010). Nomenclature of monocytes and dendritic cells in blood. *Blood*, *116*(16), e74-80. https://doi.org/10.1182/blood-2010-02-258558

Appendices

Appendix figures

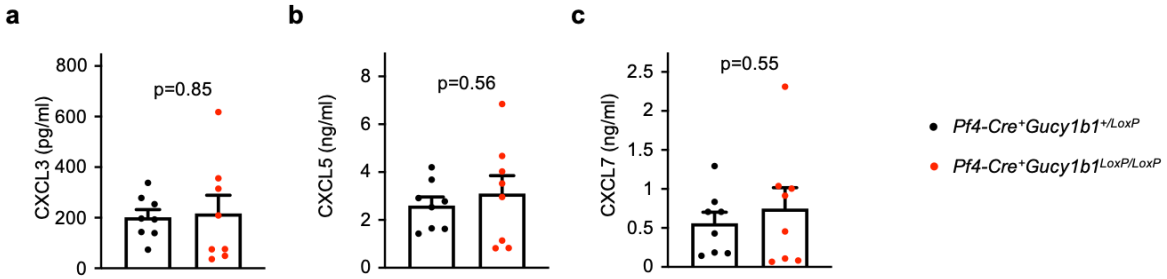

Appendix Figure 1 Plasma levels of BAC clone cytokines in platelet sGC-deficient mice. Plasma levels of the cytokines CXCL3, CXCL5, and CXCL7 did not differ between *Pf4-Cre*$^{+}$*Gucy1b1*$^{+/LoxP}$ and *Pf4-Cre*$^{+}$*Gucy1b1*$^{LoxP/LoxP}$ mice. CXCL15 was not detectable in plasma. Each symbol represents one animal. Unpaired t-test. Data are mean ± s.e.m. Abbreviations: *CXCL*, C-X-C motif ligand.

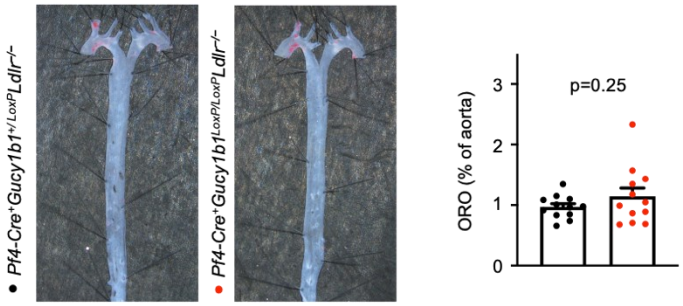

Appendix Figure 2 Early phase atherogenesis in platelet sGC-deficient mice. No significant difference in early atherosclerotic plaque formation after 6 weeks of Western diet in *Pf4-Cre*$^{+}$*Gucy1b1*$^{LoxP/LoxP}$*Ldlr*$^{-/-}$ compared with *Pf4-Cre*$^{+}$*Gucy1b1*$^{+/LoxP}$*Ldlr*$^{-/-}$ mice. Each symbol represents one animal. Unpaired t-test. Data are mean ± s.e.m. Abbreviations: *ORO*, Oil Red O.

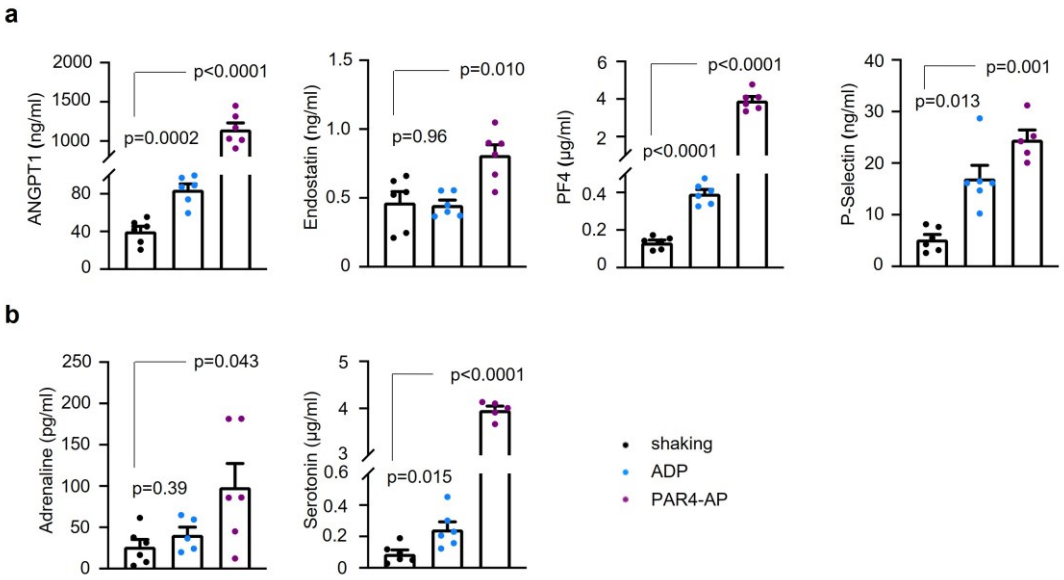

Appendix Figure 3 Differential release of granule proteins from platelets upon shaking compared with agonist-stimulated release. Differential (**a**) α-granule and (**b**) dense granule component release from wildtype platelets after activation by shaking, adenosine diphosphate, and the thrombin-receptor agonist PAR4-AP. Each symbol represents paired samples derived from 6 independent animals. One outlier was removed from the PAR4-AP group in the measurement of serotonin and P-selectin, as well as in the ADP group in adrenaline (n=5) according to the ROUT's test. Ordinary one-way ANOVA/mixed-effects analysis in case of missing values with Dunnett's multiple comparisons test. Data are mean ± s.e.m. Abbreviations: *ADP*, adenosine diphosphate; *ANGPT1*, angiopoietin-1; *PF4*, platelet factor 4.

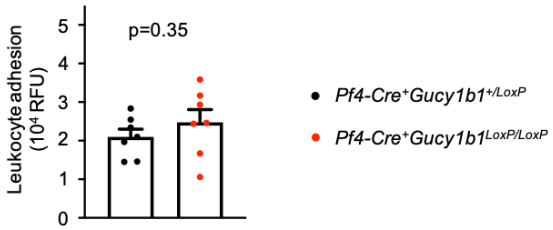

Appendix Figure 4 *In vitro* leukocyte adhesion of mice lacking sGC in platelets. *Pf4-Cre*$^{+}$*Gucy1b1*$^{+/LoxP}$ and *Pf4-Cre*$^{+}$*Gucy1b1*$^{LoxP/LoxP}$ monocyte and neutrophil adhesion to wildtype endothelial cells in presence of shake-activated wildtype platelet releasate does not differ between both groups. Each symbol represents one animal. Unpaired t-test. Data are mean ± s.e.m.

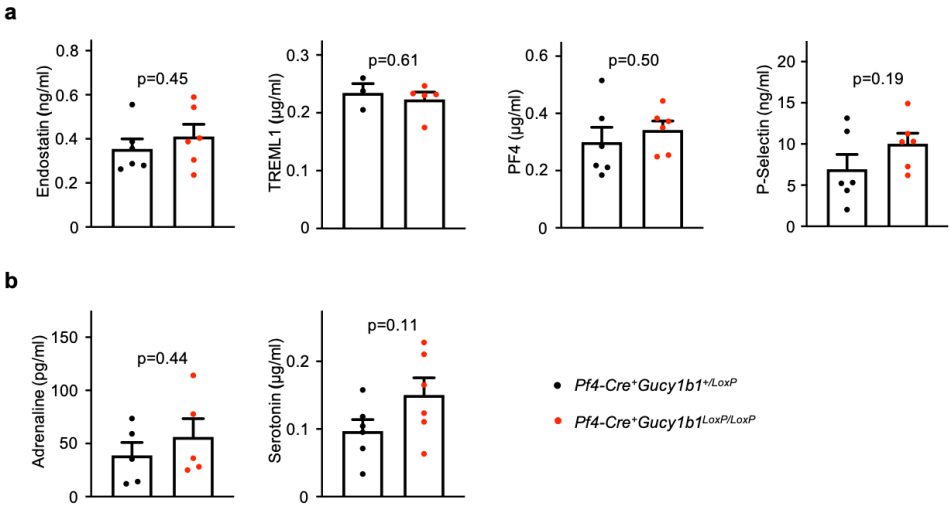

Appendix Figure 5 α- and dense granule release from sGC-deficient platelets. Release of selected important α-granule (**a**) and dense granule (**b**) components did not significantly differ between control and *Pf4-Cre*$^{+}$*Gucy1b1*$^{LoxP/LoxP}$ platelets after activation by shaking. VEGF was not detectable in either of the samples. Each symbol represents one animal. Unpaired t-test. Data are mean ± s.e.m. Abbreviations: *PF4*, platelet factor 4; *TREML1*, triggering receptor expressed on myeloid cells like 1.

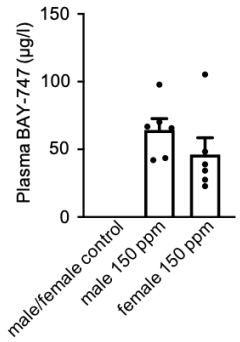

Appendix Figure 6 Plasma concentrations of mice during pharmacological sGC stimulation. BAY-747 plasma levels as determined by liquid chromatography and mass spectrometry analysis in female and male mice treated with 0 or 150 ppm of the soluble guanylyl cyclase stimulator BAY-747 for 10 weeks accompanied by Western diet. Each symbol represents one animal. Data are mean ± s.e.m. Reprinted under the terms of the Creative Commons CC BY license: Extended Data Figure 1e from reference (Mauersberger et al., 2022). Measurement was conducted by Dr. Lisa Dietz (Bayer AG, Wuppertal, Germany).

Appendix tables

Appendix Table 1 Kinase activity following sGC stimulation of platelets in vitro. List of activated kinases in shake-activated platelet lysate after preincubating platelets with vehicle or BAY-747 (n=6 each) by using the PamGene Serine/Threonine Kinase array. Mean Kinase statistic denotes directionality: a negative value displays reduced activity; a positive value displays increased activity in BAY-747 *vs.* vehicle-treated platelets. A Median Final score > 1.2 denotes statistical significance. Reprinted under the terms of the Creative Commons CC BY license: Supplemantary Table 5 from reference (Mauersberger et al., 2022). Data were obtained from Dr. Emiel van der Vorst (RWTH Aachen, Germany).

Kinase Uniprot ID	Kinase Name	Mean Kinase Statistic	Median Final score	Mean peptide set size
Q05655	PKC[delta]	1,130534003	4,017728767	21
Q96GD4	AurB/Aur1	1,842519447	3,966576245	4,111111111
Q05513	PKC[zeta]	1,409749871	3,935542011	8,444444444
Q04759	PKC[theta]	1,109819547	3,89279003	21,33333333
O14757	CHK1	1,445007704	3,841637508	8
P05771	PKC[beta]	1,459035801	3,841637508	7
O14965	AurA/Aur2	1,628922625	3,707743929	4,111111111
P31749	Akt1/PKB[alpha]	0,968654879	3,634512015	26,55555556
P11309	Pim1	0,808835832	3,627087997	59,11111111
Q13535	ATR	1,318854713	3,627087997	5,888888889
Q13131	AMPK[alpha]1	1,171440519	3,578396073	10,77777778
P05129	PKC[gamma]	1,177257426	3,571865206	12,22222222
Q15418	RSK3	1,163851085	3,565431096	10
P16066	ANP[alpha]	1,03010862	3,534617149	22,88888889
O95819	HGK/ZC1	1,324783645	3,500312917	5,285714286
P31751	Akt2/PKB[beta]	0,934008829	3,484126156	24,11111111
Q9UIK4	DAPK2	1,484170011	3,468521083	3
Q8NI60	ADCK3	1,173536306	3,438898616	8,777777778
Q9P1W9	Pim2	0,846929813	3,424812155	37,77777778
O00141	SGK1	1,354429672	3,411168274	3
O15075	DCAMKL1	1,202951418	3,3495545	3,5
P41743	PKC[iota]	0,953649545	3,304518324	11,88888889
Q9HBY8	SGK2	1,137355247	3,294136288	13,77777778
P68400	CK2[alpha]1	1,087043366	3,280668713	4
Q15349	RSK1/p90RSK	1,03411878	3,274088368	6
P23443	p70S6K	0,921611984	3,258060922	17
Q02156	PKC[epsilon]	0,911089701	3,227678293	18,66666667
P49137	MAPKAPK2	0,859129979	3,162411562	29,77777778
P24723	PKC[eta]	1,017573452	3,084072788	13,33333333
Q16644	MAPKAPK3	0,782153059	3,055517328	33,33333333
Q86V86	Pim3	0,764201039	3,032452024	56,11111111
Q9UKE5	TNIK/ZC2	1,241097254	2,907021648	3
Q14164	IKK[epsilon]	0,974173783	2,887394998	5,777777778

P42345	mTOR/FRAP	1,117639876	2,791558644	4,888888889
O96017	CHK2	0,780030989	2,635261445	21,55555556
Q9Y6S9	RSKL2	0,885785053	2,533312245	3,5
Q13153	PAK1	0,620772837	2,48945499	6
Q9UQM7	CaMK2[alpha]	0,721702046	2,396206296	3
P45984	JNK2	0,569677017	2,388064375	16
Q16539	MAPK14	0,740365841	2,323123568	12
P17252	PKC[alpha]	0,681218845	2,280668713	28,22222222
Q15759	p38[beta]	0,621057491	2,278684119	5,2
P51812	RSK2	0,596371472	2,27083521	8
P06493	CDC2/CDK1	0,636484075	2,232102384	12,77777778
P17612	PKA[alpha]	0,674270512	2,232102384	50,66666667
O75116	ROCK2	0,639308186	2,15490196	4,8
O75582	MSK1	0,62802422	2,139542205	8
Q9UPZ9	ICK	0,641690517	1,944927618	3
P51817	PRKX	0,710991456	1,871600731	30,66666667
Q16566	CaMK4	0,707887703	1,864422147	12,55555556
Q00535	CDK5	0,512221791	1,811240207	6
P04049	RAF1	0,641641019	1,773039406	7,222222222
Q13976	PKG1	0,594562032	1,76025019	42
O15264	p38[delta]	0,612539299	1,707655306	13,33333333
Q8IWB6	SgK307	0,684115928	1,666351243	3
P53779	JNK3	0,505238007	1,601712695	20,22222222
P45983	JNK1	0,492381529	1,573293594	20,55555556
Q13237	PKG2	0,612393489	1,552160042	36,33333333
P49840	GSK3[alpha]	0,512055697	1,550861147	4
Q9UBS0	p70S6K[beta]	0,610891435	1,504178247	25
Q16512	PKN1/PRK1	0,609467916	1,370916754	5
Q15131	CDK10	0,514124218	1,303084719	6
P50750	CDK9	0,49353533	1,27730028	5,666666667

Appendix Table 2 Peptide phosphorylation following sGC stimulation of platelets in vitro. List of phosphorylated peptides in shake-activated platelet lysate after preincubating platelets with vehicle or BAY-747 (n=6 each) by using the PamGene Serine/Threonine Kinase array. Only statistically significant hits (adjusted $p<0.05$) are listed. Effect size values indicate extent and directionality (negative – down-regulation, positive – up-regulation) in BAY-747 *vs.* vehicle treated platelets. Reprinted under the terms of the Creative Commons CC BY license: Supplemantary Table 6 from reference (Mauersberger et al., 2022). Data were obtained from Dr. Emiel van der Vorst (RWTH Aachen, Germany).

Peptide ID	Assigned protein	Peptide sequence	Effect size
NOS3_1171_1183	Nitric oxide synthase, endothelial	SRIRTQSFSLQER	0,414994568
ERBB2_679_691	Receptor tyrosine-protein kinase erbB-2	QQKIRKYTMRRLL	1,425183296
H2B1B_ 27_40	Histone H2B type 1-B	GKKRKRSRKESYSI	0,960534573
CENPA_1_14	Histone H3-like centromeric protein A	MGPRRRSRKPEAPR	1,391188502
KPCB_19_31_A25S	Protein kinase C beta type	RFARKGSLRQKNV	1,116446376
ESR1_160_172	Estrogen receptor	GGRERLASTNDKG	0,615124702
VASP_271_283	Vasodilator-stimulated phosphoprotein	LARRRKATQVGEK	0,550091267
KIF2C_105_118_S106G	Kinesin-like protein KIF2C	EGLRSRSTRMSTVS	0,801053345
ANDR_785_797	Androgen receptor	VRMRHLSQEFGWL	0,471784443
MPIP3_208_220	M-phase inducer phosphatase 3	RSGLYRSPSMPEN	1,052611828
PLEK_106_118	Pleckstrin	GQKFARKSTRRSI	0,762111664
RYR1_4317_4329	Ryanodine receptor 1	VRRLRRLTAREAA	0,496296734
PTN12_32_44	Tyrosine-protein phosphatase non-receptor type 12	FMRLRRLSTKYRT	0,394804806
FRAP_2443_2455	Serine/threonine-protein kinase mTOR	RTRTDSYSAGQSV	0,415469795
RAF1_253_265	RAF proto-oncogene serine/threonine-protein kinase	QRQRSTSTPNVHM	0,947622299
ADDB_706_718	Beta-adducin	KKKFRTPSFLKKS	0,649356782
RBL2_655_667	Retinoblastoma-like protein 2	GLGRSITSPTTLY	0,453680128
CREB1_126_138	Cyclic AMP-responsive element-binding protein 1	EILSRRPSYRKIL	0,21201627
PTK6_436_448	Protein-tyrosine kinase 6	ALRERLSSFTSYE	0,188092232
KAPCG_192_206	cAMP-dependent protein kinase catalytic subunit gamma	VKGRTWTLCGTPEYL	0,488101482
GYS2_1_13	Glycogen [starch] synthase, liver	MLRGRSLSVTSLG	0,386413723
E1A_ADE05_212	Early E1A protein	AILRRPTSPVSRE	0,188306496

_224			
GPR6_349_361	G-protein coupled receptor 6	QSKVPFRSRSPSE	0,426840454
GSUB_61_73	Protein phosphatase 1 regulatory subunit 17	KKPRRKDTPALHI	-0,363381147
KCNA2_442_454	Potassium voltage-gated channel subfamily A member 2	PDLKKSRSASTIS	0,374373436
KCNA3_461_473	Potassium voltage-gated channel subfamily A member 3	EELRKARSNSTLS	0,34637928
NCF1_296_308	Neutrophil cytosol factor 1	RGAPPRRSSIRNA	0,142123058
BAD_69_81	Bcl2-associated agonist of cell death	IRSRHSSYPAGTE	0,294188827
C1R_201_213	Complement C1r subcomponent	ASGYISSLEYPRS	0,284779072
CFTR_730_742	Cystic fibrosis transmembrane conductance regulator	EPLERRLSLVPDS	-0,118124641
NEK3_158_170	Serine/threonine-protein kinase Nek3	FACTYVGTPYYVP	0,281368822
PDE5A_95_107	cGMP-specific 3',5'-cyclic phosphodiesterase	GTPTRKISASEFD	0,580832005
MPIP1_172_184	M-phase inducer phosphatase 1	FTQRQNSAPARML	0,251359463
ANXA1_209_221	Annexin A1	AGERRKGTDVNVF	0,320334285
NMDZ1_890_902	Glutamate receptor ionotropic, NMDA 1	SFKRRRSSKDTST	0,119470917
ACM1_444_456	Muscarinic acetylcholine receptor M1	KIPKRPGSVHRTP	-0,268279642
BCKD_45_57	[3-methyl-2-oxobutanoate dehydrogenase [lipoamide]] kinase, mitochondrial	ERSKTVTSFYNQS	0,204482242
ERF_519_531	ETS domain-containing transcription factor ERF	GEAGGPLTPRRVS	0,631763935

List of publications

Major parts of this thesis have been published in Nature Cardiovascular Research:

Mauersberger, C.*, Sager, H. B.*, Wobst, J., Dang, T. A., Lambrecht, L., Koplev, S., Stroth, M., Bettaga, N., Schlossmann, J., Wunder, F., Friebe, A., Björkegren, J. L. M., Dietz, L., Maas, S. L., van der Vorst, E. P. C., Sandner, P., Soehnlein, O., Schunkert, H., & Kessler, T. (2022). Loss of soluble guanylyl cyclase in platelets contributes to atherosclerotic plaque formation and vascular inflammation. *Nat Cardiovasc Res*, *1*(12), 1174-1186. https://doi.org/10.1038/s44161-022-00175-w

Other contributions (Original Research):

Meyer-Lindemann, U.*, **Mauersberger, C.***, Schmidt, A.-C.*, Moggio, A.*, Hinterdobler, J., Li, X., Khangholi, D., Hettwer, J., Gräßer, C., Dutsch, A., Schunkert, H., Kessler, T., & Sager, H. B. (2022). Colchicine impacts leukocyte trafficking in atherosclerosis and reduces vascular inflammation. *Front Immunol*, *13*. https://doi.org/10.3389/fimmu.2022.898690

Hettwer, J., Hinterdobler, J., Miritsch, B., Deutsch, M. A., Li, X., **Mauersberger, C.**, Moggio, A., Braster, Q., Gram, H., Robertson, A. A. B., Cooper, M. A., Gross, O., Krane, M., Weber, C., Koenig, W., Soehnlein, O., Adamstein, N. H., Ridker, P., Schunkert, H., Libby, P., Kessler, T., & Sager, H. B. (2021). Interleukin-1beta suppression dampens inflammatory leukocyte production and uptake in atherosclerosis. *Cardiovasc Res*. https://doi.org/10.1093/cvr/cvab337

Hinterdobler, J., Schott, S., Jin, H., Meesmann, A., Steinsiek, A. L., Zimmermann, A. S., Wobst, J., Muller, P., **Mauersberger, C.**, Vilne, B., Baecklund, A., Chen, C. S., Moggio, A., Braster, Q., Molitor, M., Krane, M., Kempf, W. E., Ladwig, K. H., Hristov, M., Hulsmans, M., Hilgendorf, I., Weber, C., Wenzel, P., Scheiermann, C., Maegdefessel, L., Soehnlein, O., Libby, P., Nahrendorf, M., Schunkert, H., Kessler, T., & Sager, H. B. (2021). Acute mental stress drives vascular inflammation and promotes plaque destabilization in mouse atherosclerosis. *Eur Heart J*. https://doi.org/10.1093/eurheartj/ehab371

Other contributions (Reviews):

Mauersberger, C., Hinterdobler, J., Schunkert, H., Kessler, T., & Sager, H. B. (2022). Where the action is – leukocyte recruitment in atherosclerosis. *Front Cardiovasc Med*, *8*. https://doi.org/10.3389/fcvm.2021.813984

Mauersberger, C., Schunkert, H., & Sager, H. B. (2021). Inflammation-related risk loci in genome-wide association studies of coronary artery disease. *Cells*, *10*(2). https://doi.org/10.3390/cells10020440

Mauersberger, C. & Sager, H. B. (2019). Inflammation als therapeutisches Target. *CardioVasc*, *19*(2), 28-33. https://doi.org/10.1007/s15027-019-1539-8

Posters and talks

Atherosclerosis – Mechanisms and novel therapeutic targets: International Symposium 2022. Munich, Germany, 10.10.2022: Contribution of platelet sGC to vascular inflammation in mice.

90th European Atherosclerosis Society Congress 2022. Milan, Italy, 23.05.2022: Platelet soluble guanylyl cyclase deficiency promotes atherosclerosis in mice.

Deutsche Gesellschaft für Kardiologie, 88. Jahrestagung. Mannheim, Germany, 23.04.2022: Loss of soluble guanylyl cyclase in platelets promotes atherosclerotic plaque formation and vascular inflammation.

9th Cardiac Regeneration & Vascular Biology Conference. San Servolo, Italy, 18.10.2021: Loss of soluble guanylyl cyclase in platelets promotes atherosclerotic plaque formation and vascular inflammation.

Munich Heart Alliance Summer Meeting 2021. Online, 19.07.2021: Loss of soluble guanylyl cyclase in platelets contributes to atherosclerotic plaque formation and vascular inflammation.